Title

Levodopa-induced gamma oscillations in patients with Parkinson's disease using chronic invasive brain recording: detection, entrainment, and functional relevance

Author

Olaru, Maria

Publication Date

2024

Peer reviewed|Thesis/dissertation

Levodopa-induced gamma oscillations in patients with Parkinson's Disease using chronic invasive brain recording: detection, entrainment, and functional relevance

by
Maria Olaru

DISSERTATION
Submitted in partial satisfaction of the requirements for degree of
DOCTOR OF PHILOSOPHY

in

Neuroscience

in the

GRADUATE DIVISION
of the
UNIVERSITY OF CALIFORNIA, SAN FRANCISCO

Approved:

DocuSigned by:
Reza Abbasi Asl
169A38ABEC6F49D...
Reza Abbasi Asl
Chair

DocuSigned by:
Wolf-Julian Neumann
Wolf-Julian Neumann

DocuSigned by:
Prasad Shirvalkar
Prasad Shirvalkar

DocuSigned by:
Philip Starr
ADB44FC349C54C9...
Philip Starr

Committee Members

Acknowledgements

I'd first like to thank all academic mentors and advisors who provided guidance and feedback for my various projects – Dr. Philip Starr recommending highly relevant research topics and effectively communicating scientific findings. Dr. Reza Abbasi Asl for his ability to consistently recommend tractable analytic methods. Dr. Prasad Shirvalkar and Dr. Julian Neumann for their continual encouragement, interest, and shrewd eye for data interpretation.

I'd also like to thank various lab members for their contributions to the research projects—Amelia Hahn and Maria Scherbakova for collecting patient data and any relevant preprocessing. I will be forever grateful for their ability to navigate the finicky research equipment and provide the data I used for these research projects. I'd also like to thank Lauren Hammer, Stephanie Cernera, and Stephanie Pistorius for their encouragement and for making themselves available for miscellaneous data-related and grant submission questions. Lastly, I'd like to thank Cora de Hemptinne for helping me onboard onto ongoing lab protocols and pipelines, despite no longer being a research scientist in the Starr Lab.

Lastly, I'd like to thank Dr. Leo Sugrue, whose mentorship in the Department of Radiology and Biomedical Imaging provided me with foundational skills in coding, data interpretation, and scientific communication. Your hands-on guidance and unwavering attention to detail during my early years as a budding researcher enabled me to hit the ground running at the Starr lab.

Dedication

To my dog, Lumi, for always being by my side and reminding me to unplug from the computer and go for a walk every few hours. Our countless agility classes and beach runs also provided me with the necessary companionship and much-needed distraction from research.

To my sister, Sofia, for accompanying me on memorable adventures throughout my PhD. Your spontaneity and willingness to explore gave me the much-needed breaks to recharge and refocus.

To my partner, Sahand, for your unwavering support throughout my research career. Your willingness to help with late-night statistics and signal-processing questions, endless encouragement, and genuine passion for science have been such a delight.

Contributions

Chapter 1 is written by Maria Olaru.

Chapter 2 is reproduced in an adapted form from:

> *Olaru M.*, Cernera S., Hahn A., Wozny T.A., Anso J., de Hemptinne C., Little S., Neumann W.-J., Abbasi-Asl R., Starr P.A. (2024). Motor network gamma oscillations in chronic home recordings predict dyskinesia in Parkinson's disease. Brain: A Journal of Neurology. 147, 2038-2052*

M.O., R.A. & P.A.S. Designed Research; M.O., C. H., & A.H Performed Research; M.O. Analyzed Data; S.C., C.H., S.L. & R.A Validated Research; M.O., S.C., W.-J. N. & P.A.S Wrote Paper.

Chapter 3 is reproduced in adapted form from:

> *Olaru M.*, Hahn A., Shcherbakova M., Little S., Neumann W.-J., Abbasi-Asl R., Starr P.A. (2024). Deep brain stimulation-entrained gamma oscillations in chronic home recordings in Parkinson's disease. Brain stimulation, Submitted*

M.O. & P.A. Designed Research; M.O., A.H., & M.S Performed Research; M.O. & M.S. Analyzed Data; P.A.S, W.-J. N., & R.A Validated Research; M.O. & P.A.S Wrote Paper.

Chapter 4 is reproduced in an adapted form from:

Sermon J. J., Olaru M., Anso J, Cernera S, Little S. Shcherbakova M., Bogacz R., Starr P.A., Denison T., Duchet B. (2023). Sub-harmonic entrainment of cortical gamma oscillations to deep brain stimulation in Parkinson's disease: Model-based predictions and validation in three human subjects. Brain stimulation, 16(5), 1412-1424.*

J.J.S., M.O., & J.A. Designed Research; J.J.S., M.O., S.C., & M.S. Performed Research; J.J.S & MO Analyzed Data; S.C., R.B., T.D., P.A.S., J.A., & B.D. Validated Research; J.J.S., M.O., J.A., S.C., S.L., M.S., R.B., P.A.S., T.D., & B.D. Wrote Paper

“Well-behaved women seldom make history.”

-Laurel Thatcher Ulrich

Levodopa-induced gamma oscillations in patients with Parkinson's disease using chronic invasive brain recording: detection, entrainment, and functional relevance

Maria Olaru

Abstract

In Parkinson's disease, imbalances between "antikinetic" and "prokinetic" patterns of neuronal oscillatory activity are thought to be related to motor dysfunction. Invasive brain recordings from the motor network have suggested that medical or surgical therapy can promote a prokinetic state by inducing narrowband gamma rhythms (60-90 Hz), which are associated with dyskinesia. Here, I investigate the behavioral and statistical properties of levodopa-induced and deep brain stimulation-entrained narrowband gamma rhythms. Collaborating with Oxford researchers, we also model the deep brain stimulation induced entrainment of gamma oscillations using interacting neuronal populations and patient-specific features of the levodopa-induced gamma oscillations. Using a sensing-enabled deep brain stimulation system, attached to both motor cortex and subthalamic or pallidal leads, the Starr Lab recorded over 900 hours of multisite field potentials prior to initiating deep brain stimulation, and over 600 hours during deep brain stimulation. I find that levodopa-induced gamma oscillations are more strongly associated with dyskinesia than deep brain stimulation-entrained gamma oscillations. Statistical comparisons revealed that levodopa-induced gamma oscillations exhibit increased variance in peak frequency, decreased spectral power, and higher variance in spectral power. Furthermore, I also work with collaborators at Oxford to show that entrainment can be predicted using neural circuit models fitted to patient data at various stimulation parameters. Put together, this

work suggests that gamma oscillations as programming biomarkers should be leveraged distinctly across medical and surgical interventions to mitigate dyskinesia – while excessive levodopa-induced gamma oscillations are a marker for dyskinesia, increased entrained gamma oscillations may be a marker of a non-pathological prokinetic movement state. Our modeling work can subsequently be leveraged to predict the frequency and power of entrained gamma oscillations across stimulation parameters.

Table of Contents

Chapter 1: ***Introduction*** **1**

References 4

Chapter 2: ***Levodopa-induced gamma oscillations co-fluctuate with dyskinesia*** **6**

Introduction 6

Methods 7

Results 15

Discussion 24

Figures 30

Tables 40

Supplemental Figures 42

Supplemental Tables 49

References 50

Chapter 3: ***Entrained gamma oscillations are functionally and behaviorally distinct from levodopa-induced gamma oscillations*** **58**

Introduction 58

Methods 59

Results 62

Discussion 67

Figures 73

Tables 79

Supplemental Figures 81

References 85

Chapter 4: ***Deep brain stimulation entrainment of gamma oscillations can be modelled by neuronal population models*** **……...90**

Introduction ……..……90

Methods ……..……92

Results ……..……95

Discussion ……..……96

Figures ……..……..103

Tables ……...107

References ……..…109

List of Figures

Chapter 2:

Figure 2.1 : Anatomic localization of recording contacts and data processing method ……30

Figure 2.2 : Narrowband gamma oscillations across subjects: frequency distribution and relation to clinical history of dyskinesia ..……..……..……..32

Figure 2.3 : Narrowband gamma correlates with simulatenous contralateral wearable dyskinesia scores ….....……..…….…….…..33

Figure 2.4 : Stratification analysis shows narrowband gamma-dyskinesia correlations are not driven by outliers ……..……...35

Figure 2.5 : Other neural correlates of dyskinesia ……...36

Figure 2.6 : Low gamma processing method, frequency distribution, relation to clinical dyskinesia and correlation with contralateral dyskinesia scores .....…….38

Supplemental Figure 2.7 : Methodology for defining the peak frequency of narrowband gamma in a timeseries …...……..……..42

Supplemental Figure 2.8 : Segregation of wearable dyskinesia scores and integrated gamma scores by preoperative UPDRS IV ….....…….…...43

Supplemental Figure 2.9 : Presence of cortical gamma oscillations in relation to electrode placement ….....……..…….…….……...44

Supplemental Figure 2.10 : Differences in absolute power of average peak narrowband gamma spectral power across subjects ……..…....…..45

Supplemental Figure 2.11 : Correlates of cortical narrowband gamma with contralateral wearable scores for off-state motor signs …….....…..46

Supplemental Figure 2.12 : Correlates of subthalamic narrowband gamma with contralateral wearable scores for off-state motor signs ….....….47

Supplemental Figure 2.13 : Relationship between wearable dyskinesia scores in on-state subdomains versus ordinal groupings ….....…..48

Chapter 3:

Figure 3.1 : Anatomical localization of recording contacts and processing pipelines …73

Figure 3.2 : Levodopa-induced and entrained gamma at chronic therapeutic settings across subjects: presence, anatomical localization, and relation to the clinical history of dyskinesia ..……74

Figure 3.3 : The relationship of dyskinesia to entrained gamma across stimulation amplitude increases ……..……76

Figure 3.4 : Spectral features of cortical levodopa-induced gamma and chronic therapeutic entrained gamma: fluctuations in peak frequency and power across epochs ……....77

Supplemental Figure 3.5 : The power of entrained gamma across stimulation amplitude increases ……..……..……...81

Supplemental Figure 3.6 : Spectral features of subcortical levodopa-induced gamma and chronic therapeutic entrained gamma: fluctuations in peak frequency and power across epochs ……..……...82

Supplemental Figure 3.7 : The relationship between the difference in peak gamma frequency between levodopa-induced gamma and entrained gamma statistical properties ..……..……...83

Chapter 4:

Figure 4.1 : Contact localization across the three subjects ……..103

Figure 4.2 : Testing model predictions of a cortical circuit's response to an external stimulus using human neural data during neurostimulation ……..……..…….105

List of Tables

Chapter 2:

Table 2.1 : Subject demographics…..……..……..…..40

Table 2.2 : Presence and localization of narrowband gamma across study subjects 41

Supplementary Table 2.3 : Presence and localization of low gamma across study subjects ……....48

Chapter 3:

Table 3.1 : Subject demographics ..……....79

Table 3.2 : Presence of levodopa-induced and entrained gamma across study subjects ……...…….80

Chapter 4:

Table 4.1 : Patient information summary ……...……..107

Table 4.2 : Patient information summary ……..……...……...108

Chapter 1:

Introduction

Dyskinesia, a common side effect of Parkinson's disease treatment, severely impacts the quality of life for many patients. Since the introduction of levodopa therapy in the 1960s, it has remained the most effective treatment for alleviating motor symptoms [1]. However, prolonged use of levodopa often leads to the development of dyskinesia, characterized by involuntary, erratic, and writhing movements. The incidence of dyskinesia increases with the duration and dosage of levodopa treatment, affecting up to 80% of patients after a few years of chronic therapy [2].

Despite therapeutic advancements with deep brain stimulation, managing dyskinesia remains a major clinical challenge. The majority of patients with deep brain stimulation for Parkinson's disease receive stimulation at the subthalamic nucleus [3]. However, stimulation of the subthalamic nucleus can also induce dyskinesia [4]. As the population ages, the number of individuals affected by Parkinson's disease and its associated dyskinesia is expected to double in the next 30 years [5], underscoring the need for more effective and sustainable treatment strategies.

Invasive brain recordings from the motor network have suggested that medical or surgical therapy can promote a prokinetic state by inducing narrowband gamma rhythms (60-90 Hz). Excessive narrowband gamma in the motor cortex promotes dyskinesia in rodent models [6–8]. Recently, narrowband gamma oscillations have also been observed in the motor cortex of subjects with Parkinson's disease in the on-medication state with first-generation [9] and second-generation [10] sensing-enabled deep brain stimulation devices. In humans with Parkinson's disease, Swann et al. [9] suggested a relationship between cortical narrowband gamma and dyskinesia in two subjects from multiple brief recordings at home in dyskinetic and non-dyskinetic states. However,

those findings were based on short recordings (30-second to five-minute duration) and subject self-ratings for dyskinesia.

Deep brain stimulation can entrain levodopa-induced gamma oscillations to one-half of the stimulation frequency and are observed in clinically therapeutic stimulation settings, suggesting that these oscillations may be clinically therapeutic [9,10]. However, the impact of entraining levodopa-induced gamma oscillations on dyskinesia, and their possible mechanisms, remain an active area of research. As sensing-enabled stimulators are becoming widely available, beta-band desynchronization oscillatory activity, which aims to reduce the antikinetic movement state, is increasingly used to guide stimulator programming [11]. Given that some sensing-enabled stimulators can also detect gamma oscillations, understanding the effect of entrainment on levodopa-induced gamma oscillations may improve programming protocols.

Once the behavioral correlates of entrained gamma oscillations are better understood, programming protocols may benefit from optimizing stimulation parameters for the optimal amount of entrained gamma oscillation. Currently, optimizing stimulation parameters is a laborious and manual process that spans several months. The approach involves clinical programming sessions followed by the patient going home and returning for iterative adjustments [12]. Developing a model that can predict the amount of entrained gamma across stimulation parameters could streamline this process, saving both time and costs by identifying optimal programming protocols more efficiently.

The current findings raise intriguing questions about the role of narrowband gamma oscillations as a physiological marker of dyskinesia in patients with Parkinson's disease. Do levodopa-induced gamma oscillations fluctuate in relation to dyskinesia, and does this relationship change with entrainment, suggesting that entrained gamma oscillations correspond to a healthier

prokinetic state? If so, then can we predict the stimulation parameters that will lead to maximal gamma entrainment at one-half of the stimulation frequency? The interplay between deep brain stimulation, neuronal oscillatory activity, and their behavioral correlates necessitates further investigation. Whether these insights will redefine our understanding of optimal programming or simply add a nuanced layer to existing models, they represent a promising avenue for future research. As sensing-enabled stimulators become more advanced, the potential to fine-tune therapy based on real-time neural feedback could revolutionize treatment paradigms for Parkinson's disease.

References

1. Tolosa E, Martí MJ, Valldeoriola F, Molinuevo JL. History of levodopa and dopamine agonists in Parkinson's disease treatment. Neurology. 1998;50: S2–10; discussion S44–8.

2. Voon V, Napier TC, Frank MJ, Sgambato-Faure V, Grace AA, Rodriguez-Oroz M, et al. Impulse control disorders and levodopa-induced dyskinesias in Parkinson's disease: an update. Lancet Neurol. 2017;16: 238–250.

3. Mahajan A, Butala A, Okun MS, Mari Z, Mills KA. Global Variability in Deep Brain Stimulation Practices for Parkinson's Disease. Front Hum Neurosci. 2021;15: 667035.

4. Zheng Z, Li Y, Li J, Zhang Y, Zhang X, Zhuang P. Stimulation-induced dyskinesia in the early stage after subthalamic deep brain stimulation. Stereotact Funct Neurosurg. 2010;88: 29–34.

5. Rocca WA. The burden of Parkinson's disease: a worldwide perspective. Lancet neurology. 2018. pp. 928–929.

6. Güttler C, Altschüler J, Tanev K, Böckmann S, Haumesser JK, Nikulin VV, et al. Levodopa-Induced Dyskinesia Are Mediated by Cortical Gamma Oscillations in Experimental Parkinsonism. Mov Disord. 2021;36: 927–937.

7. Halje P, Tamtè M, Richter U, Mohammed M, Cenci MA, Petersson P. Levodopa-induced dyskinesia is strongly associated with resonant cortical oscillations. J Neurosci. 2012;32: 16541–16551.

8. Salvadè A, D'Angelo V, Di Giovanni G, Tinkhauser G, Sancesario G, Städler C, et al. Distinct roles of cortical and pallidal β and γ frequencies in hemiparkinsonian and dyskinetic rats. Exp Neurol. 2016;275 Pt 1: 199–208.

9. Swann NC, de Hemptinne C, Miocinovic S, Qasim S, Wang SS, Ziman N, et al. Gamma Oscillations in the Hyperkinetic State Detected with Chronic Human Brain Recordings in Parkinson's Disease. J Neurosci. 2016;36: 6445–6458.

10. Gilron R, Little S, Perrone R, Wilt R, de Hemptinne C, Yaroshinsky MS, et al. Long-term wireless streaming of neural recordings for circuit discovery and adaptive stimulation in individuals with Parkinson's disease. Nat Biotechnol. 2021;39: 1078–1085.

11. Sandoval-Pistorius SS, Hacker ML, Waters AC, Wang J, Provenza NR, de Hemptinne C, et al. Advances in Deep Brain Stimulation: From Mechanisms to Applications. J Neurosci. 2023;43: 7575–7586.

12. Wagle Shukla A, Zeilman P, Fernandez H, Bajwa JA, Mehanna R. DBS Programming: An Evolving Approach for Patients with Parkinson's Disease. Parkinsons Dis. 2017;2017: 8492619.

Chapter 2:

Levodopa-induced gamma oscillations co-fluctuate with dyskinesia

INTRODUCTION

Much has been learned about the physiological basis for Parkinsonian motor signs by recording local field potentials from deep brain stimulator leads implanted in basal ganglia nuclei. Early work utilized externalized leads in subjects at rest in a perioperative setting [1]. A seminal early observation using externalized leads was that therapeutic levodopa suppressed subthalamic nucleus beta band (13-30 Hz) oscillatory activity while promoting gamma band activity at 65-90 Hz, often referred to as “narrowband gamma” or as “finely-tuned gamma” [2]. This led to the hypothesis that alleviating bradykinesia requires rebalancing basal ganglia “antikinetic” beta oscillations with “prokinetic” higher frequency oscillations. This model suggests an excess of the “prokinetic” narrowband gamma rhythm could lead to hyperkinetic states such as dyskinesia. However, this link has been difficult to demonstrate with short perioperative recordings from externalized leads.

In rodent models of Parkinson’s disease treated chronically with levodopa, phenomenologically identical 65-90 Hz narrowband gamma oscillations have been recorded from the motor cortex, where they are linked to dyskinesia [3-5]. Recently, narrowband gamma has been observed in the motor cortex of subjects with Parkinson’s disease in the on-medication state with first-generation [6] and second-generation [7] sensing-enabled deep brain stimulation (DBS) devices connected to subdural cortical leads. In humans with Parkinson’s disease, Swann et al [6]. suggested a relationship between cortical narrowband gamma and dyskinesia in two subjects from multiple brief recordings at home in dyskinetic and non-dyskinetic states. However, those findings were based on short recordings (30-second to five-minute duration) and subject self-ratings for dyskinesia. The remaining questions include (1) whether narrowband gamma spectral

power in the motor network scales with the severity of dyskinesias, (2) the temporal relationship between variations in narrowband gamma and variations in dyskinesia, (3) the relative value of cortical versus basal ganglia narrowband gamma as markers of dyskinesia, and (4) the contribution of the other frequencies, such as beta and theta, as covariate predictors of dyskinesia [8].

To address these questions, we utilized an investigational second-generation sensing-enabled pulse generator capable of performing four-channel recordings continuously at home [7]. Prior to initiating therapeutic basal ganglia stimulation, we recorded 984 hours of cortical and basal ganglia field potentials in 30 hemispheres of 16 subjects with Parkinson's disease, with 608 hours recorded while continuously measuring dyskinesia using wearable sensors. We collected recordings in naturalistic settings while subjects were awake, performing normal activities of daily living, and on their usual schedule of antiparkinsonian medications. We found fluctuations in narrowband gamma spectral power in both the motor cortex and subthalamic nucleus correlate to fluctuations in continuous metrics of dyskinesia with minimal time lag.

METHODS

Subject Selection and Assessment

The institutional review board approved the study protocol and we registered the study on clinicaltrials.gov (NCT03582891) under a physician-sponsored investigational device exemption for Medtronic's Summit RC+S (G180097/R003). We collected data from 16 subjects with Parkinson's disease implanted with an investigational bidirectional neural interface, Summit RC+S (Medtronic Inc., Minneapolis, MN, USA), designed for chronic sensing of field potentials during activities of daily living [9]. We attached depth leads to the device in either the subthalamic nucleus (11 subjects) or globus pallidus (five subjects) and paddle-type leads placed subdurally

over precentral and postcentral gyri [7]. Data from the first five subjects have been published previously in an unrelated analysis that did not specifically address dyskinesias [7]. We recruited participants from the movement disorders surgery clinic at the University of California, San Francisco in accordance with the Declaration of Helsinki. Inclusion criteria were a diagnosis of idiopathic Parkinson's disease by a movement disorders neurologist and standard clinical indications for subthalamic nucleus or globus pallidus deep brain stimulation [10-11]. Exclusion criteria were significant cognitive impairment as determined by a Montreal Cognitive Assessment score of 20 or lower or an untreated mood disorder as evaluated by a neuropsychologist. A movement disorders specialist evaluated baseline motor function prior to implantation using the Movement Disorder Society revision of the Unified Parkinson's Disease Rating Scale part III in the off- and on-medication states. The off-medication state is 12 hours after withdrawal of antiparkinsonian medication, and the on-medication state is 30-45 minutes after a supratherapeutic dose of carbidopa-levodopa. We characterized the baseline severity of dyskinesia in daily life using UPDRS IVa 4.1 (time spent with dyskinesia). We determined whether motor signs in one hemibody were more severe than the other using UPDRS III off-medication scores for rigidity, bradykinesia, and tremor in each limb.

Surgical implantation

We implanted all subjects with quadripolar cylindrical leads in either the subthalamic nucleus (Medtronic 3389 lead) or globus pallidus (Medtronic 3387 lead), consisting of 1.5 mm or 3 mm intercontact spacing, respectively, and quadripolar paddle-type cortical leads (10 mm intercontact spacing) using methods previously described (**Figure 2.1A**) [7,12]. The surgeon placed cortical leads along a parasagittal trajectory such that either two or three contacts were anterior to the central sulcus, 2-4 cm from the midline. We confirmed electrode localization intraoperatively using cone beam CT (Medtronic O-arm) [13] fused to preoperative MRI (**Figure 2.1B**). For each

implanted hemisphere, we connected brain leads to a Medtronic Summit RC+S interface (model B35300R) in the ipsilateral pectoral area via 60 cm lead extenders (model 37087). We covered the connection between the lead extender and implantable pulse generator (Summit RC+S) with medical adhesive to reduce leakage of the electrocardiogram signal into neural recordings [14].

Precise anatomic electrode localization was refined post-hoc using established image analysis pipelines for deep brain stimulation [15] and cortical electrodes [16]. Briefly, we coregistered post-implantation high-resolution CT images using a rigid, linear affine transformation and resliced into a preoperative T1-weighted 3T MRI [17]. We verified placement by visual inspection and, when necessary, implemented an additional brain shift correction to refine subcortical anatomy coregistration [18]. Then, we localized electrodes to CT artefacts. Lastly, we applied an additional surface projection correction [19]. to localize cortical leads to the MRI-rendered pial surface [17]. For group analyses, we normalized electrode locations into Montreal Neurological Institute space [17] and visualized either on the FreeSurfer average cortical surface [20] (**Figure 2.1D**) or a standardized Parkinson's disease-specific subcortical atlas (**Figure 2.1E**) [21].

Signal Recording

Neural

We analyzed intracranial sensorimotor cortical and basal ganglia field potentials from subjects with chronically implanted cortical paddles and depth leads in the home environment while engaging in activities of daily living. Recordings were completed more than one week after implantation, before initiating therapeutic deep brain stimulation one month after implantation, and for recording durations of at least eight hours per hemisphere. For cortical recordings in subjects 1-5, we configured overlapping bipolar recording channels (contacts 1-3 and 2-4) and configured all subsequent subjects with non-overlapping bipolar recording channels (contacts 1-2 and 3-4).

For the non-overlapping recording channels from the cortical site, the recording configuration from contacts 1-2 sampled the precentral gyrus, while the recording configuration from contacts 3-4 sampled the postcentral gyrus. For depth leads, we configured subthalamic-implanted subjects with overlapping recording channels and pallidal-implanted subjects with non-overlapping recording channels (**Figure 2.1C**). Subjects streamed neural data from the Summit RC+S interface to a Microsoft Windows tablet using a custom-made graphical user interface on the device's application program made available by Medtronic Inc (all software is compliant with FDA code CFR 820.30 and accessible at https:// openmind-consortium. github. io) [7]. Subjects with bilateral implants streamed data from both hemispheres simultaneously. Each RC+S streamed potentials in the time domain from two channels per cortical paddle at a sampling rate of 250 or 500 Hz. The device enables up to 30 hours of continuous recording prior to recharging.

Wearable

Subjects streamed neural data at home while wearing Global Kinetics PTY LTD Personal KinetiGraph® (PKG®) monitors [22-23] on both wrists during normal daily activities while on their preoperative dose of antiparkinsonian medication (**Table 2.1**). This wearable device provides continuous tremor, bradykinesia, and dyskinesia scores in two-minute intervals using a three-axis accelerometer and a proprietary, validated commercial algorithm [24]. Each wearable device records data for a maximum of nine days before requiring an additional charge. We removed outliers from the wearable data by excluding all values more than four standard deviations from each subject's mean score, a standard practice for large datasets [25]. While PKG® scores have been clinically validated with respect to UPDRS ratings [26], we performed additional validation within our data, showing a correlation of averaged wearable dyskinesia scores and UPDRS IV ratings of ρ=0.51 (P=0.004, **Supplementary Figure 2.8A**). The relationship between averaged

wearable dyskinesia scores and UPDRS IV ratings suggests that these scores can approximate involuntary hyperkinetic movement, versus primarily normal voluntary movement.

Signal Processing

Neural

We first derived timestamps for field potentials and reformatted cortical and basal ganglia field potentials from the RC+S system using a validated open-source toolbox in MATLAB R2019b [27]. For subjects with recordings containing multiple channel configurations, we processed the channel configuration with the longest recorded data to increase the dyskinetic fluctuations during recordings (for subject-specific channel configurations, see Signal Recording – Neural, **Figure 2.1C** description). Then, we downsampled the potentials to 250 Hz and calculated the power spectral density for each channel in non-overlapping two-minute intervals using the *Welch* method (Python 3.8.3 *SciPy* package) [28]. We used non-overlapping *Hann* windows of 256 data points per fast *Fourier* transform for the cortical (**Figure 2.1F**) and subcortical (**Figure 2.1H**) channels.

Power spectra from all two-minute epochs were overlaid for each channel and processed to identify narrow band peaks within a frequency band of interest (65-90 Hz for narrowband gamma). Given the temporal variability of peak presence and dyskinesia in this large dataset, we employed three steps to increase the signal-to-noise ratio and focus on epochs with high oscillatory activity. First, we flattened the spectra by removing the aperiodic component from all two-minute epochs using the Fitting Oscillations and One-Over-F (FOOOF) algorithm [29]. Second, we defined the peak frequency oscillation as the most commonly occurring frequency (within the frequency band of interest) with maximum spectral power (at least two standard deviations above the mean at 65 Hz) across all epochs (**Supplementary Figure 2.7A**). A single peak frequency was used for all data epochs from a given recording site and hemisphere but was individualized across hemispheres, recording sites within a hemisphere, and frequency bands within a recording site.

Additional analyses regarding the variability of peak gamma frequency across epochs within a subject hemisphere can be found in the intra-subject hemisphere variability section of the Supplementary material. We used the 65 Hz frequency as a baseline because even after removing aperiodic activity, lower frequency activity may exhibit higher power values. Third, we defined epochs as containing oscillatory signals if the peak frequency power was at least two standard deviations above the mean peak frequency power. We included all visually detectable FOOOF peaks in the unflattened overlaid power spectra (when identifying narrow band peaks using the low-gamma frequency band, some FOOOF peaks detected were broadband gamma, not narrowband peaks).

To generate summary statistics for the oscillatory signal, we defined an integrated narrowband gamma score that considers not only the power but also the temporal duration of the oscillation. To do this, we averaged the power spectral densities for all epochs that met the criteria for having an oscillatory peak and multiplied this by the percentage of the recording time during which the oscillation was present. For each electrode (two channels per electrode), we defined the dominant channel as having the largest integrated narrowband gamma score. The dominant channel was defined independently for each spectral power band. For comparisons of spectral power to wearable scores, we used the peak frequency of the dominant channel as determined from flattened spectra (as in Figure 2.1G and 2.1I), with the amplitude of that frequency in the unflattened, log scaled power spectra (as in Figure 2.1F and 2.1H) for each subject hemisphere, since the latter is more relevant for evaluation of these signals in adaptive deep brain stimulation.

Lastly, we characterized narrowband gamma coherence using Python's *SciPy* package [28] between the recording site with the maximal integrated narrowband gamma score and the two channels from the remaining recording site **(Figure 2.1J)**. Then, we determined the dominant

paired channels as those with the largest integrated narrowband gamma score using the above methods. We also visually observed distinct low gamma spectral peaks (40-60 Hz) in three subjects and thus employed these methods to characterize low gamma cortical (**Figure 2.6A-B**) and subcortical (**Figure 2.6C-D**) oscillations.

Wearable

Wearable dyskinesia and tremor scores were labeled such that higher scores indicated more severe motor signs. We transformed wearable bradykinesia scores from negative to positive values, such that higher scores also indicated more severe motor signs. Next, we removed data from periods of sleep using immobility as a surrogate marker, defined as two or more minutes with a bradykinesia score greater than 80 [30].

Time-alignment

To align neural and wearable data, we set the wearable devices to computer clock time as determined by the network time protocol. We used computer clock timestamps from the neural data stream. To verify synchronization, we compared the root-mean-square voltage of the built-in internal accelerometer of the RC+S to the wearable accelerometer across synchronized timestamps in a subset of five subjects [7].

Statistics

We used modules in Python for our statistical analyses. We measured time series correlations using *Spearman's* statistics as the default statistic, as this measure is robust to outliers. For correlations across aggregate/non-continuous measures, we used *Pearson's* statistics in the *SciPy* statistics module [28]. To visually compare time series data between neural and wearable datasets of a subject hemisphere and the contralateral wrist, we rescaled each signal using minimum-maximum normalization from the *sklearn* module [31] onto a common scale.

Normalization is standard practice for variables with large differences in scale. It does not impact statistical tests that do not rely on distance measures between examples (such as *Spearman* or *Pearson* statistics) [25]. For linear regression analysis, we used the *sklearn* package. We split data into an 80/20 ratio of training and testing subsets. Utilizing the training subset, we trained a linear regression model and calculated the correlation coefficient (*r*) between the predicted and actual dependent variable from the testing subset. For cross-validation, we re-generated the data split ratio five times across non-overlapping epochs of the data. Then, we averaged all statistics across each split.

We corrected all *P*-values for multiple comparisons within each subject hemisphere using false discovery rate correction in the *statsmodel* statistics multitest module [32]. We assessed effect size using *Cohen's d* statistic with the built-in statistics module. We compared distributions of gamma-wearable correlations across neural sites and wearable motor signs using *one-way ANOVA* tests. We assessed normality in each distribution with the *Shapiro* normality test from the *SciPy* statistics module. We used *t-tests* to compare distributions that did meet the criteria for normality and the *Mann-Whitney U test* for distributions that did not. We averaged the integrated gamma scores across hemispheres for clinical measures available at the subject but not the hemibody level. To determine the total hours recorded, we summed the hemisphere with the maximal recorded configuration of each subject.

Outlier values may influence standard linear correlation techniques. Thus, in addition to using *Spearman's* coefficient, we use another stratification method, described below, to assess the relationship between narrowband gamma activity and dyskinesia within individual subjects. We transformed the wearable dyskinesia numerical output to have discrete ordinal labels [25]. We binned the dyskinesia scores from bins 0-3 in an exponential manner, such that each consecutive

bin contains half the amount of values as the previous bin, to mimic the duration of time subjects experience dyskinesia theoretically. Bin 4 contains all the remaining values. The ordinal bin with a label of 0 corresponds to the lowest 50th percentile of dyskinesia scores, with each consecutive label containing the remaining lowest 50th percentile of scores such that bin 0 contains percentiles 0-50, bin 1 contains percentiles 51-75, bin 2 contains percentiles 76-87.5, bin 3 contains percentiles 87.6-93.75, and bin 4 contains percentiles 93.76-100. We compared differences in narrowband gamma power for each subject hemisphere across paired sets of binned wearable dyskinesia scores (0-1, 1-2, 2-3, 3-4) with *t-tests* in the *SciPy* statistics module [28]. We excluded subjects without a clinical history of dyskinesia using UPDRS part IVa scores in data visualization for **Figures 2.3-5** (*n*=4).

RESULTS

Subject characteristics

We implanted 30 hemispheres from 16 subjects with Parkinson's disease with cortical and basal ganglia leads (2/16 female, mean age at surgery 57±12 years). Subject demographics are in **Table 2.1**. Twelve subjects had a clinical history of dyskinesia (UPDRS IVa dyskinesia score>0), 10 of whom had implants in the subthalamic nucleus. In the off-medication state, 15 subjects had mild to moderate tremor scores in at least one limb (MDS-UPDRS III 15–17), and all subjects had non-zero bradykinesia scores in all limbs (MDS–UPDRS III 4–9, 14, recorded in the off-medication state).

Narrowband gamma oscillations across subjects: characteristics and relationship to the clinical history of dyskinesia

We defined the presence of narrowband gamma at the hemisphere level by inspecting each two-minute flattened power spectral density epoch for spectral power greater than two standard

deviations above the 1/*f* background (see methods, **Figure 2.1G, 2.1I**). Cortical narrowband gamma was present in 20/30 hemispheres (13/16 subjects), and subthalamic narrowband gamma was present in 13/22 hemispheres and one or both hemispheres of 8/11 subjects (**Table 2.2**). None of the five subjects with pallidal depth leads met the criteria for subcortical narrowband gamma; thus all subsequent analyses of subcortical activity utilized only subthalamic recordings.

Frequency distribution and anatomic localization

We visualized the distribution of cortical and subthalamic narrowband gamma peak frequencies between 65-90 Hz (**Figure 2.2A**). Subject hemispheres with cortical and subthalamic oscillations (*n*=11) tended to have similar peak frequencies across sites, with a median frequency peak absolute difference of 1 Hz between the cortical and subthalamic sites (**Figure 2.2B)**.

All cortical electrode arrays spanned the precentral gyrus, with at least one contact over the postcentral gyrus. For later subjects in the protocol, the central sulcus was used as the midpoint of cortical quadripolar arrays. For these subjects, we recorded cortical field potentials using non-overlapping bipolar montages (**Figure 2.1C**) to distinguish oscillatory activity in the precentral versus postcentral gyrus. Narrowband gamma localized to the precentral gyrus in all 13 hemispheres with narrowband gamma and non-overlapping bipolar montages.

Relation to clinical history of dyskinesia

Here, we report subject-level metrics because clinical dyskinesia scores were available at the level of the subject but not the hemisphere. We defined subjects as having narrowband gamma if the signal was present in one or both hemispheres. Of the subjects who met the criteria for dyskinesia preoperatively (UPDRS IVa score>0), cortical narrowband gamma was present in 17/23 hemispheres (*n*=11/12 subjects), and subthalamic narrowband gamma was present in

13/20 hemispheres (*n*=8/10 subjects). Of the subjects who did *not* meet the clinical criteria for dyskinesia, cortical narrowband gamma was present in *n*=2/4 subjects. Subthalamic narrowband gamma was absent in the subject who did not meet the clinical criteria for dyskinesia (**Figure 2.2C**). The observed patterns among the subjects suggest narrowband gamma oscillations in the motor network likely occur in subjects with a clinical history of dyskinesia, though this comparison was underpowered for formal statistical analysis. Additionally, the mean integrated gamma scores were smaller in hemispheres of subjects without a clinical history of dyskinesia than in subjects with a clinical history of dyskinesia at the cortical (t=2.15, P=0.046) and subthalamic (t=3.25, P=0.007) sites (**Supplementary Figure 2.8B**). These results show that narrowband gamma differs between subjects as a function of the presence or absence of dyskinesia. To further investigate whether the lack of narrowband gamma in some patients with a history of dyskinesia may be due to electrode placement, we also plotted anatomic coordinates of cortical leads segregated by presence or absence of narrowband gamma, and did not find a systematic difference (**Supplementary Figure 2.8C**).

Spectral power of narrowband gamma oscillations correlates to wearable dyskinesia scores

We examined the relationship between fluctuations in narrowband gamma power and fluctuations in continuous dyskinesia scores from the contralateral wearable device for each hemisphere of subjects with non-zero UPDRS dyskinesia preoperative scores. Examples of the narrowband gamma and dyskinesia time series are shown in **Figure 2.3A**. Cortical narrowband gamma, subthalamic narrowband gamma, and narrowband gamma coherence between the two sites correlated to the wearable dyskinesia signal (false discovery rate-corrected P<0.05) in 15/17, 12/13, and 11/13 hemispheres (**Figure 2.3B**).

Correlations between narrowband gamma oscillations and wearable dyskinesia scores yielded mean correlation coefficients of ρ=0.48 for the motor cortex, ρ=0.53 for the subthalamic nucleus, and ρ=0.31 for subthalamic-motor cortex coherence. Each correlation was significant using a *one-sample t-test*, with P<0.005. The distributions differed across sites (F=5.11, P=0.01, **Figure 2.3C**) and were driven by differences between coherence and cortical distributions (F=2.39, P=0.02) and coherence and subthalamic distributions (F=2.83, P=0.009). However, cortical and subthalamic distributions did not differ (t=0.73, P=0.47), indicating narrowband gamma oscillations at multiple sites in the motor network have similar predictive power for the occurrence of dyskinesia in a group-level analysis. Narrowband gamma fluctuations were anticorrelated with bradykinesia scores at the cortical (**Supplementary Figure 2.11**) and subthalamic (**Supplementary Figure 2.12**) sites. Narrowband gamma fluctuations were also anticorrelated with tremor scores but relatively less than with bradykinesia scores.

Power distribution of correlated narrowband gamma signal

Electrocorticography field potential recordings generally have a higher signal spectral power than local field potentials from subcortical structures [12]. To assess their relative spectral power in the narrowband gamma ranges, we compared the average peak narrowband gamma spectral power across the 15 cortical and 12 subthalamic sites of the subject hemispheres with correlated narrowband gamma signals and a history of clinical dyskinesia. The spectral power of the narrowband gamma oscillations was not significantly different across sites when comparing spectral power after normalization to the 1/f baseline (t=1.05, P=0.30, **Figure 2.3D**). However, spectral power comparisons for absolute spectral power values (not normalized to baseline 1/f) showed a greater spectral power in the cortex, consistent with its generally higher 1/f baseline (**Supplementary Figure 2.10**).

Time-lag comparison of narrowband gamma correlation distributions

To assess whether variations in narrowband gamma oscillations led or lagged the variations in dyskinesia scores, we compared correlations at various sample lags up to ± 10 data points (20 minutes) lag time (**Figure 2.3E**). For the cortical narrowband gamma lag analysis, the median maximal correlation occurred at a sample lag of zero, indicating simultaneity with dyskinesia scores (within the temporal resolution of two minutes). For the subthalamic narrowband gamma lag analysis, the median maximal correlation occurred at a sample lag of -1. We assessed the significance of this apparent sample lag by comparing the distributions of sample lags at -1 with those for zero (simultaneous occurrence). The increased occurrence at a sample lag of -1 compared to zero (no lag) approached significance (χ^2=3.0, p=0.08) (**Figure 2.3F**). This indicates that fluctuations in narrowband gamma oscillations occur at the same time as, or slightly precede, fluctuations in dyskinesia scores within the two-minute resolution available in wearable scores.

Stratification analysis shows outliers do not drive correlations

Correlations can be driven by outliers, for example, when dyskinesia scores are in the bottom 10th percentile. Thus, a correlation is insufficient to demonstrate whether narrowband gamma fluctuates as a function of dyskinesia over a wide range of severity versus indexing mainly the presence or absence of dyskinesia. To control for this possibility, we binned the continuous dyskinesia scores into ordinal bins (**Figure 2.4A**, **2.4D**, dashed horizontal lines) and compared narrowband gamma across the paired, ordinal bins in single subjects with cortical (**Figure 2.4B**) and subthalamic (**Figure 2.4E**) narrowband gamma oscillations. We confirmed that narrowband gamma between paired ordinal bins of dyskinesia scores differed across subjects. Differences in narrowband gamma comparisons across paired ordinal bins remained significant (P<0.05) with consistent effect sizes at cortical (**Figure 2.4C**) and subthalamic (**Figure 2.4F**) sites. These relationships indicate that gamma-band oscillations scale with dyskinesia scores over a wide range of severity.

In the absence of neurostimulation, dyskinesias can only occur during on-medication states, so assessing whether narrowband gamma is more predictive of the dyskinetic state compared to the on-medication state without dyskinesia is important. First, we removed all data collected during off-medication states, which we defined as the top 70th percentile of bradykinesia scores within subjects. Then, we stratified narrowband gamma oscillations from the remaining on-medication state data into three categories: non-dyskinetic (bottom 30th percentile dyskinesia scores within subjects), dyskinetic (top 30th percentile), and transitional (middle 40th percentile) at both cortical (**Figure 2.4G**) and subthalamic (**Figure 2.4I**) sites. Comparisons showed dyskinetic on-states had higher narrowband gamma spectral power than non-dyskinetic on-states in 11/17 and 10/13 subject hemispheres at cortical and subthalamic sites, respectively, with $P<0.05$. Average *t*-statistics and *Cohen's d* values were 3.77 and 1.14 at cortical (**Figure 2.4H**) and 4.22 and 1.12 at subthalamic (**Figure 2.4J**) locations. Comparisons between the binned dyskinesia categories generated from the entire set of wearable scores (**Figure 2.4C, 2.4F**) and the clinical subdomain categories (**Figure 2.4G, Figure 2.4I**) can be found in Supplementary Figure 2.13.

Relation of narrowband gamma to normal voluntary movement

We collected wearable dyskinesia scores across our subject cohort, regardless of whether subjects had a history of dyskinesia. In two subjects without a clinical history of dyskinesia but who exhibited cortical narrowband gamma (subject 7 left and subject 11 right hemispheres), the correlation coefficients between wearable dyskinesia scores and cortical narrowband gamma were significantly positive, with $\rho=0.02$ and $\rho=0.16$, respectively (mean integrated narrowband gamma score of 0.036, versus 0.113 in subjects with a history of dyskinesia). This suggests that (1) the dyskinesia monitor may generate non-zero dyskinesia scores from normal voluntary

movement and (2) narrowband gamma may also correlate with normal movement, consistent with its prokinetic function.

Relation of other frequencies to dyskinesia and use of multiple bands to predict dyskinesia

Subthalamic theta (4-10 Hz) oscillations have also been implicated in the pathophysiology of dyskinesia [8]. On the cortical level, this relationship has not been investigated, but the spectral overlap of the subthalamic 4-10 Hz activity with the mu-rhythm (8-12 Hz) that is suppressed with movement and is less modulated in PD may suggest an inverse relationship [33]. The majority of subjects had theta/mu oscillations (*n*=10/16 subjects, cortical and subcortical site), regardless of a clinical history of dyskinesia (*n*=3/4 subjects without dyskinesia, cortical and subcortical site) (**Figure 2.5A**). We processed these theta peaks using the same methods as for narrowband gamma, but with 4 Hz as the baseline spectral power and the use of flattened spectra to remove noise artifact in lower frequency bands. Then, we compared the absolute values of theta-dyskinesia and gamma-dyskinesia correlations (**Figure 2.5B**), and found narrowband gamma was a stronger correlate than theta at the cortical (**Figure 2.5B**) and subthalamic (**Figure 2.5C**) sites, with $P<0.05$.

Since subthalamic beta oscillations (13-30 Hz) are a known off-state neural biomarker and cortical beta oscillations are reduced by movement, we expect beta band oscillations would anticorrelate with dyskinesia scores. Therefore, we examined the absolute value of correlations between beta oscillations (using 13 Hz as the baseline spectral power and using flattened spectra) and dyskinesia. We found the absolute correlations of narrowband gamma oscillations and dyskinesia scores were comparable at the cortical and (**Figure 2.5B**) subthalamic (**Figure 2.5C**) sites.

This raises the possibility that incorporating beta, theta, and narrowband gamma as independent variables in a model could increase the predictive power for dyskinesia. We therefore compared the model's predictive power (*r*) across linear regression models with either narrowband gamma alone, the combination of narrowband gamma and beta, or the combination of all three rhythms as predictors. The inclusion of additional frequencies in a linear model did not significantly improve the predictive power for dyskinesia at the cortical (**Figure 2.5D**) or subthalamic (**Figure 2.5E**) sites at the group level.

However, within individual subject hemispheres, there were two cortical and four subthalamic recording sites for which predictive power for dyskinesia scores increased by more than 5% when adding beta and gamma as independent variables, versus solely gamma, to the linear regression model. As a visual aid to understanding the regression results, we generated scatterplots of beta versus gamma peak frequency power for each two-minute epoch with dyskinesia severity represented by color intensity (**Figure 2.5 F–G**). In an example subject hemisphere for which beta band activity provided additional predictive power (**Figure 2.5F**), one can see that for a constant level of prokinetic gamma (dotted line), the spectral power of beta influences the occurrence of dyskinesia. The distributions of spectral power for beta and gamma oscillations are also provided (**Figure 2.5 F–G**) to show that these distributions can be either relatively continuous (gamma) or binary (beta) in nature, behaving as either “dimmer” switches or “binary on/off” switches, respectively.

A distinct 40-60 Hz oscillation in some subjects

We noticed a distinct oscillation at 40-60 Hz, with a relatively broad spectral peak, in three subjects. We describe these as “low gamma oscillations” to distinguish them from the more classic narrowband 65-90 Hz oscillations and quantify their correlations with dyskinesia scores using the

same methods as for narrowband gamma (**Supplementary Table 2.3**, **Figure 2.6**). These oscillations occurred in the cortex, subthalamic nucleus, or both sites in some subjects with a clinical history of dyskinesia (**Figure 2.6G**). Low gamma oscillations differed from classical narrowband gamma oscillations not only in their frequency distribution (**Figure 2.6E**), spectral peak width (**Figure 2.6 A-D**), and variation in peak frequency across sites (**Figure 2.6F**), but also in their relationship to dyskinesia scores. In contrast to the positive correlations between subthalamic low gamma power and contralateral dyskinesia scores, cortical low gamma spectral power was anticorrelated with contralateral dyskinesia scores (**Figure 2.6H, I**). The sample lag between dyskinesia and oscillatory activity was not distinguishable from zero (no lag) (**Figure 2.6J, K**).

DISCUSSION

We investigated the relationship between narrowband gamma oscillations and dyskinesia in subjects with Parkinson's disease using a sensing-enabled neurostimulator in conjunction with a wearable monitor providing continuous dyskinesia scores. We analyzed 984 hours of neural recordings from both sensorimotor cortex and basal ganglia nuclei in 16 individuals during normal daily activities on their usual dose of dopaminergic medications prior to initiating therapeutic stimulation. Both subthalamic and cortical narrowband gamma as well as intersite coherence correlated with dyskinesia scores with a minimal time lag. However, in individual cases, one site often exhibited a greater prediction accuracy than the other.

The physiologic role of narrowband gamma oscillations

Narrowband oscillatory activity in the 40-90 Hz range is a ubiquitous feature of healthy cortical function. It has been studied extensively in rodents and nonhuman primates, though mainly in networks unrelated to motor function [34]. This activity is thought to arise from rhythmic interactions between excitatory neurons and inhibitory interneurons. Gamma band oscillations dominate in the second and third layers of the neocortex and are thought to reflect "bottom-up" sensory input. Throughout the neocortex, gamma oscillations anticorrelate with alpha/beta oscillations, which dominate in layers five and six and are thought to reflect "top-down" cognitive control [35].

Narrowband gamma in the motor cortex has not been directly observed outside of disease states or disease models. Nevertheless, a potential role of motor network gamma oscillations in normal movement should be considered. The small, but significant, correlation between peak gamma spectral power and dyskinesia scores in our two subjects without a clinical history of dyskinesia can be interpreted in several ways. It is possible that the continuous dyskinesia monitors are more sensitive than the UPDRS assessment, and thus, narrowband gamma signals in these subjects

indicate subclinical dyskinesia. Alternatively, the dyskinesia monitor may score some patterns of normal voluntary movement as dyskinesias. If so, narrowband gamma oscillations may be tracking voluntary movement in patients without a clinical history of dyskinesia. Consistent with this, prior studies in Parkinson's disease patients in the on-medication state show scaling of subthalamic gamma oscillations with the velocity of normal movement during cued movement tasks [36-37].

It is important to distinguish narrowband gamma, an oscillatory rhythm, from broadband gamma activity (sometimes referred to as "high gamma"). Movement-related broadband gamma increases are often apparent at 50-200 Hz frequencies in the sensorimotor cortex during movement initiation [38]. They are related to local cortical activation and likely reflect asynchronous underlying spiking activity rather than a narrowband oscillatory rhythm [39].

Models of dyskinesia genesis

The primary clinically effective therapies for Parkinson's disease, including dopaminergic medication [2], deep brain stimulation [6], and pallidal thermolesion [40], all induce narrowband gamma oscillations and reduce beta oscillations at various nodes of the motor network. These observations have led to the hypothesis that in the context of Parkinson's disease, gamma and beta oscillations serve as "prokinetic" and "antikinetic" rhythms, respectively, and that therapeutic interventions rebalance their relative contributions to provide a more normokinetic state. Our results generally support the hypothesis that an *excess* of narrowband gamma oscillations creates a hyperkinetic movement state [6, 40]. However, in some subjects (**Figure 2.5F**), beta activity can also influence dyskinesia severity independently of gamma band activity, supporting a model in which the *balance* between prokinetic and antikinetic frequencies is important in dyskinesia genesis.

Whether narrowband gamma oscillations cause dyskinesia or are simply a physiological correlate is not yet clear. Many experiments have investigated narrowband gamma oscillations in the 6-hydroxydopamine-treated rodent model of Parkinson's disease [3-5], where experimental interventions to probe causality are more readily performed than in humans. In this model, the induction of dyskinesia by administration of levodopa or dopamine agonists was associated with the simultaneous emergence of pathological gamma-band oscillations in the cortico-basal ganglia-thalamic circuitry. The suppression of cortical gamma oscillations by administration of topical dopamine antagonists also immediately eradicated dyskinesia, suggesting a causal relationship. Nevertheless, the mechanistic link between the dopamine-depleted, levodopa-treated state and the emergence of abnormal "prokinetic" oscillations has not been established.

Other physiological models for the generation of dyskinesia have also been proposed. Mouse optogenetic studies suggest a model that attributes dyskinesia to abnormal firing rates of specific populations of neurons in the basal ganglia, particularly within the striatum [41-42]. In this model, dyskinesia is thought to originate from the excessive activation of a subpopulation of D1-positive, direct pathway striatal neurons. A strength of the neuronal firing rate model is that it offers a specific cellular basis for dyskinesia, which can be directly manipulated using optogenetics. However, when applied to humans, models based on abnormal firing rates in the basal ganglia-thalamocortical circuit have difficulty accounting for some important clinical phenomena. Interventions that reduce activity in the internal globus pallidus, such as reversible or irreversible lesioning, suppress rather than exacerbate dyskinesia [43]. A mechanistic neural model of dyskinesia that accounts for physiological and surgical observations across species has yet to be developed.

Gamma oscillations at other frequencies are functionally distinct

The existing literature on narrowband gamma in Parkinson's disease in animal models of parkinsonism has focused on oscillatory rhythms in the 65-90 Hz range. Gamma oscillations at other frequencies are likely functionally distinct in the motor network. High-frequency oscillations at 250-350 Hz have been described in both the subthalamic nucleus and globus pallidus. Their attributes may delineate the two current motor subtypes of Parkinson's disease, tremor dominant versus postural instability with gait disorder subtypes [44-45]. These oscillations increase during voluntary movements and with dopaminergic medication, indicating their potential role in normal basal ganglia function. However, these high-frequency signals, particularly in the globus pallidus, are more pronounced in a dopamine-depleted state, unlike 65-90 Hz narrowband gamma oscillations.

Furthermore, our study reveals the presence, in some subjects, of distinct oscillations in the gamma band at lower frequencies (40-60 Hz) than the classical narrowband gamma range. These low gamma rhythms do not show functional or temporal co-occurrence with 65-90 Hz narrowband gamma oscillations. While the spectral power of 65-90 Hz narrowband gamma correlates with dyskinesia (**Figure 2.3B**), the spectral power of cortical low gamma anticorrelates to dyskinesia (**Figure 2.6G**). The greater bandwidth of the low gamma power spectral density peak may also hint at a different underlying physiologic mechanism.

Narrowband gamma as a marker for closed-loop deep brain stimulation

Adaptive deep brain stimulation relies on neural signals to infer the subject's clinical state and auto-adjust stimulation parameters to meet changing brain needs [46]. A prospective closed-loop marker requires that signals be sensitive and specific to the pathological state, and time-locked to motor signs. The use of narrowband gamma as a control signal for adaptive deep brain stimulation with existing sensing-enabled neurostimulators has been demonstrated [47-48], and

the entrainment of gamma rhythms by therapeutic neurostimulation at a stable and predictable frequency (subharmonics of stimulation frequency) is an advantage for the use of this signal [49]. The present work supports the utility of narrowband gamma as a control signal for adaptive deep brain stimulation by showing that this rhythm correlates to symptom fluctuations across varying spectral power of dyskinesia with minimal temporal lag. Either the subthalamic nucleus or the motor cortex may serve as the site for signal detection since narrowband gamma spectral power at either site are roughly equal predictors of dyskinesia in a cross-subjects analysis. However, adaptive deep brain stimulation in Parkinson's disease may require sensing neural signals *during* active stimulation, and stimulation artefacts will likely interfere with subthalamic sensing more than cortical sensing. Of note, theta oscillations in the subthalamic nucleus have been shown to correlate to dyskinesia [50]. We replicated this finding but found that, unlike narrowband gamma, the relationship of theta band activity to dyskinesia relationship is not present in the motor cortex. Further, theta-alpha oscillations may be strongly affected by off-period tremor [51], limiting their utility as a control signal in adaptive deep brain stimulation.

Limitations

Although the analysis of the relationship between dyskinesia scores and gamma oscillations had high statistical power within subjects due to the long duration of recordings, the cross-subject correlations were underpowered due to the relatively small number of subjects, as is typical of invasive human studies. Subjects wore wearables on the wrist; therefore, the sensor captured upper body dyskinesia rather than leg dyskinesia. Additionally, dyskinetic motor signs on the contralateral side may influence the lateralized dyskinesia scores. The proprietary algorithm generating the dyskinesia scores used is not personalised to each subject [52] and is susceptible to false positives, as voluntary movement elicits a non-zero dyskinesia score. A similar gyroscope-based heuristic algorithm to classify tremor results in a false positive rate of 10% when tested on

healthy controls [53]. Future studies may benefit from personalised dyskinesia monitors that include lower as well as upper extremities for precise assessment.

Within the detection threshold employed here, we did not always detect narrowband gamma at cortical and subcortical sites in dyskinetic subjects. This may be due to limited spatial sampling using single quadripolar lead arrays at each site, which is a particularly important consideration for cortical recording since the precentral gyrus is both large and functionally heterogeneous [54]. Even within the motor territories of basal ganglia nuclei, electrophysiologic markers of motor signs in PD are known to differ in adjacent subregions [44, 55-57]. Further, we did not detect pallidal narrowband gamma – possibly because we were underpowered in our sample size, did not sample the relevant regions of the pallidum, or because narrowband gamma is not present in the pallidum. Prior findings of strong narrowband gamma coherence between pallidum and subthalamic nucleus in the on-medication state suggest that a larger sample of pallidal recordings might allow the detection of pallidal narrowband gamma [2, 37].

FIGURES

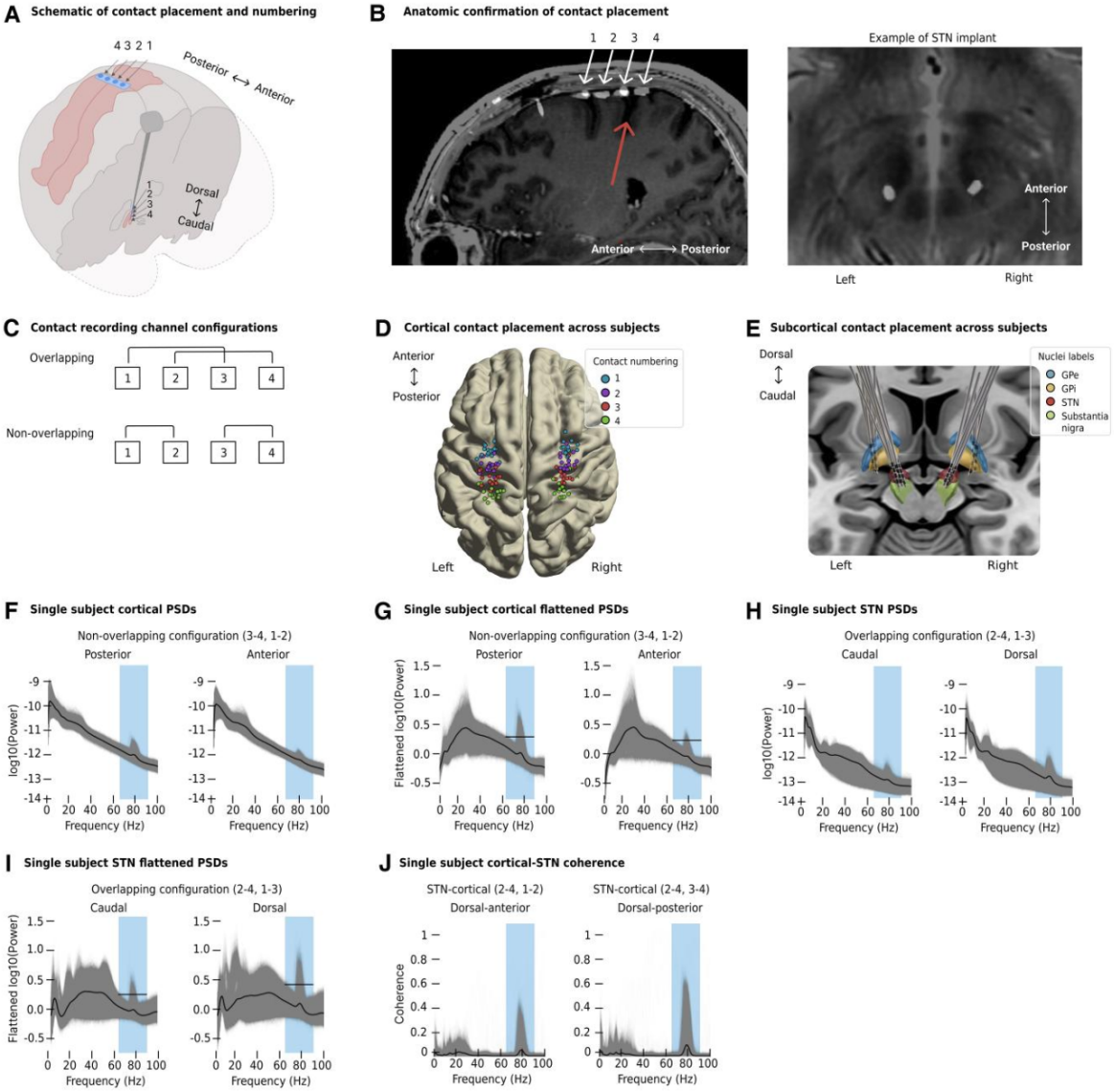

Fig. 2.1: Anatomic localization of recording contacts and data processing method. A) A schematic of the cortical paddle and subcortical depth lead locations (hardware shown on only one side for clarity), where each contact is labeled 1-4 (anterior-posterior for the cortical paddle, dorsal-caudal for the subcortical depth lead). B) An example of cortical (left column) and subthalamic (right column) leads in an individual subject (subject 1) on a parasagittal MRI (left column) and on an axial MRI at the level of the dorsal subthalamic nucleus (right column). The red arrow marks the central sulcus. C) Top, the overlapping bipolar recording configuration using contact pairs 1-3 and 2-4. For cortical recordings, this is the configuration used to record from subjects 1-5. For subcortical recordings, this is the configuration used to record from subthalamic-implanted subjects. Bottom, the non-overlapping bipolar recording configuration using contact pairs 1-2 and 3-4. For cortical recordings, this is the configuration used to record from subjects 6-16. For subcortical recordings, this is the configuration used to record from pallidal-implanted subjects. (Figure caption continued on the next page)

(Figure caption continued from the previous page) D) Cortical contact placement across subjects represented on a template brain. Each contact is labeled by color. E) Location of all subcortical depth leads represented on a template brain. F) Single subject example (subject 4, right hemisphere) of overlaid power spectral densities from the posterior (left) and anterior (right) recording configurations of the cortical paddle (log scaled) during everyday life at home. Each power spectral density line (grey) is derived from a two-minute recording length. The average power spectra is overlaid as the black line. The blue rectangle spanning 65-90 Hz denotes the signal frequencies that characterize narrowband gamma. G) Overlaid power spectral densities from panel F after removing aperiodic activity using FOOOF.[29] The flattened average power spectra is overlaid as the black line. The black horizontal line is the power threshold used to detect the peak narrowband gamma frequency. H) Example of overlaid power spectral densities from the caudal (left) and dorsal (right) recording configurations of the subthalamic lead using the same format as panel F. I) Overlaid power spectral densities from panel H after removing aperiodic activity using FOOOF, similar to panel G. J) The coherence between the channel with the maximum integrated gamma score (dorsal) and the two channels (anterior and posterior) from the remaining implant site (cortical).

GPe = globus pallidus external, GPi = globus pallidus internal, STN = subthalamic nucleus, NBG = narrowband gamma.

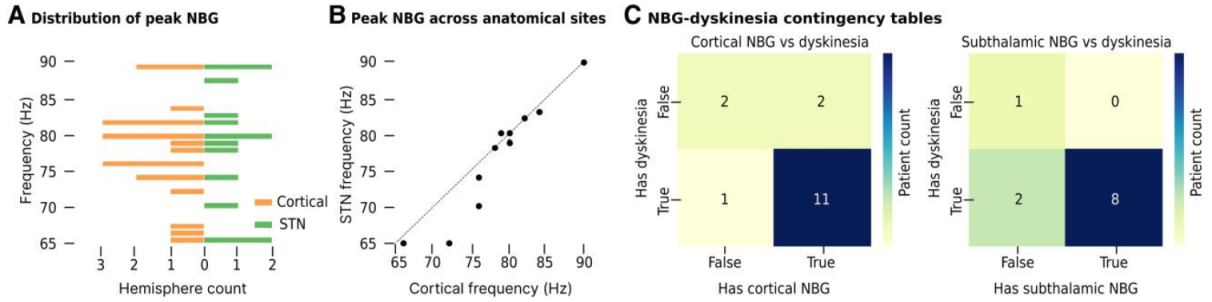

Fig. 2.2: Narrowband gamma oscillations across subjects: frequency distribution and relation to clinical history of dyskinesia.

A) The distribution of peak narrowband gamma frequencies in cortical (orange) and subthalamic (green) sites. B) A scatterplot of peak narrowband gamma frequencies across sites in subject hemispheres where narrowband gamma was recorded at both sites. The dotted line indicates where the frequency would be the same at both sites, serving as a visual aid for comparing the frequencies across sites. C) Contingency tables relating clinical history of dyskinesia with narrowband gamma for cortical (left) and subthalamic (right) electrode sites. Each data point represents a subject, where each subject was classified as exhibiting narrowband gamma if one or both hemispheres had narrowband gamma oscillations exceeding the detection threshold.

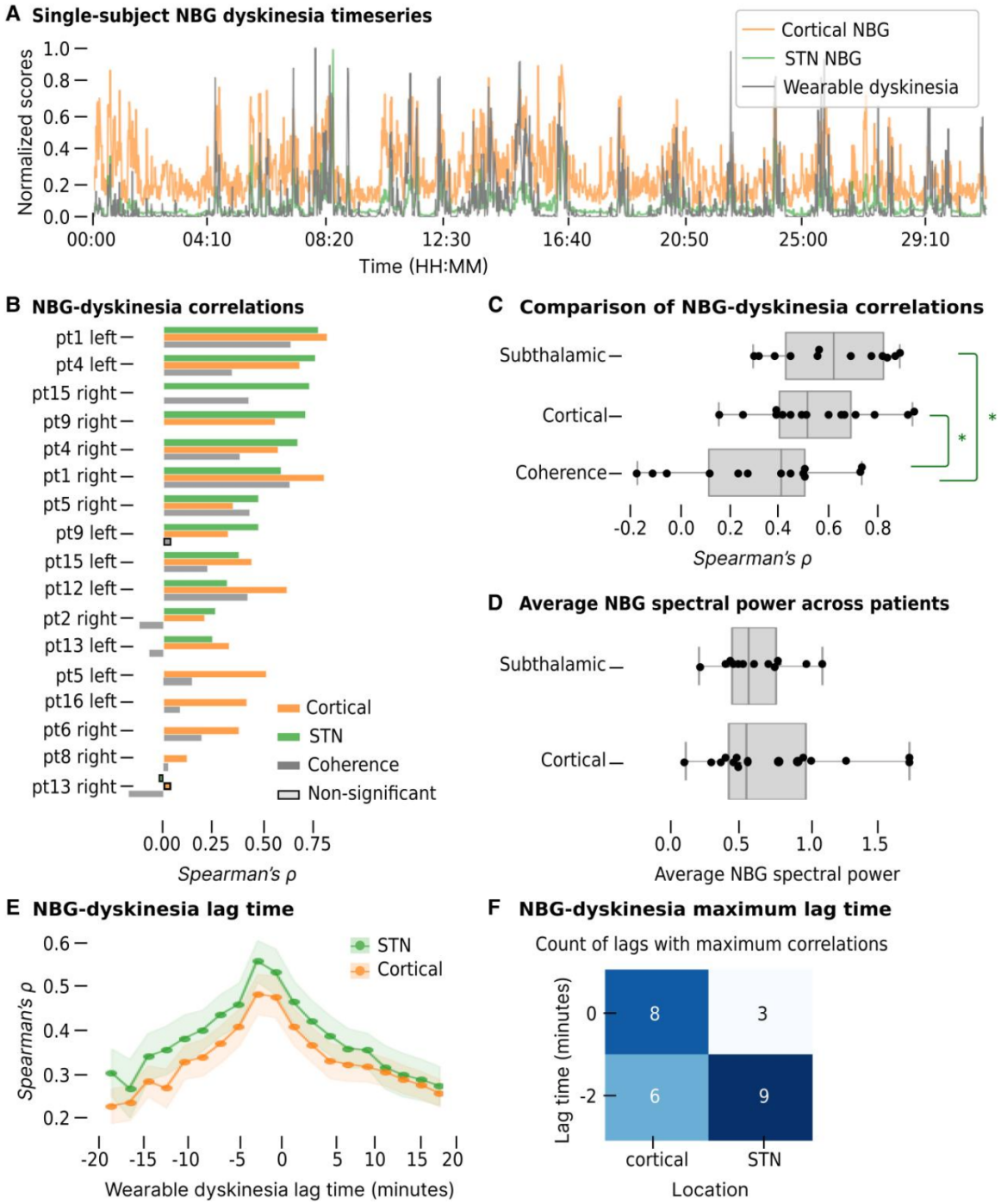

Fig. 2.3: Narrowband gamma correlates with simultaneous contralateral wearable dyskinesia scores.

A) Example of a time series of power at the peak frequency of the cortical narrowband gamma (orange) and subthalamic narrowband gamma (green) in comparison to the dyskinesia scores from the contralateral wearable devices (grey) of subject 4's left hemisphere. B) The correlations with false discovery rate-corrected $P<0.05$ between the time series narrowband gamma signal and wearable dyskinesia scores across our subject subcohort with a clinical history of dyskinesia. (Figure caption continued on the next page)

(Figure caption continued from the previous page) Green labels represent correlations from subthalamic narrowband gamma, orange labels represent correlations from cortical narrowband gamma, and grey labels represent correlations from narrowband gamma coherence between cortical and subthalamic electrode sites. C) Boxplots of correlation coefficients across subject hemispheres for subthalamic narrowband gamma, cortical narrowband gamma, and narrowband gamma coherence across the sites, showing higher correlation for single site spectral power than for intersite coherence. D) Boxplots of the average narrowband gamma spectral power (normalized to 1/*f* baseline) across hemispheres showing similar spectral power at cortical and subthalamic sites using an *independent t-test*. The signal spectral power also did not differ in a paired subset analysis of 10 subject hemispheres with both cortical and subthalamic narrowband gamma (t=1.43, P=0.19). E) Pearson correlation lag analysis illustrates the strength and direction of the correlation of each lag value. The maximum correlation showed an apparent negative lag of one sample (gamma leading dyskinesia by two minutes) for subthalamic nucleus (green line), but this did not meet statistical significance across subjects by chi-square testing of categorical sample lags across subjects, shown in panel F.

NBG = narrowband gamma, STN = subthalamic nucleus, FDR = false discovery rate

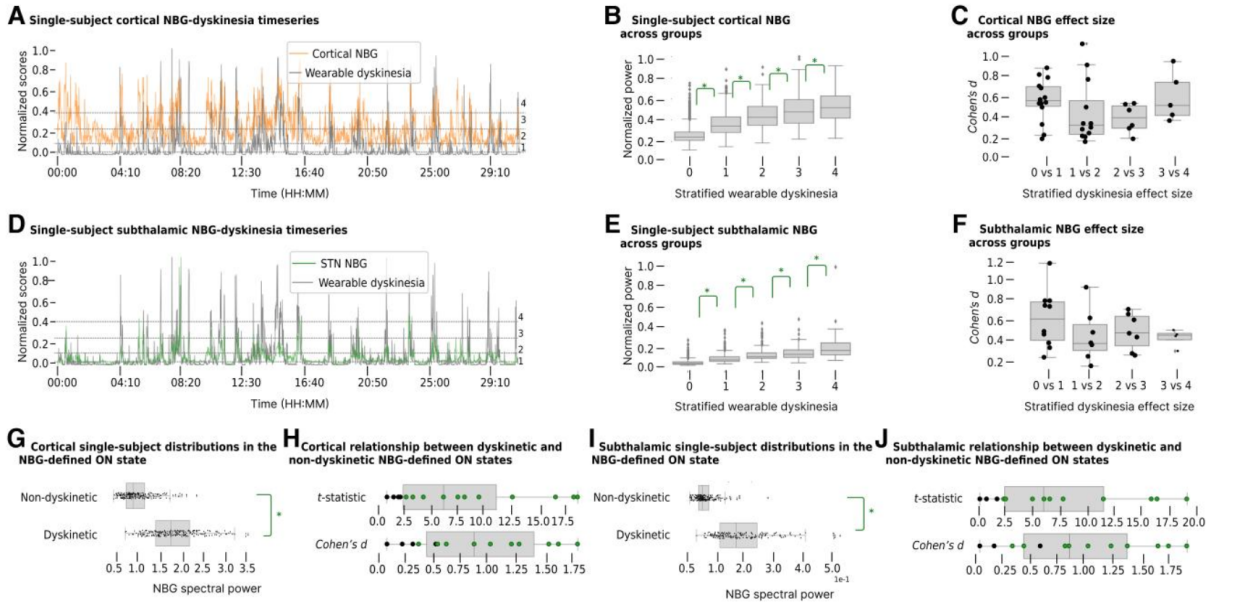

Fig. 2.4: Stratification analysis shows narrowband gamma-dyskinesia correlations are not driven by outliers.

Data are from subjects who have narrowband gamma oscillations at the specified site, as well as a clinical history of dyskinesia. A) Example time series of cortical narrowband gamma (orange) and dyskinesia scores (grey), derived from Figure 2.3A but with horizontal grey dotted lines that denote the thresholds used to bin the wearable dyskinesia scores. Bins are labelled 0, 1, 2, 3, 4. B) Single-subject example (subject 4, left hemisphere) showing the *t-test* comparison for cortical narrowband gamma between each paired, ordinal wearable dyskinesia category. C) The effect size using *Cohen's d* between cortical narrowband gamma of each ordinal pair of dyskinesia categories with false discovery rate-corrected $P<0.05$ across subjects. D) Example time series of subthalamic narrowband gamma (green) and dyskinesia scores (grey) derived from Figure 2.3A with the same structure as Figure 2.4A. E) A single-subject example (subject 4, left hemisphere) for subthalamic narrowband gamma, same format as Figure 2.4B. F) The effect size using *Cohen's d* between subthalamic narrowband gamma of each ordinal bin with false discovery rate-corrected $P<0.05$ across the cohort. G) A single-subject example from subject 4's left hemisphere shows the *t-test* comparison of cortical narrowband gamma between the non-dyskinetic and dyskinetic states. H) The significance and effect size for cortical narrowband gamma between the dyskinetic and non-dyskinetic states across subjects, with significant data points (false discovery rate-corrected $P<0.05$) denoted in green. I) A single-subject example (subject 4, left hemisphere) showing the *t-test* comparison for subthalamic narrowband gamma spectral power between the non-dyskinetic and dyskinetic states. J) The significance and effect size for subthalamic narrowband gamma between the dyskinetic and non-dyskinetic states across subjects, with significant data points (false discovery rate-corrected $P<0.05$) denoted in green.

The asterisk (*) denotes a comparison with false discovery rate-corrected $P<0.05$, NBG = narrowband gamma, STN = subthalamic nucleus

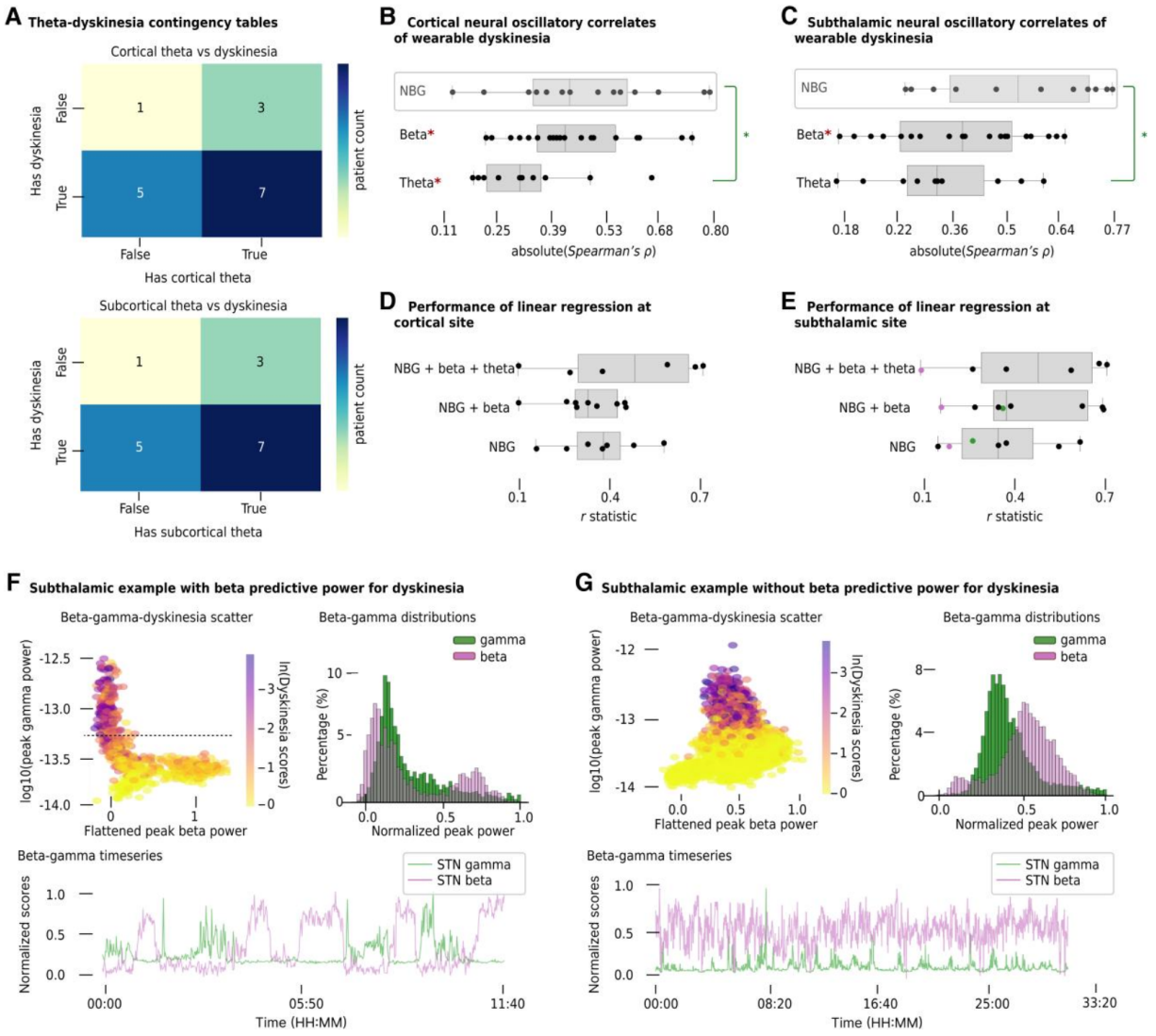

Fig. 2.5: Other neural correlates of dyskinesia.
A) Contingency tables relating a clinical history of dyskinesia with the presence of theta for cortical (left) and subthalamic (right) electrode sites, using the same format as Figure 2.2C.
B,C) For neural correlates of dyskinesia, the magnitude of the absolute correlations of dyskinesia to theta, beta and narrowband gamma at the cortical site (B) and subthalamic site (C), where anticorrelated are denoted with a red asterisk (*). The distributions of correlations were compared using an *independent t-test* with $P<0.05$. D,E) The ability to predict dyskinesia scores using linear regression models with various sets of predictors: narrowband gamma alone, the combination of narrowband gamma and beta, or the combination of all three rhythms, at the cortical site (D) and subthalamic site (E). The green and red dots in (E) denote data points corresponding to subjects analyzed in greater detail in the subsequent panels. F,G) Single-subject examples of beta-gamma-dyskinesia interactions in the right subthalamic nucleus of subject 15 (green labeled data point in Figure 2.5E), for which including beta as an independent predictor increased predictive power by 37% (F) and the left hemisphere of subject 4 (red labeled data point in Figure 2.5E), for which including beta did not add predictive power (G). (Figure caption continued on the next page)

(Figure caption continued from the previous page) Top left plot illustrates how dyskinesia scores (colored data points) fluctuate at a constant gamma power as a function of beta power (for example, note how dyskinesia intensity varies along the horizontal dotted line). The top right plot shows how peak beta (red) and gamma (green) are distributed across the timeseries. The bottom plot shows how beta (red) and gamma (green) fluctuate throughout the timeseries.

The green asterisk (*) denotes a comparison with $P<0.05$. NBG = narrowband gamma

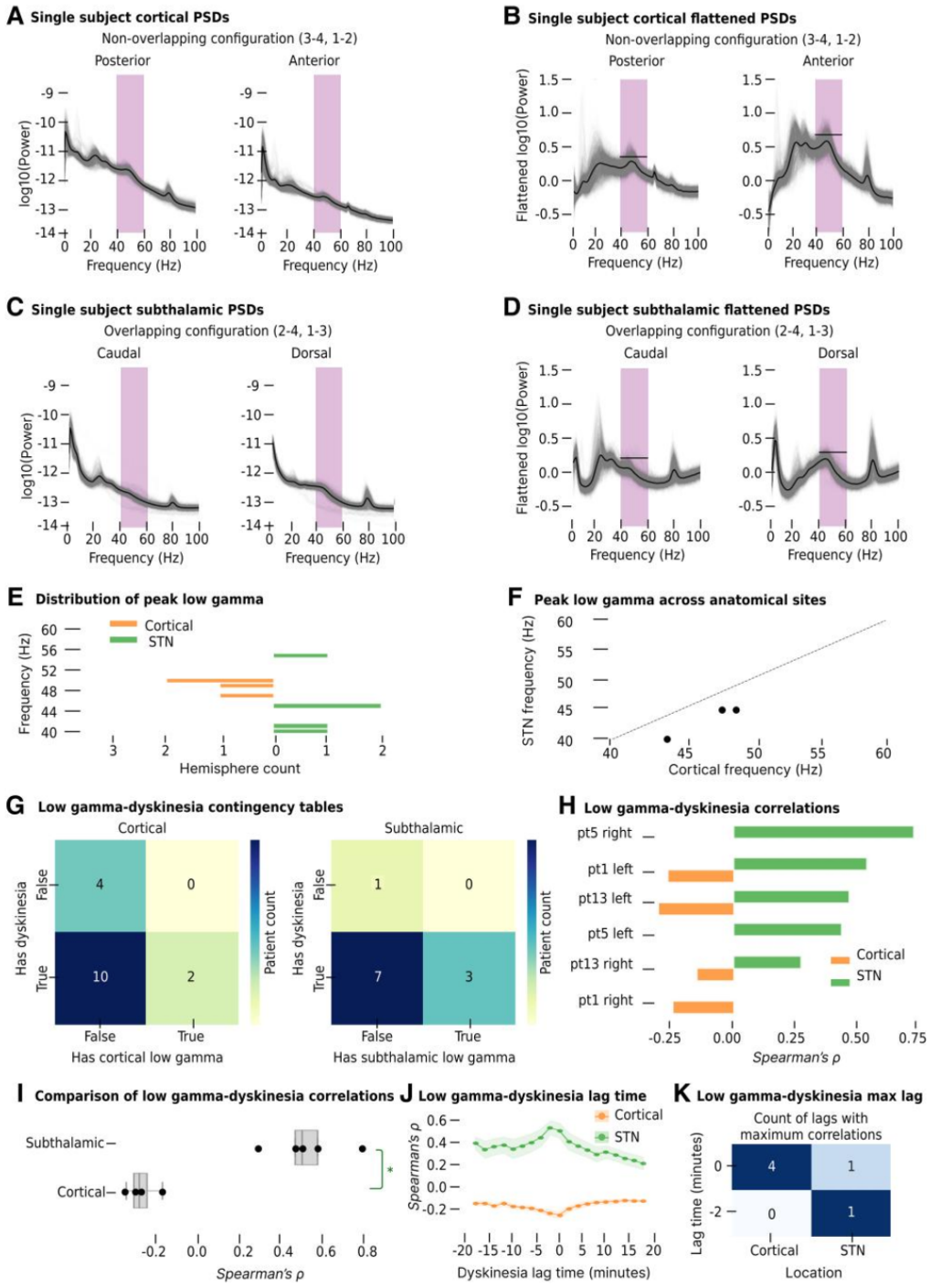

Fig. 2.6: Low gamma processing method, frequency distribution, relation to clinical dyskinesia, and correlation to contralateral dyskinesia scores.
A) Single subject example (subject 13, right hemisphere) of overlaid power spectral densities from the posterior (left) and anterior (right) recording configurations of the cortical paddle (log scaled) during everyday life at home. Each power spectral density line (grey) is derived from a two-minute recording length. (Figure caption continued on the next page)

(Figure caption continued from the previous page) The average power spectra is overlaid as the black line. The purple rectangle spanning 40-60 Hz denotes the signal frequencies that characterize low gamma. B) Overlaid power spectral densities from panel A after removing aperiodic activity using FOOOF.[29] The average flattened power spectra is overlaid as the black line. The black horizontal line is the power threshold used to detect the peak low gamma frequency. C) Example of overlaid power spectral densities from the caudal (left) and dorsal (right) recording configurations of the subthalamic lead using the same format as panel A. D) Overlaid power spectral densities from panel C after removing aperiodic activity using FOOOF, similar to panel B. E) The distribution of peak low gamma frequencies in cortical (orange) and subthalamic (green) sites. F) A scatterplot of low gamma frequencies across sites in subject hemispheres where low gamma was recorded at both sites. The dotted line indicates where the frequency would be the same at both sites, serving as a visual aid for comparing the frequencies across sites. G) Contingency tables relating a clinical history of dyskinesia with low gamma for cortical (left) and subthalamic (right) electrode sites. Each data point represents a subject, where each subject was classified as exhibiting low gamma if one or both hemispheres had low gamma. H) The distribution of peak low gamma frequencies in cortical (orange) and subthalamic (green) sites. I) Boxplots of correlation coefficients across subject hemispheres for subthalamic low gamma and cortical low gamma, showing that while subthalamic low gamma positively correlated to dyskinesia scores, cortical low gamma anticorrelated to the scores. J) *Pearson* correlation lag analysis illustrates the strength and direction of the correlation of each lag value. Dyskinesia scores are temporally shifted either prior to (positive lag scores) or after (negative lag scores) low gamma spectral power from either subthalamic (green) or cortical (orange) electrode sites. K) Comparison of 0 and -2 minute lag times with maximum low-gamma dyskinesia correlations across electrode sites.

The asterisk (*) denotes a comparison with a $P<0.05$ using a *t-test*, STN = subthalamic, FDR = false discovery rate

TABLES

Table 2.1 Subject demographics

Pt	Symptoms (years)	UPDRS (OFF)	UPDRS IV	Levodopa (mg)	Age (years)	Gender	MOCA	UPDRS tremor L	UPDRS tremor R	UPDRS (OFF-ON)	Implant site	Implant side
1	7	49	4	1425	54	M	26	2	0	0.9	STN	Bilateral
2	19	45	1	955	63	M	30	3	4	0.51	STN	Bilateral
3	12	61	2	1550	28	F	27	12	9	0.73	STN	Bilateral
4	4	41	1	1314	40	M	30	6	3	0.65	STN	Bilateral
5	12	44	2	2100	58	M	27	0	0	0.75	STN	Bilateral
6	10	39	2	1755	48	M	27	6	14	0.59	GP	Bilateral
7	13	89	0	1083	64	F	27	9	11	0.53	GP	Bilateral
8	7	29	2	1525	71	M	26	0	4	0.58	STN	Bilateral
9	10	34	2	800	58	M	28	4	10	0.73	STN	Bilateral
10	4	31	0	1580	65	M	26	7	4	0.51	GP	Unilateral
11	6	35	0	570	61	M	27	7	7	0.67	STN	Bilateral
12	12	32	1	920	45	M	26	3	3	0.84	STN	Bilateral
13	7	49	2	2031	67	M	27	1	1	0.76	STN	Bilateral
14	8	49	0	1213	51	M	27	14	3	0.61	GP	Bilateral
15	13	31	1	1036	73	M	28	4	4	0.67	STN	Bilateral
16	9	66	1	900	66	M	29	12	11	0.64	GP	Unilateral

Table 2.2 Presence and localization of narrowband gamma across study subjects

Pt	Implant site	UPDRS IV	Left cortical		Right cortical		Left subcortical		Right subcortical	
			NBG	Correlation	NBG	Correlation	NBG	Correlation	NBG	Correlation
1	STN	4	True	True	True	True	True	True	True	True
2	STN	1	False	False	True	True	False	False	True	True
3	STN	2	False	False	False	False	False	False	False	False
4	STN	1	True	True	True	True	True	True	True	True
5	STN	2	True	False	True	True	False	False	True	True
8	STN	2	False	False	True	True	False	False	False	False
9	STN	2	True	True	True	True	True	True	True	True
11	STN	0	False	False	True	False	False	False	False	False
12	STN	1	True	True	False	False	True	True	False	False
13	STN	2	True	True	True	False	True	True	True	False
15	STN	1	True	True	False	False	True	True	True	True
6	GP	2	True	True	True	True	False	True	False	False
7	GP	0	True	True	True	True	False	False	False	False
10	GP	0	False	False	NA	NA	False	False	NA	NA
14	GP	0	False	False	False	False	False	False	False	False
16	GP	1	True	True	NA	NA	False	False	NA	NA

SUPPLEMENTAL FIGURES

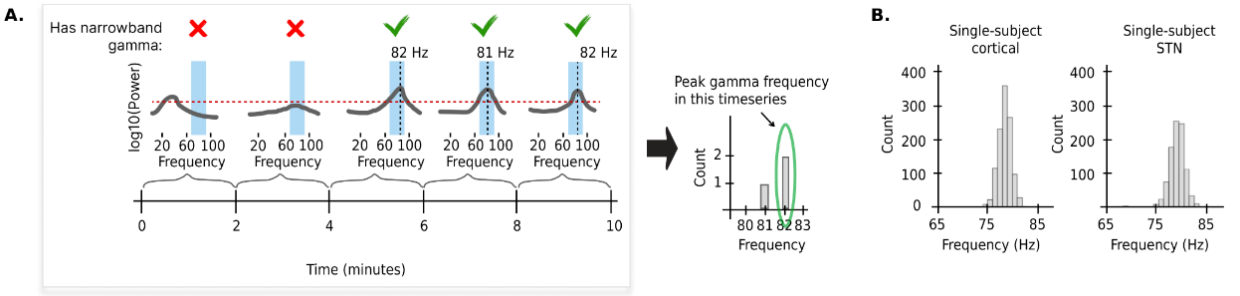

Fig. 2.7: Methodology for defining the peak frequency of narrowband gamma in a timeseries.
A) In this schematic, we apply our method of defining the peak frequency for narrowband gamma (65-90 Hz, range denoted in the blue inset rectangle). First, we inspect whether each epoch contains narrowband signal greater than the threshold, defined as two standard deviations greater than the mean at 65 Hz (red dotted line). Epochs with eligible signal are denoted with a green check mark. The maximum peak frequency of each eligible epoch is then counted, and the peak frequency with the maximum counts is used as the peak frequency for all subsequent analyses. B) An example of the intra-subject variability of peak narrowband gamma is shown with a histogram of peak narrowband gamma frequency counts across the epochs from the right hemisphere of subject 4 at the cortical (left) and subthalamic (right) sites.
STN = subthalamic nucleus

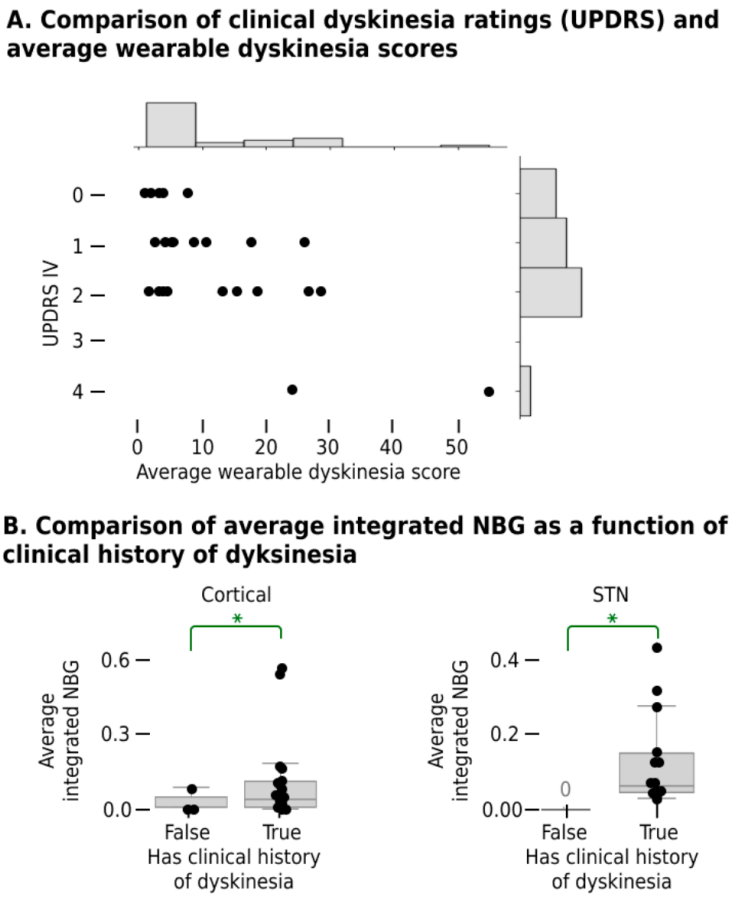

Fig. 2.8: Segregation of wearable dyskinesia scores and integrated gamma scores by preoperative UPDRS IV.

A) A scatterplot of the UPDRS scores and average wearable dyskinesia scores across subject hemispheres used for *Spearman's* statistics. The relationship between UPDRS scores and averaged wearable dyskinesia scores remains significant with $P<0.05$ regardless whether the UPDRS=4 datapoints, which could be construed as outliers, are included. Residual histograms display the distribution of respective counts. B) Box plots representing the averaged integrated narrowband gamma scores, differentiated by clinical history of dyskinesia at the cortical (left) and subthalamic (right) sites, with a significance of $P=0.045$ and $P=0.007$, respectively. The green asterisk (*) denotes a *Welch's t*-test with $P<0.05$.

UPDRS = Unified Parkinson's Disease Rating Scale, NBG = narrowband gamma, STN = subthalamic nucleus

A. Cortical electrode localization of subject hemispheres with UPDRS dyskinesia

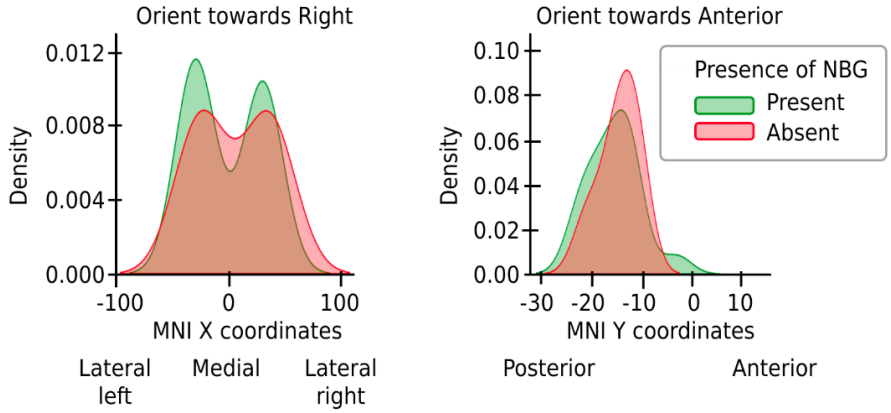

Fig. 2.9: Presence of cortical gamma oscillations in relation to electrode placement A) Density plots of cortical electrode localisation of subject hemispheres with a clinical history of dyskinesia with narrowband gamma present (green) and absent (red). The coordinates are shown as MNI X (left) and Y (right) coordinates with the “Right-Anterior-Superior” orientation system.

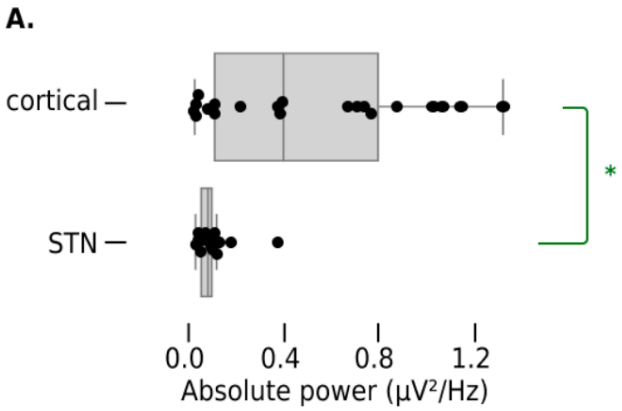

Fig. 2.10: Differences in absolute power of average peak narrowband gamma spectral power across subjects.
A) A boxplot comparison of the unflattened, non-log transformed power spectra values of peak narrowband gamma at the cortical and subthalamic sites. The mean cortical power was 0.51, and the mean subthalamic power was 0.0970. The cortical oscillations have greater absolute spectral power than the subthalamic oscillations (*t*-statistic = 3.353, *p*-value = 0.0021). The green asterisk (*) denotes a *t*-test with $P<0.05$.

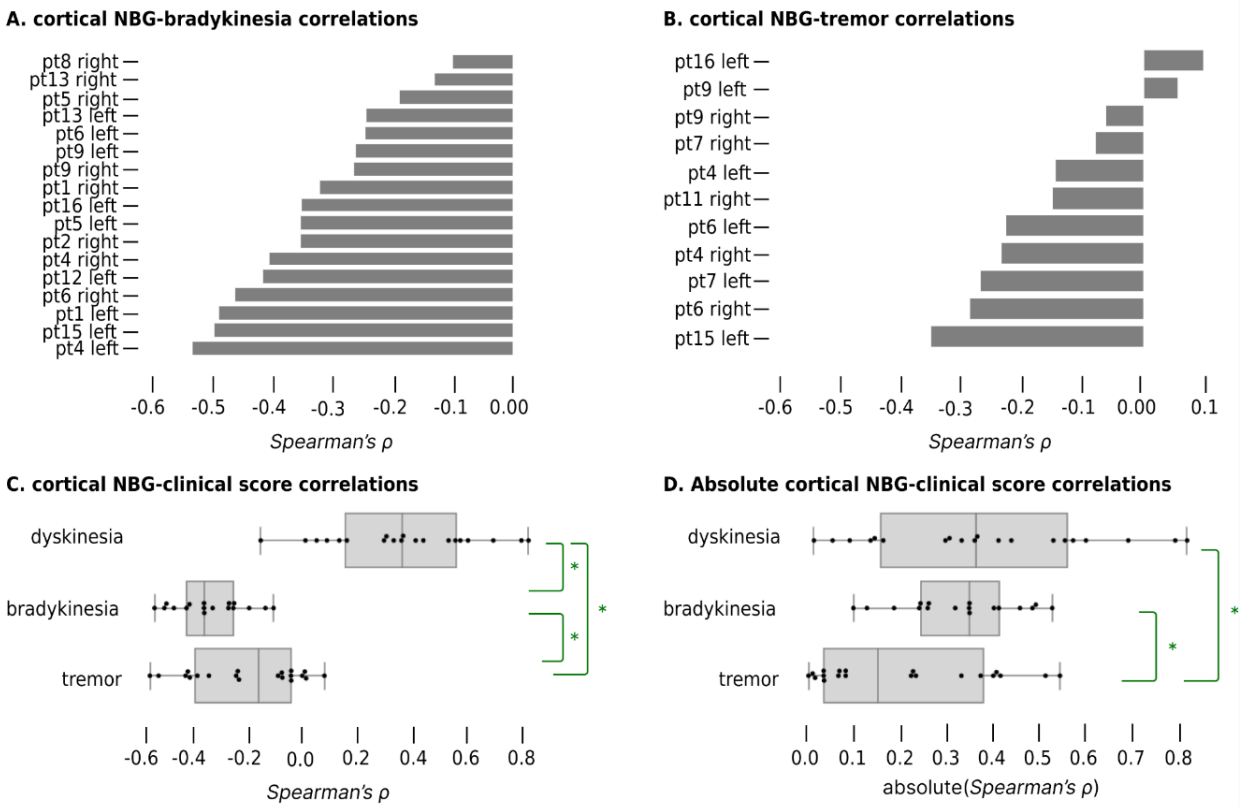

Fig. 2.11: Correlates of cortical narrowband gamma to other contralateral motor sign wearable scores.

A) The correlations between the time series of cortical narrowband gamma and wearable bradykinesia scores from the contralateral side across our subject subcohort with cortical narrowband gamma and a clinical history of dyskinesia. B) The correlations between the time series of narrowband gamma and wearable tremor scores across the subject subcohort with narrowband gamma and a clinical history of tremor and dyskinesia. C) Boxplots of correlation coefficients of cortical narrowband gamma signal to motor scores derived from wearable devices of dyskinesia, bradykinesia, and tremor. D) Boxplots of absolute values of correlation coefficients from Supplementary Figure 2.11C. We used different statistical tests to compare the results against tremor and bradykinesia scores: the *Mann-Whitney U test* for tremor scores and *t-test* for bradykinesia scores.

Asterisk denotes significance at false discovery rate-corrected $P<0.05$, NBG = narrowband gamma, UPDRS = Unified Parkinson's Disease Rating Scale

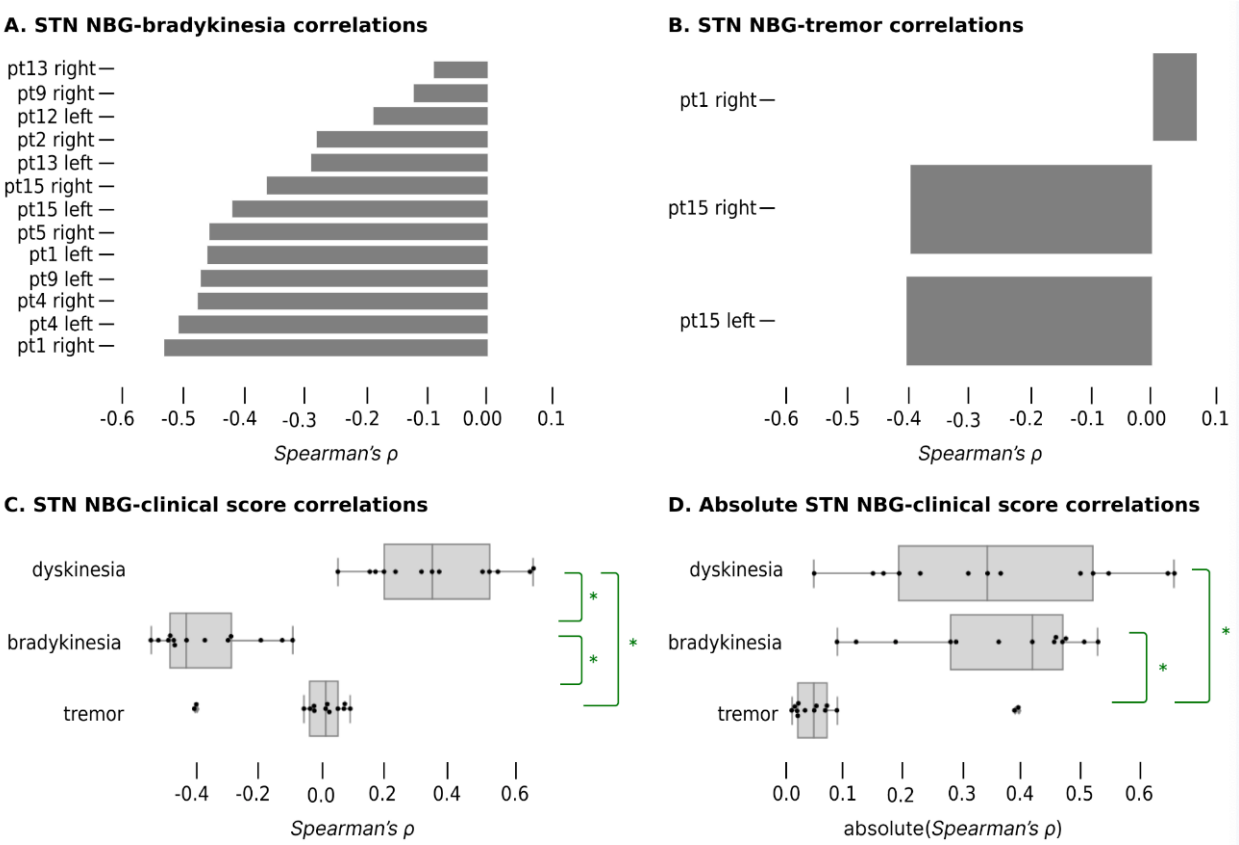

Fig. 2.12: Correlates of subthalamic narrowband gamma with contralateral wearable scores for off-state motor signs.

A) The correlations between the time series of subthalamic narrowband gamma and wearable bradykinesia scores from the contralateral side across our subject subcohort with subthalamic narrowband gamma and a clinical history of dyskinesia. B) The correlations between the time series of subthalamic narrowband gamma power and wearable tremor scores across the subject subcohort with subthalamic narrowband gamma and a clinical history of tremor and dyskinesia. C) Boxplots of correlation coefficients of subthalamic narrowband gamma signal to wearable device motor scores of dyskinesia, bradykinesia, and tremor. D) Boxplots of absolute values of correlation coefficients from Supplementary Figure 2.12C. We used *t-test* comparisons across all motor sign distributions.

Asterisk denotes significance at false discovery rate-corrected $P<0.05$ using ANOVA, STN = subthalamic nucleus, NBG = narrowband gamma, UPDRS = Unified Parkinson's Disease Rating Scale

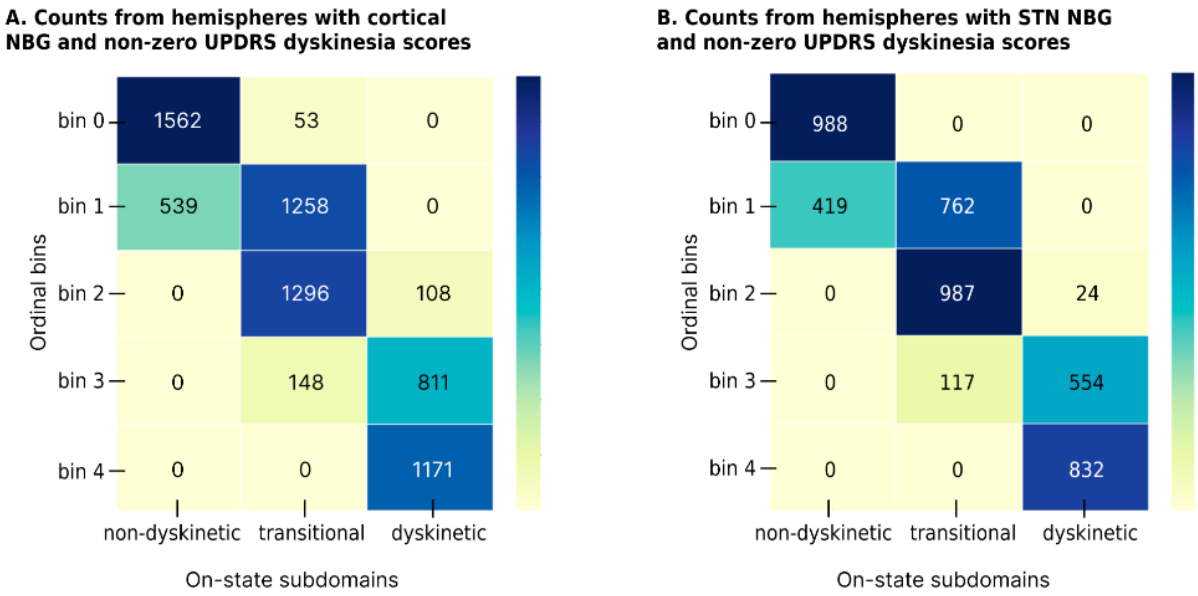

Fig. 2.13: Relationship between wearable dyskinesia scores in on-state subdomains versus ordinal groupings

A,B) The counts of on-state subdomain (Figure 2.4G, Figure 2.4I) wearable scores from subject hemispheres with cortical (A) and subthalamic (B) narrowband gamma within each ordinal grouping (Figure 2.4C, Figure 2.4F). There is a highly significant relationship ($P < 1e\text{-}15$) between the binned dyskinesia categories generated from each ordinal grouping and the three on-state subdomain categories when comparing across both the cortical ($\chi^2 = 10080$, *Cramer's V* = 0.85) and subthalamic ($\chi^2 = 7087$, *Cramer's V* = 0.71) sites.

SUPPLEMENTAL TABLES

Table 2.3 Presence and localization of low gamma across study subjects

			Left cortical		Right cortical		Left subcortical		Right subcortical	
Subject id	Implant site	UPDRS IV	Low gamma	Correlation	Low gamma	Correlation	Low gamma	Correlation	Low gamma	Correlation
1	STN	4	True	True	True	True	True	True	False	False
2	STN	1	False	False	False	False	False	False	False	False
3	STN	2	False	False	False	False	False	False	False	False
4	STN	1	False	False	False	False	False	False	False	False
5	STN	2	False	False	False	False	True	True	True	True
8	STN	2	False	False	False	False	False	False	False	False
9	STN	2	False	False	False	False	False	False	False	False
11	STN	0	False	False	False	False	False	False	False	False
12	STN	1	False	False	False	False	False	False	False	False
13	STN	2	True	True	True	True	True	True	True	True
15	STN	1	False	False	False	False	False	False	False	False
6	GP	2	False	False	False	False	False	False	False	False
7	GP	0	False	False	False	False	False	False	False	False
10	GP	0	False	False	NA	NA	False	False	NA	NA
14	GP	0	False	False	False	False	False	False	False	False
16	GP	1	False	False	NA	NA	False	False	NA	NA

REFERENCES

1. Brown P, Williams D. Basal ganglia local field potential activity: character and functional significance in the human. Clin Neurophysiol. 2005;116: 2510–2519.

2. Brown P, Oliviero A, Mazzone P, Insola A, Tonali P, Di Lazzaro V. Dopamine dependency of oscillations between subthalamic nucleus and pallidum in Parkinson's disease. J Neurosci. 2001;21: 1033–1038.

3. Güttler C, Altschüler J, Tanev K, Böckmann S, Haumesser JK, Nikulin VV, et al. Levodopa-Induced Dyskinesia Are Mediated by Cortical Gamma Oscillations in Experimental Parkinsonism. Mov Disord. 2021;36: 927–937.

4. Halje P, Tamtè M, Richter U, Mohammed M, Cenci MA, Petersson P. Levodopa-induced dyskinesia is strongly associated with resonant cortical oscillations. J Neurosci. 2012;32: 16541–16551.

5. Salvadè A, D'Angelo V, Di Giovanni G, Tinkhauser G, Sancesario G, Städler C, et al. Distinct roles of cortical and pallidal β and γ frequencies in hemiparkinsonian and dyskinetic rats. Exp Neurol. 2016;275 Pt 1: 199–208.

6. Swann NC, de Hemptinne C, Miocinovic S, Qasim S, Wang SS, Ziman N, et al. Gamma Oscillations in the Hyperkinetic State Detected with Chronic Human Brain Recordings in Parkinson's Disease. J Neurosci. 2016;36: 6445–6458.

7. Gilron R, Little S, Perrone R, Wilt R, de Hemptinne C, Yaroshinsky MS, et al. Long-term wireless streaming of neural recordings for circuit discovery and adaptive stimulation in individuals with Parkinson's disease. Nat Biotechnol. 2021;39: 1078–1085.

8. Alonso-Frech F, Zamarbide I, Alegre M, Rodríguez-Oroz MC, Guridi J, Manrique M, et al. Slow oscillatory activity and levodopa-induced dyskinesias in Parkinson's disease. Brain. 2006;129: 1748–1757.

9. Stanslaski S, Herron J, Chouinard T, Bourget D, Isaacson B, Kremen V, et al. A Chronically Implantable Neural Coprocessor for Investigating the Treatment of Neurological Disorders. IEEE Trans Biomed Circuits Syst. 2018;12: 1230–1245.

10. Follett KA, Weaver FM, Stern M, Hur K, Harris CL, Luo P, et al. Pallidal versus subthalamic deep-brain stimulation for Parkinson's disease. N Engl J Med. 2010;362: 2077–2091.

11. Okun MS, Fernandez HH, Wu SS, Kirsch-Darrow L, Bowers D, Bova F, et al. Cognition and mood in Parkinson's disease in subthalamic nucleus versus globus pallidus interna deep brain stimulation: the COMPARE trial. Ann Neurol. 2009;65: 586–595.

12. Swann NC, de Hemptinne C, Miocinovic S, Qasim S, Ostrem JL, Galifianakis NB, et al. Chronic multisite brain recordings from a totally implantable bidirectional neural interface: experience in 5 patients with Parkinson's disease. J Neurosurg. 2018;128: 605–616.

13. Shahlaie K, Larson PS, Starr PA. Intraoperative computed tomography for deep brain stimulation surgery: technique and accuracy assessment. Neurosurgery. 2011;68: 114–24; discussion 124.

14. Hammer LH, Kochanski RB, Starr PA, Little S. Artifact Characterization and a Multipurpose Template-Based Offline Removal Solution for a Sensing-Enabled Deep Brain Stimulation Device. Stereotact Funct Neurosurg. 2022;100: 168–183.

15. Horn A, Li N, Dembek TA, Kappel A, Boulay C, Ewert S, et al. Lead-DBS v2: Towards a comprehensive pipeline for deep brain stimulation imaging. Neuroimage. 2019;184: 293–316.

16. Davis TS, Caston RM, Philip B, Charlebois CM, Anderson DN, Weaver KE, et al. LeGUI: A Fast and Accurate Graphical User Interface for Automated Detection and Anatomical Localization of Intracranial Electrodes. Frontiers in Neuroscience. 2021. doi:10.3389/fnins.2021.769872

17. Penny WD, Friston KJ, Ashburner JT, Kiebel SJ, Nichols TE. Statistical Parametric Mapping: The Analysis of Functional Brain Images. Elsevier; 2011.

18. Horn A, Kühn AA. Lead-DBS: a toolbox for deep brain stimulation electrode localizations and visualizations. Neuroimage. 2015;107: 127–135.

19. Hermes D, Miller KJ, Noordmans HJ, Vansteensel MJ, Ramsey NF. Automated electrocorticographic electrode localization on individually rendered brain surfaces. J Neurosci Methods. 2010;185: 293–298.

20. Fischl B, Sereno MI, Tootell RBH, Dale AM. High-resolution intersubject averaging and a coordinate system for the cortical surface. Human Brain Mapping. 1999. pp. 272–284. doi:10.1002/(sici)1097-0193(1999)8:4<272::aid-hbm10>3.0.co;2-4

21. Xiao Y, Fonov V, Bériault S, Al Subaie F, Mallar Chakravarty M, Sadikot AF, et al. Multi-contrast unbiased MRI atlas of a Parkinson's disease population. International Journal of Computer Assisted Radiology and Surgery. 2015. pp. 329–341. doi:10.1007/s11548-014-1068-y

22. Griffiths RI, Kotschet K, Arfon S, Xu ZM, Johnson W, Drago J, et al. Automated assessment of bradykinesia and dyskinesia in Parkinson's disease. J Parkinsons Dis. 2012;2: 47–55.

23. Braybrook M, O'Connor S, Churchward P, Perera T, Farzanehfar P, Horne M. An Ambulatory Tremor Score for Parkinson's Disease. Journal of Parkinson's Disease. 2016. pp. 723–731. doi:10.3233/jpd-160898

24. Horne MK, McGregor S, Bergquist F. An objective fluctuation score for Parkinson's disease. PLoS One. 2015;10: e0124522.

25. Brownlee J. Data preparation for machine learning. 2022. Available: http://14.99.188.242:8080/jspui/bitstream/123456789/14557/1/Data%20Preparation%20for%20Machine%20Learning%20-%20Data%20Cleaning%2C%20Feature%20Selection%2C%20and%20Data%20by%20Jason%20Brownlee.pdf

26. Chen L, Cai G, Weng H, Yu J, Yang Y, Huang X, et al. More Sensitive Identification for Bradykinesia Compared to Tremors in Parkinson's Disease Based on Parkinson's KinetiGraph (PKG). Front Aging Neurosci. 2020;12: 594701.

27. Sellers KK, Gilron R 'ee, Anso J, Louie KH, Shirvalkar PR, Chang EF, et al. Analysis-rcs-data: Open-Source Toolbox for the Ingestion, Time-Alignment, and Visualization of Sense and Stimulation Data From the Medtronic Summit RC+S System. Front Hum Neurosci. 2021;15: 714256.

28. Virtanen P, Gommers R, Oliphant TE, Haberland M, Reddy T, Cournapeau D, et al. SciPy 1.0: fundamental algorithms for scientific computing in Python. Nat Methods. 2020;17: 261–272.

29. Donoghue T, Haller M, Peterson EJ, Varma P, Sebastian P, Gao R, et al. Parameterizing neural power spectra into periodic and aperiodic components. Nat Neurosci. 2020;23: 1655–1665.

30. Kotschet K, Johnson W, McGregor S, Kettlewell J, Kyoong A, O'Driscoll DM, et al. Daytime sleep in Parkinson's disease measured by episodes of immobility. Parkinsonism Relat Disord. 2014;20: 578–583.

31. Buitinck L, Louppe G, Blondel M, Pedregosa F, Mueller A, Grisel O, et al. API design for machine learning software: experiences from the scikit-learn project. arXiv [cs.LG]. 2013. Available: http://arxiv.org/abs/1309.0238

32. Seabold S, Perktold J. Statsmodels: Econometric and statistical modeling with python. Proceedings of the 9th Python in Science Conference. Austin, TX; 2010. pp. 10–25080.

33. Heida T, Poppe NR, de Vos CC, van Putten MJAM, van Vugt JPP. Event-related mu-rhythm desynchronization during movement observation is impaired in Parkinson's disease. Clin Neurophysiol. 2014;125: 1819–1825.

34. Miller EK, Lundqvist M, Bastos AM. Working Memory 2.0. Neuron. 2018;100: 463–475.

35. Fernandez-Ruiz A, Sirota A, Lopes-Dos-Santos V, Dupret D. Over and above frequency: Gamma oscillations as units of neural circuit operations. Neuron. 2023;111: 936–953.

36. Brücke C, Kempf F, Kupsch A, Schneider G-H, Krauss JK, Aziz T, et al. Movement-related synchronization of gamma activity is lateralized in patients with dystonia. Eur J Neurosci. 2008;27: 2322–2329.

37. Cassidy M, Mazzone P, Oliviero A, Insola A, Tonali P, Di Lazzaro V, et al. Movement-related changes in synchronization in the human basal ganglia. Brain. 2002;125: 1235–1246.

38. Crone NE, Miglioretti DL, Gordon B, Lesser RP. Functional mapping of human sensorimotor cortex with electrocorticographic spectral analysis. II. Event-related synchronization in the gamma band. Brain. 1998;121 (Pt 12): 2301–2315.

39. Manning JR, Jacobs J, Fried I, Kahana MJ. Broadband shifts in local field potential power spectra are correlated with single-neuron spiking in humans. J Neurosci. 2009;29: 13613–13620.

40. de Hemptinne C, Wang DD, Miocinovic S, Chen W, Ostrem JL, Starr PA. Pallidal thermolesion unleashes gamma oscillations in the motor cortex in Parkinson's disease. Mov Disord. 2019;34: 903–911.

41. Ryan MB, Bair-Marshall C, Nelson AB. Aberrant Striatal Activity in Parkinsonism and Levodopa-Induced Dyskinesia. Cell Rep. 2018;23: 3438–3446.e5.

42. Girasole AE, Lum MY, Nathaniel D, Bair-Marshall CJ, Guenthner CJ, Luo L, et al. A Subpopulation of Striatal Neurons Mediates Levodopa-Induced Dyskinesia. Neuron. 2018;97: 787–795.e6.

43. Vitek JL, Bakay RAE, Freeman A, Evatt M, Green J, McDonald W, et al. Randomized trial of pallidotomy versus medical therapy for Parkinson's disease. Ann Neurol. 2003;53: 558–569.

44. Telkes I, Viswanathan A, Jimenez-Shahed J, Abosch A, Ozturk M, Gupte A, et al. Local field potentials of subthalamic nucleus contain electrophysiological footprints of motor subtypes of Parkinson's disease. Proc Natl Acad Sci U S A. 2018;115: E8567–E8576.

45. Johnson LA, Aman JE, Yu Y, Escobar Sanabria D, Wang J, Hill M, et al. High-Frequency Oscillations in the Pallidum: A Pathophysiological Biomarker in Parkinson's Disease? Mov Disord. 2021;36: 1332–1341.

46. Neumann W-J, Gilron R, Little S, Tinkhauser G. Adaptive Deep Brain Stimulation: From Experimental Evidence Toward Practical Implementation. Mov Disord. 2023;38: 937–948.

47. Swann NC, de Hemptinne C, Thompson MC, Miocinovic S, Miller AM, Gilron R 'ee, et al. Adaptive deep brain stimulation for Parkinson's disease using motor cortex sensing. J Neural Eng. 2018;15: 046006.

48. Oehrn CR, Cernera S, Hammer LH, Shcherbakova M, Yao J, Hahn A, et al. Personalized chronic adaptive deep brain stimulation outperforms conventional stimulation in Parkinson's disease. medRxiv. 2023. doi:10.1101/2023.08.03.23293450

49. Sermon JJ, Olaru M, Ansó J, Cernera S, Little S, Shcherbakova M, et al. Sub-harmonic entrainment of cortical gamma oscillations to deep brain stimulation in Parkinson's disease: Model based predictions and validation in three human subjects. Brain Stimul. 2023;16: 1412–1424.

50. di Biase L, Pecoraro PM, Carbone SP, Caminiti ML, Di Lazzaro V. Levodopa-Induced Dyskinesias in Parkinson's Disease: An Overview on Pathophysiology, Clinical Manifestations, Therapy Management Strategies and Future Directions. J Clin Med Res. 2023;12. doi:10.3390/jcm12134427

51. Contarino MF, Bour LJ, Bot M, van den Munckhof P, Speelman JD, Schuurman PR, et al. Tremor-specific neuronal oscillation pattern in dorsal subthalamic nucleus of parkinsonian patients. Brain Stimul. 2012;5: 305–314.

52. Khodakarami H, Shokouhi N, Horne M. A method for measuring time spent in bradykinesia and dyskinesia in people with Parkinson's disease using an ambulatory monitor. J Neuroeng Rehabil. 2021;18: 116.

53. Mahadevan N, Demanuele C, Zhang H, Volfson D, Ho B, Erb MK, et al. Development of digital biomarkers for resting tremor and bradykinesia using a wrist-worn wearable device. NPJ Digit Med. 2020;3: 5.

54. Gordon EM, Chauvin RJ, Van AN, Rajesh A, Nielsen A, Newbold DJ, et al. A somato-cognitive action network alternates with effector regions in motor cortex. Nature. 2023;617: 351–359.

55. van Wijk BCM, Neumann W-J, Kroneberg D, Horn A, Irmen F, Sander TH, et al. Functional connectivity maps of theta/alpha and beta coherence within the subthalamic nucleus region. Neuroimage. 2022;257: 119320.

56. Lofredi R, Neumann W-J, Bock A, Horn A, Huebl J, Siegert S, et al. Dopamine-dependent scaling of subthalamic gamma bursts with movement velocity in patients with Parkinson's disease. Elife. 2018;7: e31895.

57. Horn A, Neumann W-J, Degen K, Schneider G-H, Kühn AA. Toward an electrophysiological "sweet spot" for deep brain stimulation in the subthalamic nucleus. Hum Brain Mapp. 2017;38: 3377–3390.

Chapter 3:

Entrained gamma oscillations are functionally and behaviorally distinct from levodopa-induced gamma oscillations

INTRODUCTION

Narrowband gamma oscillations (60-90 Hz) may play a role in the genesis of levodopa-induced dyskinesia. Cortical recordings of Parkinsonian rodent models treated chronically with levodopa have shown that 60-90 Hz narrowband gamma oscillations are predictive of dyskinesia [1–3]. Very similar narrowband gamma oscillations have been detected in humans with Parkinson's disease in the on-medication state [4]. In a prior study, we used a sensing-enabled implantable neurostimulator attached to both basal ganglia and cortical leads to study levodopa-induced gamma oscillations, prior to initiating therapeutic stimulation, during normal daily activities. Recordings were paired with data from wrist-wearable sensors providing ratings of dyskinesia severity. Our findings showed that levodopa-induced gamma oscillations scale with dyskinesia severity, in close temporal precision, similarly across the subthalamic nucleus and motor cortex [5].

Several small case series have shown that deep brain stimulation (DBS) can entrain subthalamic or cortical gamma oscillations to a subharmonic of the stimulation frequency, often to one-half of the stimulation frequency [6,7]. The stimulation parameters leading to entrainment have been modeled using a coupled oscillator framework, in which the driven oscillator is the motor network that has a natural oscillation frequency in the gamma range, and the driving oscillator is the neurostimulator [6]. However, DBS-entrained gamma oscillations have not been systematically studied in a larger cohort [8], raising several important questions: (1) How common are entrained gamma oscillations during chronic stimulation, (2) which basal ganglia stimulation sites are

associated with cortical entrainment, and (3) does entraining levodopa-induced gamma oscillations alter their behavioral correlates and statistical properties.

To answer these questions, we studied entrained gamma oscillations in the same cohort of subjects in which we previously characterized levodopa-induced gamma oscillations [5]. We analyzed 993 hours of cortical and basal ganglia field potential recordings at home during normal daily activities, with 656 hours recorded prior to initiating stimulation, in 20 hemispheres of 13 patients with Parkinson's disease. We collected data in three stimulation conditions: (1) prior to initiating basal ganglia stimulation [5], (2) during the initial slow increase in DBS amplitude to therapeutic settings, and (3) after at least five months of chronic therapeutic stimulation. For the stimulation increase condition, we also recorded 31 hours of dyskinesia scores using wrist-wearable sensors. We found that entrained cortical gamma oscillations are common and equally likely to entrain from the pallidal and subthalamic stimulation sites. Chronic entrainment of levodopa-induced gamma oscillations reduces their pro-dyskinetic effect and alters the distributions of peak frequencies and spectral power.

METHODS

Subject Selection and Assessment

The study was approved by the IRB, registered on clinicaltrials.gov (NCT03582891), and included data from 13 subjects with Parkinson's disease using Medtronic's Summit RC+S device [9]. Two subjects were excluded due to lack of chronic stable stimulation recordings. Depth leads were placed in the subthalamic nucleus or globus pallidus, with paddle leads over pre-central and post-central gyri [10]. Data from these subjects have been published in an analysis of neural recordings prior to the onset of DBS, paired with wearable measures of dyskinesia [5]. Subjects were recruited from UCSF's movement disorders clinic, with inclusion criteria of idiopathic Parkinson's

and standard DBS indications [11,12], and exclusion criteria of significant cognitive impairment or untreated mood disorder. Baseline motor function and dyskinesia severity were assessed using UPDRS scales.

Surgical implantation

Subjects were implanted with cortical leads (**Figure 3.1A**) and quadripolar cylindrical leads in the subthalamic nucleus (**Figure 3.1B**) or globus pallidus (**Figure 3.1C**), and quadripolar paddle-type cortical leads using established methods [4,7]. Cortical leads were placed parasagittally and confirmed intraoperatively with CT fused to MRI. Brain leads connected to a Medtronic interface [13]. Post-implantation, precise electrode localization was refined using CT and MRI image analysis, verified by visual inspection, and adjusted for brain shift [14,15]. Electrode locations were then mapped to standardized brain spaces for group analysis [16,17].

Signal Recording

Neural field potentials from sensorimotor cortical and basal ganglia regions were recorded from subjects with implanted cortical paddles and depth leads at home. Data were streamed via the Summit RC+S interface to a tablet, with each RC+S device recording from two channels per cortical paddle and depth lead. Recordings started one to four weeks post-implantation, with adjustments for optimal signal-to-noise ratio. During stimulation amplitude increases, recordings were made up to two months post-stimulation onset, while monitoring for adverse effects. Chronic recordings were made at least five months after stimulation onset. **Table 3.1** lists the subject cohorts included in each stimulation paradigm. Six subjects used Apple Watch monitors to stream data to the StrivePD app during stimulation adjustments.

Signal Processing

Neural field potentials were downsampled to 250 Hz, and power spectral density was calculated using non-overlapping Hann windows in 2-minute intervals for chronic entrained gamma and 1-minute intervals for stimulation amplitude increases (**Figure 3.1D**). A processing pipeline was utilized to determine which epochs contained gamma oscillations (60-90 Hz), and of those epochs, the corresponding frequency with maximal power (**Figure 3.1E**). An integrated narrowband gamma score, considering both power and duration, determined the dominant channel for analysis. Wearable data from Apple Watch monitors provided validated dyskinesia scores in 1-minute intervals [18]. These scores were binarized using a 50% threshold to determine dyskinetic episodes.

Statistics

Sklearn and *SciPy* statistics modules in Python were used for statistical analyses. *Chi-squared* test of independence was used to compare distributions across categorical variables. The *Shapiro* normality test was used to assess normality. The mean gamma power in epochs with gamma oscillations was compared using independent *t-tests*. *Levene's test* assessed the equality of variance in gamma frequency and power. The kernel probability densities across distributions, the kernel probabilities were rescaled using minimum-maximum normalization [19] onto a 0-1 scale for visualization purposes. For logistic regression analysis, *statsmodels* and *sklearn* were used with a 50:50 training-test data split for statistical inference and predictive ability. To train the model across a cohort with individualized thresholds for entrainment, entrained gamma oscillations were normalized with a linear shift such that power values below the channel-specific threshold for containing entrained gamma oscillations were negative. The *log-likelihood ratio* determined the fit of the logistic regression.

A subject was scored as having gamma oscillations if either hemisphere contained gamma oscillations. The hemisphere with maximal neural recordings was used to determine the total hours recorded by each subject.

RESULTS

Subject characteristics

We studied 20 hemispheres from 13 subjects with Parkinson's disease with cortical and basal ganglia leads (1/13 female, mean age at surgery 59±9 years, **Table 3.1**). Eleven subjects had a clinical history of dyskinesia (UPDRS IVa dyskinesia score>0), nine of whom had implants in the subthalamic nucleus. Previously, we examined levodopa-induced gamma oscillations from this cohort [5]. Here, we examine how entraining levodopa-induced gamma oscillations impacts their behavioral and statistical properties.

Entrained gamma oscillations after chronic therapeutic DBS: incidence in a large cohort and relationship to levodopa-induced gamma oscillations across subjects

To objectify the relationship between levodopa-induced narrowband gamma oscillations and DBS-induced gamma entrainment, we investigated these neurophysiological phenomena prior to and during chronic DBS. Recordings were subdivided into 2-minute epochs and the presence of gamma oscillations in each epoch was determined by inspecting its flattened power spectral density plot for spectral power greater than two standard deviations above the 1/*f* background, in the range of 60-90 Hz (see methods, **Figure 3.1**). The frequency of entrained gamma oscillations was always at one-half of the stimulation frequency at either 130 Hz or 150 Hz (**Figure 3.1D**) regardless of the exact frequency at which levodopa-induced gamma oscillations occurred prior to stimulation. Cortical entrained gamma oscillations were observed in 16/20 hemispheres (11/13 subjects) and occurred in the context of either pallidal (4/5 hemispheres) or subthalamic (12/15

hemispheres) stimulation (**Figure 3.2A**). Subcortical entrained gamma oscillations appeared in 8/20 hemispheres and 6/13 subjects and occurred in the context of either pallidal (1/5) or subthalamic (7/15) hemispheres (**Figure 3.2B**). See **Table 3.2** for the subject hemisphere-labeled dataset.

During chronic DBS, once entrained gamma oscillations occurred, non-entrained oscillations (those not at a subharmonic of DBS frequency) were not typically observed. While most hemispheres had both levodopa-induced gamma oscillations prior to stimulation and entrained gamma on chronic stimulation (**Figure 3.2C-D**), in some hemispheres stimulation-entrained gamma rhythms occurred even though levodopa-induced gamma oscillations were absent without stimulation.

Anatomic localization

Cortical electrode arrays spanned the precentral gyrus, with at least one contact over the postcentral gyrus. We recorded from the same two cortical channels before and after the onset of DBS. In hemispheres with levodopa-induced gamma oscillations and entrained gamma oscillations, entrained gamma oscillation predominantly occurred at the same cortical channel as levodopa-induced gamma oscillations in 13/14 hemispheres. These findings suggest that the same cortical circuit is susceptible to levodopa-induced gamma and DBS-induced entrainment. To anatomically localize the cortical region with the most prominently entrained gamma oscillations, we examined the nine hemispheres where the cortical bipolar montages were not interleaved. Regardless of whether levodopa-induced gamma oscillations appeared, cortical gamma oscillations entrained primarily at the primary motor cortex, rather than the somatosensory cortex, in 9/9 hemispheres.

Relation to the clinical history of dyskinesia

Here, we report subject-level metrics because clinical dyskinesia scores were available at the level of the subject but not the hemisphere. We defined subjects as having entrained gamma oscillations if the signal appeared in one or both hemispheres. Entrained cortical gamma oscillations appeared in 2/3 of subjects who did not meet the criteria for dyskinesia preoperatively (UPDRS IVa score = 0), and in 9/10 subjects who did meet the criteria (**Figure 3.2E**). Entrained subcortical gamma oscillations also appeared in 2/3 subjects who did not meet the criteria for dyskinesia preoperatively and 5/10 subjects who did meet the criteria (**Figure 3.2F**). The observed patterns among subjects suggest that a clinical history of dyskinesia is not a prerequisite for the occurrence of entrained gamma oscillations compared to levodopa-induced gamma oscillations.

Entrained gamma oscillations do not co-occur with episodes of dyskinesia during stimulation amplitude increases

Although levodopa-induced gamma oscillations fluctuate in relation to wearable dyskinesia [5], the relationship between entrained oscillations and dyskinesia is unknown. Of the six patients (10 hemispheres) with stimulation amplitude increases and wearable recordings, we examined the subset of three patient hemispheres (two subjects) with entrained gamma oscillations. **Supplementary Figure 3.5** shows the relationship of entrained gamma oscillations to stimulation amplitude increases in all subjects.

Each epoch was scored for the presence of a dyskinetic episode, defined as an epoch with a wearable probability of dyskinesia score greater than 50%. Across the three hemispheres, dyskinetic episodes were most likely to occur in pt12 left hemisphere, the subject with the least cortical and subthalamic entrained gamma oscillations. The remaining analyses focus primarily

on dyskinetic episodes from pt12 left hemisphere (44 epochs with cortical recordings, 53 epochs with subthalamic recordings) since the remaining two hemispheres had dyskinetic episodes during less than 1.1% of the recordings (*n*=5 for pt13 left; *n*=7 for pt13 right). To compare the relationship of entrained gamma oscillations to dyskinesia across the cohort, the channel-specific entrained gamma threshold was subtracted from each score, such that only values with entrained power were positive. Across the normalized power distribution of cortical (**Figure 3.3A**) and subthalamic (**Figure 3.3B**) entrained gamma oscillations, there was no entrainment during 37/56 and 46/62 epochs with dyskinetic episodes. Logistic regression was used to assess the relationship between the presence/absence of a dyskinetic episode (dependent variable) and entrained/not entrained gamma oscillations (independent variable), with an intercept term to account for the imbalanced sample. Gamma oscillations that did not entrain classified epochs with dyskinesia (log-likelihood ratio *P*<1e-4; Wald coefficient of the intercept <-2.1, *P*<1e-3; Wald coefficient of gamma power <-1.6; *P*<1e-3) and had an average area under the receiver operating characteristic (AUC-ROC) curve of 0.69 for cortical (**Figure 3.3C**) and 0.77 for subthalamic (**Figure 3.3D**) gamma oscillations during chronic stimulation. These results suggest that entraining levodopa-induced gamma oscillations dissociates them from their pro-dyskinetic effect.

To validate the robustness of these findings, we evaluated the fit of the linear regression model and generated the AUC-ROC curve using dyskinesia scores that were binarized with thresholds from 10% to 40%. Our results confirm that the classifier performed similarly using either cortical (mean auc=0.67, range=0.64–0.69) or subthalamic (mean auc=0.73, range=0.66–0.79) gamma oscillations, with a log-likelihood ratio *P*<1e-4.

Statistical properties of entrained gamma oscillations during chronic therapeutic DBS are distinct from levodopa-induced gamma oscillations

To better understand the statistical oscillatory properties that might drive the behavioral differences between levodopa-induced gamma oscillations and chronic therapeutic entrained gamma oscillations, we examined potential differences in peak gamma frequency and power across 2-minute epochs in the 14 hemispheres with gamma oscillations across stimulation conditions. First, we examined variance in the peak gamma oscillation frequency across epochs with gamma oscillations. **Figure 3.4A** shows an example of overlaid power spectral epochs with gamma oscillations across the two stimulation conditions in a single hemisphere, with black arrows denoting the peak frequency distributions across each stimulation condition. The distributions of these peak frequencies in a single hemisphere are then shown in **Figure 3.4B**. Across the cohort, levodopa-induced peak frequencies varied more than entrained gamma peak frequencies in 13/14 cortical hemispheres (**Figure 3.4C**) using Levene's test of variance (false discovery rate-corrected $P<0.05$).

We also assessed differences in the distributions of gamma power at the peak frequency. **Figure 3.4D-E** shows an example of the distributions of gamma power across epochs of levodopa-induced and entrained gamma oscillations in a single hemisphere. Entrained gamma oscillations had higher overall power than levodopa-induced gamma oscillations in 12/14 cortical hemispheres (**Figure 3.4F**) with independent *t*-tests (family discovery rate-corrected $P<0.05$). Lastly, we assessed differences in the variance of the peak gamma power at the peak frequency (see **Figure 3.4G-H** for a single-subject example). Entrained gamma oscillations had more variance than levodopa-induced gamma oscillations in 11/14 cortical hemispheres (**Figure 3.4I**) using Levene's test of variance (false discovery rate-corrected $P<0.05$). **Supplemental Figure 3.6** assesses these statistical comparisons for subcortical gamma oscillations. **Supplemental**

Figure 3.7 assesses whether the difference between the entrained peak frequency and levodopa-induced gamma frequency correlates to these statistical differences.

DISCUSSION

We investigated the relationship between levodopa-induced gamma oscillations and DBS-entrained gamma oscillations in a cohort of 13 Parkinson's disease patients with 993 hours of recordings from an investigational, sensing-enabled neurostimulator. We studied stimulation-entrained gamma oscillations in the same cohort of subjects in which we previously showed that levodopa-induced gamma oscillations predict dyskinesia severity, prior to initiating neurostimulation [5]. To investigate how DBS may alter the behavioral correlates of gamma oscillations, we also concurrently collected wearable monitor recordings providing continuous dyskinesia scores in three hemispheres during DBS amplitude increases up to clinically therapeutic settings. Both pallidal and subthalamic stimulation entrained cortical gamma oscillations in most patient hemispheres and stimulation could entrain gamma rhythms even in hemispheres in which levodopa-induced gamma oscillations had not been previously identified. Entraining levodopa-induced cortical gamma oscillations decreased their prodyskinetic association. Entrainment by stimulation altered the peak frequency, frequency variance, and mean and variance of gamma power spectral density, compared with levodopa-induced oscillations in the off-stimulation state.

Physiologic and pathophysiologic role of narrowband gamma oscillations

For cortical functioning, it is crucial to differentiate between two types of gamma activities: narrowband and broadband. Narrowband gamma rhythms in field potentials reflect underlying oscillatory synchronization and have a peak in the field potential's power spectral density, typically within the 40-90 Hz range. Outside of the motor system, narrowband gamma rhythms are a

ubiquitous feature of healthy neocortical function and represent rhythmic interactions between excitatory neurons and inhibitory interneurons. On the other hand, broadband gamma activity, sometimes called "high gamma," generally appears between 50-200 Hz and is associated with movement initiation in the sensorimotor cortex [20]. It is a non-oscillatory phenomenon thought to reflect the underlying asynchronous spiking activity [21]. Our study focuses on narrowband gamma oscillations and was not confounded by underlying broadband changes because we removed the aperiodic spectral component from each epoch.

While narrowband gamma oscillations have been extensively studied in rodents and nonhuman primates, these investigations have primarily focused on networks unrelated to motor function [22]. In the neocortex, gamma oscillations are primarily observed in the second and third layers and are thought to reflect "bottom-up" sensory input, while alpha/beta oscillations, which are more prevalent in layers five and six, indicate "top-down" cognitive control and typically show an inverse relationship with gamma activity [23].

In rodent models of parkinsonism, narrowband gamma activity in the motor cortex has been causally linked to the induction of dyskinesia by levodopa. Consistent with this, in chronic invasive at-home recordings in humans with Parkinson’s disease, levodopa-induced cortical and subthalamic gamma oscillations scale with dyskinesia severity [5].

Mechanisms of DBS-entrained gamma oscillations

Some small case series examining neurophysiological effects of neurostimulation have shown that subthalamic DBS can entrain gamma oscillations in the motor cortex at a subharmonic stimulation frequency, most commonly at one-half of the stimulation frequency [5,24,25], and has since been modeled across a range of stimulation frequencies and amplitudes. The model

predicts 1:2 entrainment across stimulation parameters in relation to the peak frequency of levodopa-induced gamma oscillations, where a larger difference in levodopa-induced peak gamma frequency and stimulation frequency requires more stimulation amplitude to entrain. Furthermore, this model shows that 1:2 entrainment is nonlinear – as stimulation amplitude increases, there is a transition from 1:2 to 1:1 entrainment, during which 1:2 entrainment is subsequently lost [6]. While we captured positively correlated data from some subjects across stimulation amplitude increases up to the maximal 1:2 entrainment (pt13), other subjects recorded data during the transition to 1:1 entrainment, resulting in negative correlates (pt6) (**Supplementary Figure 3.5**).

Our findings shed light on the circuit mechanism by which subcortical stimulation entrains cortical gamma. One candidate mechanism for subthalamic stimulation-entrained cortical gamma is antidromic activation of the hyper-direct pathway, which is known to occur in both rodent models and humans [26,27]. However, we found that pallidal stimulation also entrains cortical gamma oscillations, and the pallidum does not have a known hyper-direct innervation from the motor cortex. Therefore, to account for entrainment phenomena induced by stimulation at either target, it is more likely that the mechanism of entrainment is orthodromic (STN-internal pallidum-thalamus-cortex).

Previously, entrainment at a subharmonic stimulation frequency was often dismissed as artifactual, in part due to the lack of a physiological differentiating factor when considering this signal over a short time period [28]. Recent findings have since shown that entrained gamma oscillations have a physiological origin – entrained gamma amplitude fluctuates in accordance with the medication cycle, is more prominent at a more distant site from the stimulating contact than adjacent to it, and takes additional time to “wash out” when the stimulation is turned off [25].

Our findings that entrained gamma power has more variance than levodopa-induced gamma oscillations (**Figure 3.4**) further confirm that entrained gamma oscillations are not artifactual, but tied to a physiological function.

Entrained gamma oscillations do not have a pro-dyskinetic effect

The major clinically effective treatments for Parkinson's disease – dopaminergic medication [29], DBS [24], and pallidal thermolesion [30] – induce narrowband gamma oscillations across various structures in the motor network. While dopaminergic medication has been observed to induce gamma oscillations that correlate with the severity of dyskinesia [5], treatments like pallidal DBS [31] and thermolesion [32] typically suppress dyskinesia. This variance suggests that "all gamma oscillations are not alike" in their tendency to produce a prodyskinetic state. Our findings that entrained gamma oscillations appear in the majority of patients without a clinical history of dyskinesia and that pallidal stimulation entrains cortical gamma oscillations at a similar rate to subthalamic stimulation (**Figure 3.2**) suggests that entrained gamma oscillations may not be prodyskinetic. In support of this, we found that dyskinetic episodes recorded by wrist-wearable sensors tended to occur during periods without entrained gamma oscillations (**Figure 3.3**). This is in contrast to the effect of levodopa-induced gamma oscillations, studied in the exact same cohort of subjects with similar recording and analytic methods.

Understanding the statistical properties that differentiate entrained from non-entrained gamma oscillations might resolve this apparent paradox and lead to novel therapeutic interventions. Although the power of levodopa-induced gamma oscillations scales with the severity of dyskinesia, entraining levodopa-induced gamma oscillations tend to increase their higher overall power while reducing their prodyskinetic link (**Figure 3.4**), ruling out spectral power as the sole differentiating factor. Another statistical difference lies in the frequency variance: levodopa-

induced gamma oscillations have a larger variance in peak frequency than entrained gamma oscillations, possibly because levodopa-induced gamma frequency is modulated by movement, while entrainment locks gamma oscillations to a much more monotonous frequency [8]. Entraining gamma oscillations to a subharmonic of the stimulation frequency typically shifts the peak gamma frequency away from its “natural” resonant frequency in the basal ganglia thalamocortical loop, unless a subharmonic stimulation frequency happens to fall exactly at the resonant frequency. This shift may mitigate the prodyskinetic effects of levodopa-induced gamma oscillations.

Programming

As sensing-enabled stimulators are becoming widely available, oscillatory activity, such as beta-band desynchronization, is increasingly used to guide stimulator programming [33]. Given that some sensing-enabled stimulators can also detect gamma oscillations, understanding the effect of entrainment on levodopa-induced gamma oscillations may improve programming protocols. To effectively use gamma oscillations as a programming biomarker, future research should explore the optimal relationship between entrained gamma frequency and the peak levodopa-induced gamma frequency that best mitigates dyskinesia. In theory, various combinations of stimulation amplitude and frequencies can achieve similar levels of entrainment [6]. Future studies could benefit from investigating whether similar clinical outcomes are obtained from equivalent gamma entrainment achieved through different stimulation settings. The impact of entrained gamma oscillations on classic Parkinsonian motor signs, such as bradykinesia, rigidity, and tremor, warrants further examination.

Limitations

The cross-subject correlations in this study were underpowered due to the relatively small number of subjects, as is typical of invasive human studies. Our subject cohort with both entrained gamma

oscillations and nonzero wearable dyskinetic scores was small (three hemispheres), the wristwatch-style sensor captured only upper body dyskinesia and not leg dyskinesia. This study uses a different wrist-wearable watch and dyskinesia algorithm from our previous study, which compared levodopa-induced gamma oscillations to dyskinesia scores from PKG© watches. On-stimulation chronic home recordings could only be done at the clinician-selected stimulation settings, and we did not always find entrained gamma oscillations in the clinically therapeutic stimulation settings. This may be because the clinical stimulation settings were not within the range of settings that elicited entrained gamma oscillations for that subject, which could be further investigated in shorter, in-clinic studies in which entrained gamma oscillations are mapped across a wide range of stimulation settings [6]. The decreased likelihood of subthalamic gamma oscillations to entrain relative to levodopa-induced gamma oscillations may have been due to the limited recording montages available when recording from the same contact array used for stimulation. Stimulation-induced entrainment was typically studied in bilaterally implanted subjects with both sides activated, so we could not rule out the possibility that both contralateral and ipsilateral entrainment effects occurred.

FIGURES

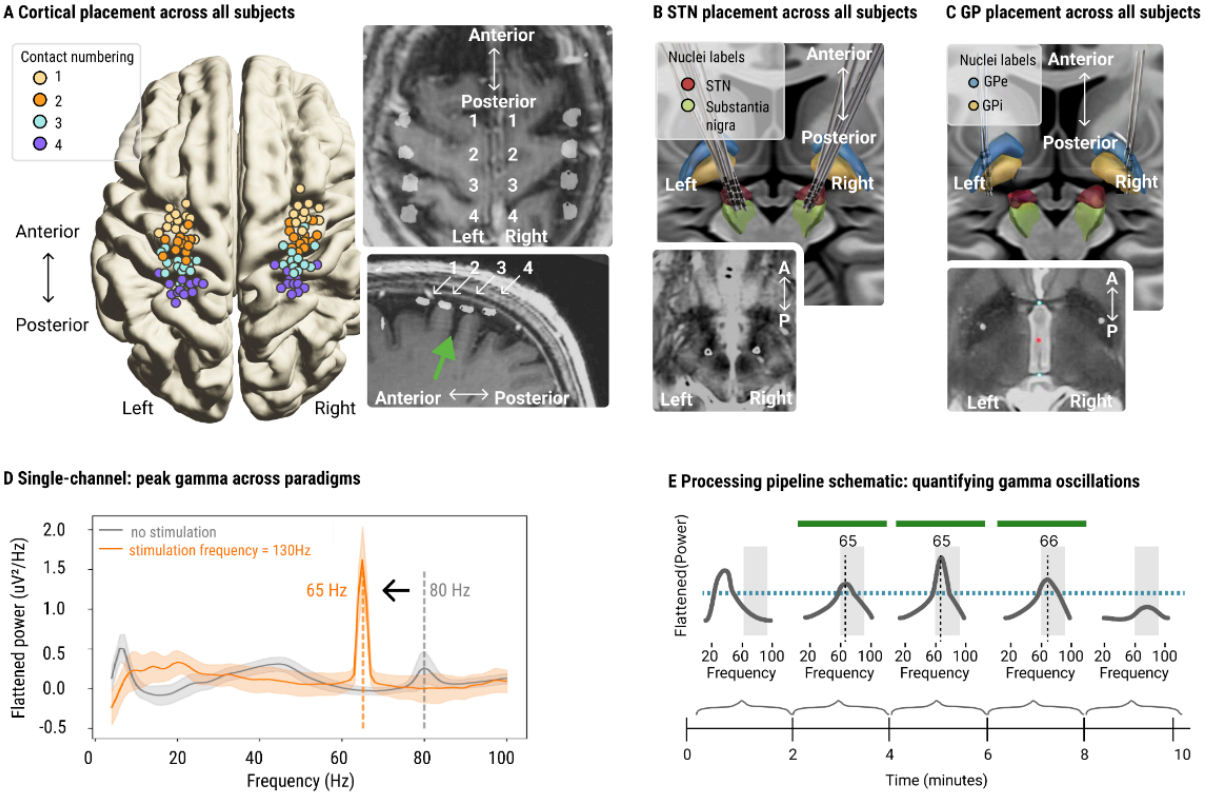

Fig. 3.1. Anatomic localization of recording contacts and signal processing pipeline
A) Cortical contact placement across subjects transformed onto a template brain, where each contact is labeled by color. An example of cortical leads in an individual subject (pt13) on a parasagittal (top row) and axial (bottom row) MRI. Each contact is labeled 1-4 in the anterior to posterior direction. The green arrow points to the central sulcus. B, C) Location of subthalamic (B) and pallidal (C) depth leads across subjects transformed onto a template brain. Each panel contains an example of leads from pt13 and pt14 on an axial MRI showing the dorsal subthalamic nucleus (B) and globus pallidus (C) at the anterior and posterior commissures. D) A single-subject example (pt13 right hemisphere) of the peak gamma frequency is shown across all epochs for each stimulation condition. The shaded regions represent one standard deviation. Prior to the onset of stimulation, the peak gamma frequency is at 80 Hz (grey). After the stimulation frequency is set to 130 Hz, the peak frequency shifts to one-half stimulation frequency, 65 Hz (orange). E) A schematic that shows how gamma oscillations are quantified in each epoch: Flattened power spectra are generated for each 2-minute neural recording epoch. Then, a threshold (horizontal blue dashed line) is computed to determine whether an epoch contains an oscillation in the gamma frequency band (frequencies from 60-90 Hz, which are included in the grey inset rectangle) by calculating two standard deviations greater than the mean at the lowest gamma frequency (60 Hz) across all epochs. Epochs with gamma are denoted with a horizontal green bar. The gamma frequency with maximal power, which we refer to as the peak frequency (vertical dotted black line) is denoted for each epoch with entrained gamma. The most commonly occurring peak gamma frequency across epochs with entrained gamma (65 Hz) is then used as the peak gamma frequency for analyses that are not epoch-specific (Supplementary Figure 3.6, Figure 3.3).

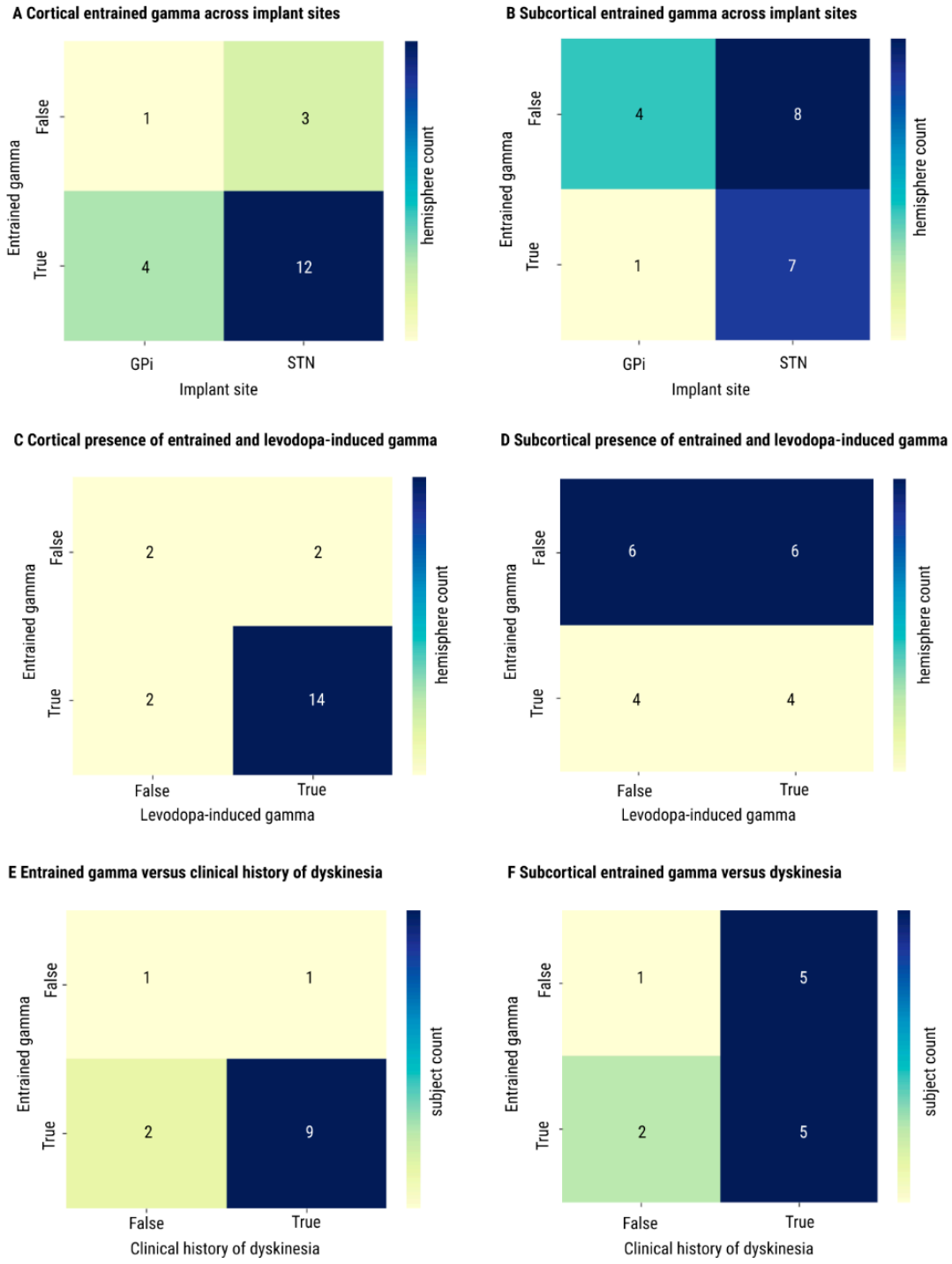

Fig. 3.2. Levodopa-induced and entrained gamma at chronic therapeutic settings across subjects: presence, anatomical localization, and relation to the clinical history of dyskinesia.

A, B) Contingency tables of the presence of cortical (A) and subcortical (B) entrained gamma across implantation sites show that cortical entrained gamma is prolifically entrained with either pallidal or subthalamic stimulation. (Figure caption continued on the next page)

(Figure caption continued from previous page) C, D) Contingency tables of hemisphere counts with the presence of levodopa-induced and entrained gamma at the cortical (C) and subcortical (D) sites show that the presence of levodopa-induced gamma and entrained gamma do not always co-occur. E, F) Contingency tables of subject counts relating the clinical history of dyskinesia with the presence of entrained gamma at the cortical (E) and subcortical (F) electrode sites show that the entrained gamma is likely to occur regardless of the clinical history of dyskinesia.

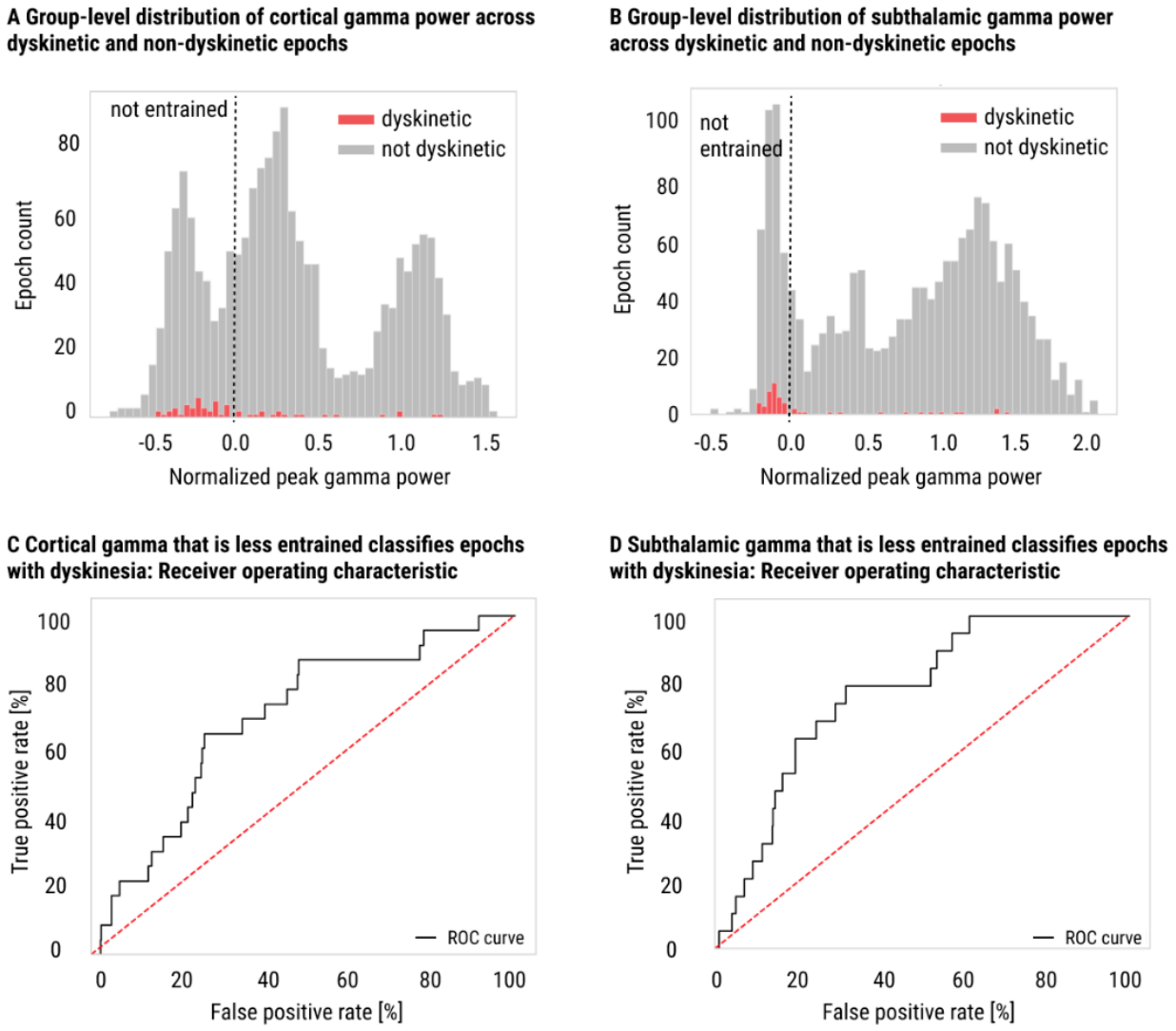

Fig. 3.3. The relationship of dyskinesia to entrained gamma across stimulation amplitude increases.

A, B) Group-level distributions of normalized gamma power (linearly shifted such that non-entrained values are negative) across epochs with cortical (A) and subthalamic (B) entrained gamma, where epochs with dyskinetic episodes are red. The cortical bimodal distribution is due to pt13's left hemisphere is entrained at a higher amplitude than the other hemispheres. Distributions of dyskinetic epochs show that 37/56 of the dyskinetic epochs occurred when cortical gamma was not entrained (normalized gamma power < 0), and 46/62 of the dyskinetic epochs occurred when subthalamic gamma was not entrained. C, D) Logistic regression shows that the presence of entrained gamma can classify the absence of a dyskinetic episode with an average area under the receiver operating characteristic curve of 0.69 for cortical (C) and 0.77 for subthalamic (D) entrained gamma.

STN = subthalamic nucleus, DBS = deep brain stimulation

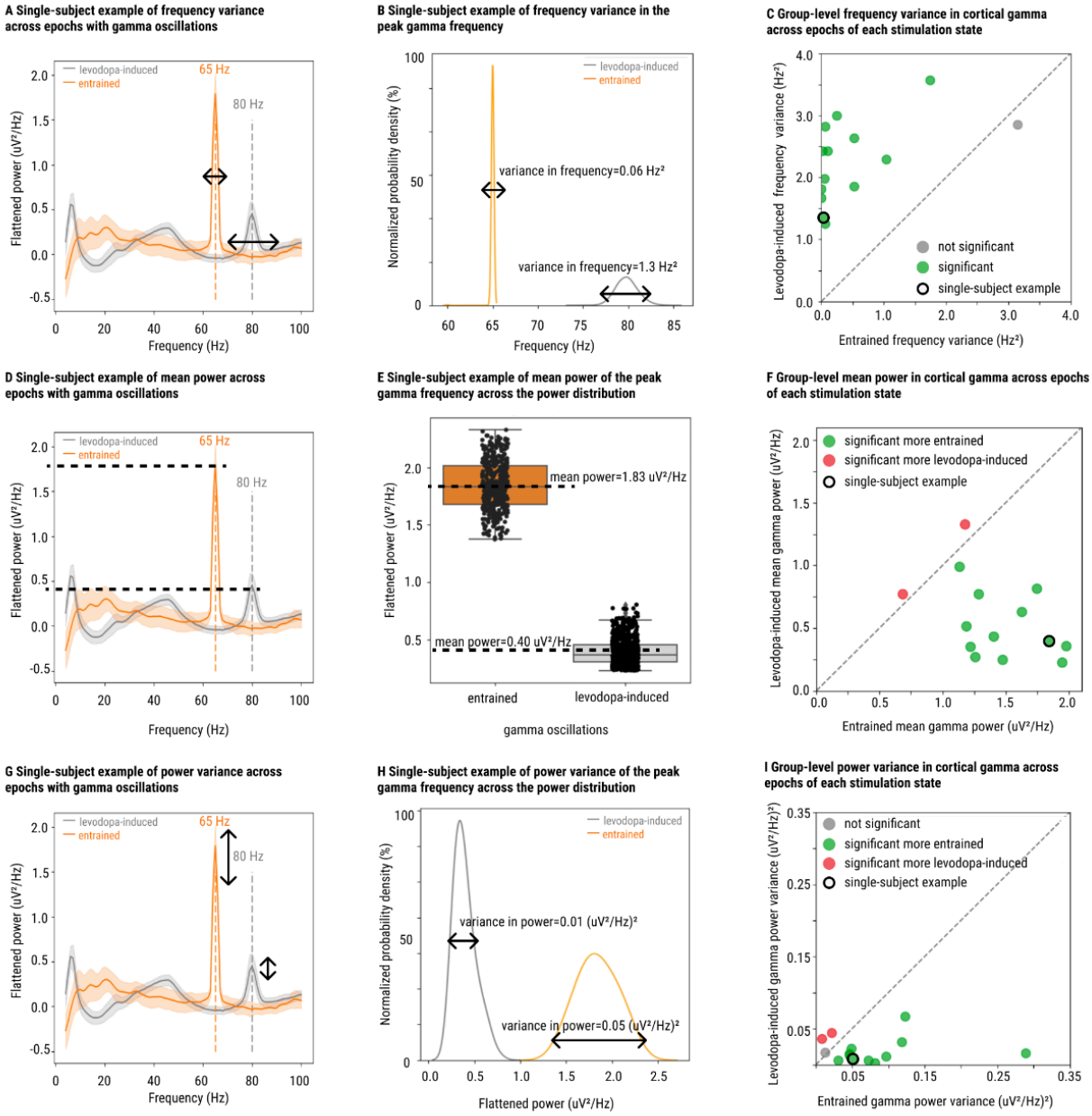

Fig. 3.4. Spectral features of cortical levodopa-induced gamma and chronic therapeutic entrained gamma: fluctuations in peak frequency and power across epochs.

A) A single-subject example (pt13 right hemisphere, STN) is shown across epochs with detected gamma oscillations for each stimulation state. Black arrows denote the distributions of peak frequencies across stimulation conditions. The remaining aspects of the plot are equivalent to Figure 3.1D. B) The same single-subject example from Figure 3.3A with probability densities of peak gamma frequency across epochs with levodopa-induced gamma in the absence of stimulation (grey) and stimulation-entrained gamma (orange). The levodopa-induced gamma frequency distribution ranges across a wider set of frequencies in relation to the entrained gamma frequency distribution. C) Group-level comparisons of the variance in peak gamma frequency across epochs for each stimulation condition at the cortical site. (Figure caption continued on the next page)

(Figure caption continued from the previous page) Most subject hemispheres have less variance in peak frequency after the onset of stimulation (green data points) using Levene's statistic with false discovery rate-corrected *p*-value < 0.05 across hemispheres. D) The same single-subject example as Figure 3.3A, with horizontal dashed lines that denote the differences in mean gamma power across stimulation conditions. E) The same single-subject example from Figure 3.3D with box plots of the gamma power at peak frequencies across epochs with levodopa-induced gamma (grey) and entrained gamma (orange) shows that entrained gamma power is larger than levodopa-induced gamma power. F) Group-level comparisons of mean power at the peak gamma frequency across stimulation conditions at the cortical site. Most subject hemispheres have more entrained mean power (green data points) using independent t-tests with false discovery-rate corrected *p*-value < 0.05 across hemispheres. A small subset of hemispheres have less entrained mean power (red data points). G) The same single-subject example as Figure 3.3D, with vertical arrows that denote the variance in mean gamma power across spectral epochs. H) The same probability densities as Figure 3.3E with arrows that show how the variance in entrained gamma is larger than the variance of levodopa-induced gamma. I) Group-level comparisons of variance in power across stimulation conditions at the cortical site. Most subject hemispheres have more variance in entrained gamma power after the onset of stimulation (green data points) using Levene's statistic with false discovery rate-corrected *p*-value < 0.05 across hemispheres. A small subset of hemispheres have less variance in entrained gamma power (red data points).

DBS = deep brain stimulation, STN = subthalamic nucleus

TABLES

Table 3.1. Subject demographics

The UPDRS dyskinesia rating is from question UPDRS IVa 4.1. The UPDRS OFF-ON score is the percent change in overall motor symptoms (UPDRS III) between clinically defined off- and on-medication states. The off-medication state is defined as 12 hours after withdrawal of antiparkinsonian medication, and the on-medication state is defined as 30-45 minutes after a supratherapeutic dose of carbidopa-levodopa.

UPDRS = Unified Parkinson's Disease Rating Scale, MOCA = Montreal Cognitive Assessment, OFF = off medication, ON = on medication, m = male, f = female, pt = subject, GP = globus pallidus, STN = subthalamic nucleus

Study id	Motor signs (yrs)	UPDRS (Off)	UPDRS IV	Levodopa (mg)	Subject age (yrs)	Gender	MOCA	UPDRS (OFF-ON)	Implant site	Implanted sides	Neural recordings > 5mo DBS onset	Neural recordings 0-2mo DBS onset	Wearable recordings 0-2mo DBS onset
pt1	7	49	4	1425	54	m	26	0.9	STN	bilateral	Yes	No	No
pt2	9	66	1	900	66	m	29	0.64	GP	unilateral	Yes	No	No
pt3	19	45	1	955	63	m	30	0.51	STN	bilateral	Yes	No	No
pt4	4	41	1	1314	40	m	30	0.65	STN	bilateral	Yes	No	No
pt5	12	44	2	2100	58	m	27	0.75	STN	bilateral	Yes	No	No
pt6	10	39	2	1755	48	m	27	0.59	GP	bilateral	Yes	Yes	No
pt7	13	89	0	1083	64	f	27	0.53	GP	bilateral	Yes	No	No
pt8	7	29	2	1525	71	m	26	0.58	STN	bilateral	Yes	No	No
pt9	10	34	2	800	58	m	28	0.73	STN	bilateral	Yes	Yes	No
pt10	4	31	0	1580	65	m	26	0.51	GP	unilateral	Yes	Yes	Yes
pt11	6	35	0	570	61	m	27	0.67	STN	bilateral	Yes	Yes	Yes
pt12	12	32	1	920	45	m	26	0.84	STN	bilateral	Yes	Yes	Yes
pt13	7	49	2	2031	67	m	27	0.76	STN	bilateral	Yes	Yes	Yes
pt14	8	49	0	1213	51	m	27	0.61	GP	bilateral	No	Yes	Yes
pt15	13	31	1	1036	73	m	28	0.67	STN	bilateral	No	Yes	Yes

Table 3.2. Presence of levodopa-induced and entrained gamma across study subjects.
The implantation sites and presence of levodopa-induced and entrained gamma at least 5 months after deep brain stimulation onset (True or False) are shown across sites for all subject hemispheres.

		presence of pre-stimulation gamma		presence of chronic entrained gamma	
subject hemispheres	**implantation site**	**cortical**	**subcortical**	**cortical**	**subcortical**
pt1l	STN	True	True	True	False
pt1r	STN	True	True	True	False
pt2l	GP	True	False	True	False
pt3l	STN	False	False	False	False
pt3r	STN	True	False	False	False
pt4l	STN	True	False	True	True
pt4r	STN	True	True	True	True
pt5l	STN	True	True	True	False
pt5r	STN	True	False	True	False
pt6r	GP	True	False	True	False
pt7l	GP	True	False	True	False
pt7r	GP	True	False	True	True
pt8l	STN	True	True	False	False
pt9l	STN	True	False	True	False
pt10l	GP	False	False	False	False
pt11l	STN	True	False	False	True
pt11r	STN	True	False	True	True
pt12l	STN	True	True	True	True
pt13l	STN	True	True	True	True
pt13r	STN	True	True	True	True

SUPPLEMENTAL FIGURES

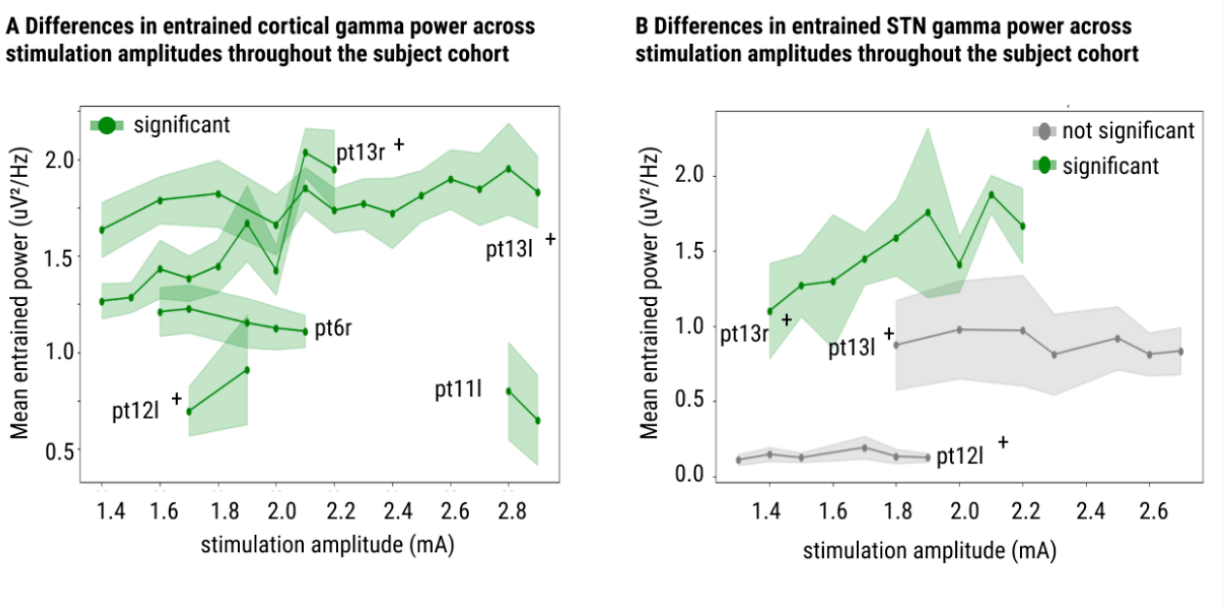

Fig. 3.5: The power of entrained gamma across stimulation amplitude increases
A, B) Comparisons of entrained gamma power across stimulation amplitudes at the cortical (A) and subthalamic (B) sites from the cohort. Error bars are included with one standard deviation. Gamma power in 5/5 hemispheres at the cortical site (A) differs across stimulation amplitudes using Spearman's rho with false discovery rate-corrected p-value<0.05 (green-labeled data points) across subject hemispheres. Gamma power in two of the three subthalamic hemispheres (B) did not differ (grey-labeled data points). Wearable dyskinesia data was also recorded across a subset of annotated subjects (+).

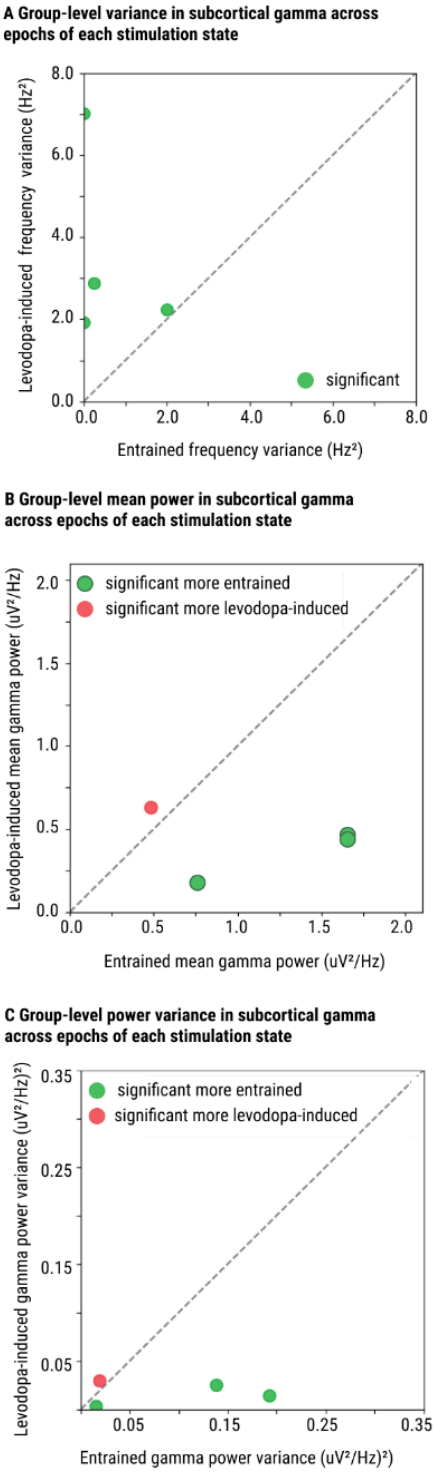

Fig. 3.6: Spectral features of subcortical levodopa-induced gamma and chronic therapeutic entrained gamma: fluctuations in peak frequency and power across epochs. A) The same statistical comparison from Figure 3.3C for subcortical gamma. B) The same statistical comparison from Figure 3.3F for subcortical gamma. C) The same statistical comparison from Figure 3.3I for subcortical gamma.

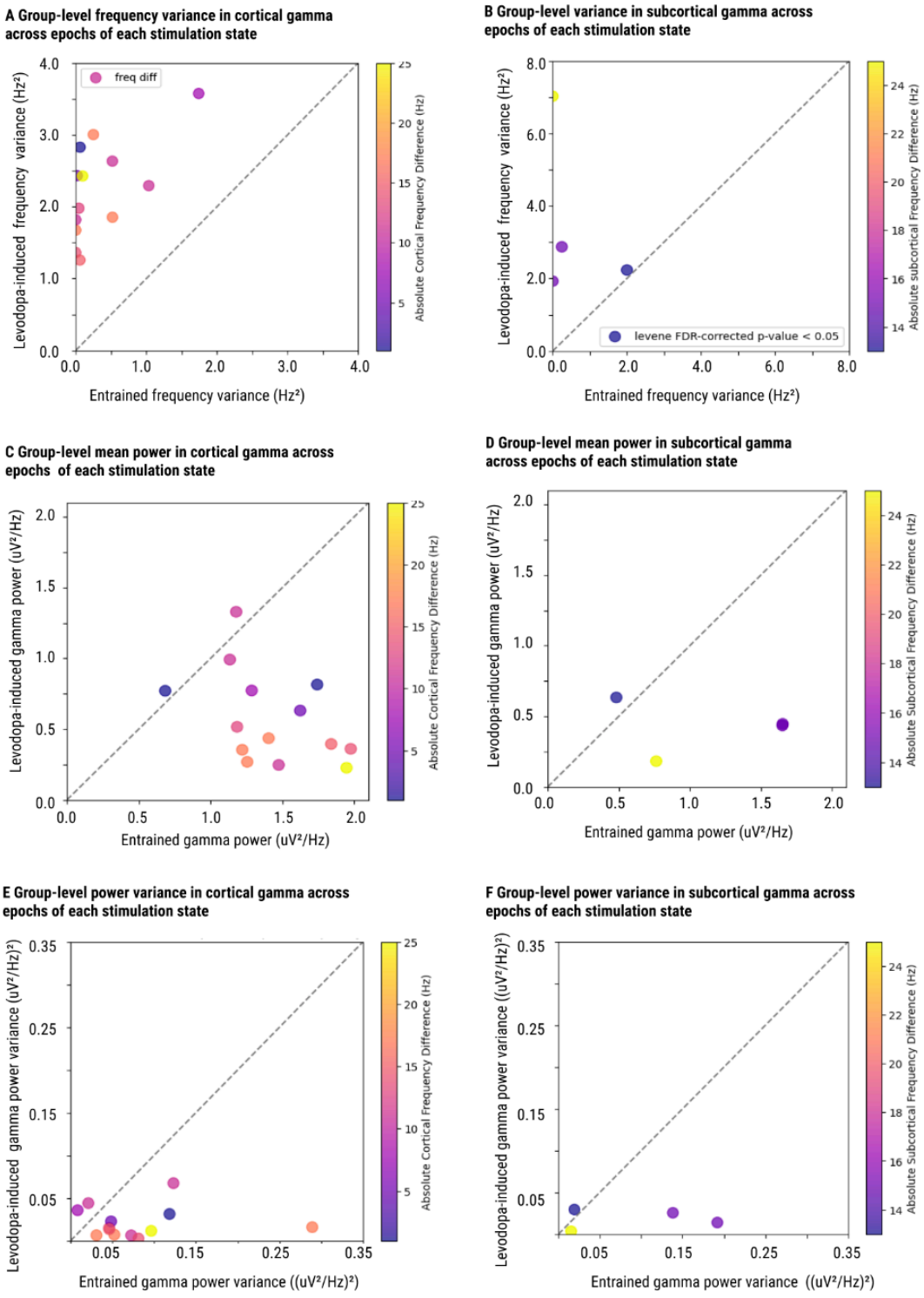

Fig. 3.7: The relationship between the difference in peak gamma frequency between levodopa-induced gamma and entrained gamma statistical properties

A, B) The same results from Figure 3.3C-D, with data points that are color-labeled by the difference between the cortical (A) and subcortical (B) peak gamma frequency in the levodopa-induced gamma oscillation and entrained gamma. (Figure caption continued on the next page)

(Figure captaion continued from the previous page) Smaller differences are darker and larger differences are lighter. C, D) The same results from Figure G-H, where the data points are color-labeled using the same method as Supplemental Figure A-B for the differences in cortical (C) and subcortical (D) peak gamma frequency. E, F) The same results from Figure 3.3K-L, where the data points are color-labeled using the same method as Supplemental Figure A-B for the differences in cortical (E) and subcortical (F) peak gamma frequency.

REFERENCES

1. Güttler C, Altschüler J, Tanev K, Böckmann S, Haumesser JK, Nikulin VV, et al. Levodopa-Induced Dyskinesia Are Mediated by Cortical Gamma Oscillations in Experimental Parkinsonism. Mov Disord. 2021;36: 927–937.

2. Halje P, Tamtè M, Richter U, Mohammed M, Cenci MA, Petersson P. Levodopa-induced dyskinesia is strongly associated with resonant cortical oscillations. J Neurosci. 2012;32: 16541–16551.

3. Salvadè A, D'Angelo V, Di Giovanni G, Tinkhauser G, Sancesario G, Städler C, et al. Distinct roles of cortical and pallidal β and γ frequencies in hemiparkinsonian and dyskinetic rats. Exp Neurol. 2016;275 Pt 1: 199–208.

4. Swann NC, de Hemptinne C, Miocinovic S, Qasim S, Ostrem JL, Galifianakis NB, et al. Chronic multisite brain recordings from a totally implantable bidirectional neural interface: experience in 5 patients with Parkinson's disease. J Neurosurg. 2018;128: 605–616.

5. Olaru M, Cernera S, Hahn A, Wozny TA, Anso J, de Hemptinne C, et al. Motor network gamma oscillations in chronic home recordings predict dyskinesia in Parkinson's disease. Brain. 2024. doi:10.1093/brain/awae004

6. Sermon JJ, Olaru M, Ansó J, Cernera S, Little S, Shcherbakova M, et al. Sub-harmonic entrainment of cortical gamma oscillations to deep brain stimulation in Parkinson's disease: Model based predictions and validation in three human subjects. Brain Stimul. 2023;16: 1412–1424.

7. Gilron R, Little S, Perrone R, Wilt R, de Hemptinne C, Yaroshinsky MS, et al. Long-term wireless streaming of neural recordings for circuit discovery and adaptive stimulation in

individuals with Parkinson's disease. Nature Biotechnology. 2021. pp. 1078–1085. doi:10.1038/s41587-021-00897-5

8. Wiest C, Torrecillos F, Tinkhauser G, Pogosyan A, Morgante F, Pereira EA, et al. Finely-tuned gamma oscillations: Spectral characteristics and links to dyskinesia. Experimental Neurology. 2022. p. 113999. doi:10.1016/j.expneurol.2022.113999

9. Stanslaski S, Herron J, Chouinard T, Bourget D, Isaacson B, Kremen V, et al. A Chronically Implantable Neural Coprocessor for Investigating the Treatment of Neurological Disorders. IEEE Trans Biomed Circuits Syst. 2018;12: 1230–1245.

10. Gilron R, Little S, Perrone R, Wilt R, de Hemptinne C, Yaroshinsky MS, et al. Long-term wireless streaming of neural recordings for circuit discovery and adaptive stimulation in individuals with Parkinson's disease. Nat Biotechnol. 2021;39: 1078–1085.

11. Follett KA, Weaver FM, Stern M, Hur K, Harris CL, Luo P, et al. Pallidal versus subthalamic deep-brain stimulation for Parkinson's disease. N Engl J Med. 2010;362: 2077–2091.

12. Okun MS, Fernandez HH, Wu SS, Kirsch-Darrow L, Bowers D, Bova F, et al. Cognition and mood in Parkinson's disease in subthalamic nucleus versus globus pallidus interna deep brain stimulation: the COMPARE trial. Ann Neurol. 2009;65: 586–595.

13. Hammer LH, Kochanski RB, Starr PA, Little S. Artifact Characterization and a Multipurpose Template-Based Offline Removal Solution for a Sensing-Enabled Deep Brain Stimulation Device. Stereotact Funct Neurosurg. 2022;100: 168–183.

14. Horn A, Li N, Dembek TA, Kappel A, Boulay C, Ewert S, et al. Lead-DBS v2: Towards a comprehensive pipeline for deep brain stimulation imaging. Neuroimage. 2019;184: 293–316.

15. Davis TS, Caston RM, Philip B, Charlebois CM, Anderson DN, Weaver KE, et al. LeGUI: A Fast and Accurate Graphical User Interface for Automated Detection and Anatomical Localization of Intracranial Electrodes. Frontiers in Neuroscience. 2021. doi:10.3389/fnins.2021.769872

16. Fischl B, Sereno MI, Tootell RBH, Dale AM. High-resolution intersubject averaging and a coordinate system for the cortical surface. Human Brain Mapping. 1999. pp. 272–284. doi:10.1002/(sici)1097-0193(1999)8:4<272::aid-hbm10>3.0.co;2-4

17. Xiao Y, Fonov V, Bériault S, Al Subaie F, Mallar Chakravarty M, Sadikot AF, et al. Multi-contrast unbiased MRI atlas of a Parkinson's disease population. International Journal of Computer Assisted Radiology and Surgery. 2015. pp. 329–341. doi:10.1007/s11548-014-1068-y

18. Powers R, Etezadi-Amoli M, Arnold EM, Kianian S, Mance I, Gibiansky M, et al. Smartwatch inertial sensors continuously monitor real-world motor fluctuations in Parkinson's disease. Science Translational Medicine. 2021. p. eabd7865. doi:10.1126/scitranslmed.abd7865

19. Buitinck L, Louppe G, Blondel M, Pedregosa F, Mueller A, Grisel O, et al. API design for machine learning software: experiences from the scikit-learn project. arXiv [cs.LG]. 2013. Available: http://arxiv.org/abs/1309.0238

20. Crone NE, Miglioretti DL, Gordon B, Lesser RP. Functional mapping of human sensorimotor cortex with electrocorticographic spectral analysis. II. Event-related synchronization in the gamma band. Brain. 1998;121 (Pt 12): 2301–2315.

21. Manning JR, Jacobs J, Fried I, Kahana MJ. Broadband shifts in local field potential power spectra are correlated with single-neuron spiking in humans. J Neurosci. 2009;29: 13613–13620.

22. Miller EK, Lundqvist M, Bastos AM. Working Memory 2.0. Neuron. 2018;100: 463–475.

23. Fernandez-Ruiz A, Sirota A, Lopes-Dos-Santos V, Dupret D. Over and above frequency: Gamma oscillations as units of neural circuit operations. Neuron. 2023;111: 936–953.

24. Swann NC, de Hemptinne C, Miocinovic S, Qasim S, Wang SS, Ziman N, et al. Gamma Oscillations in the Hyperkinetic State Detected with Chronic Human Brain Recordings in Parkinson's Disease. J Neurosci. 2016;36: 6445–6458.

25. Oehrn CR, Cernera S, Hammer LH, Shcherbakova M, Yao J, Hahn A, et al. Personalized chronic adaptive deep brain stimulation outperforms conventional stimulation in Parkinson's disease. medRxiv. 2023. doi:10.1101/2023.08.03.23293450

26. Miocinovic S, de Hemptinne C, Chen W, Isbaine F, Willie JT, Ostrem JL, et al. Cortical Potentials Evoked by Subthalamic Stimulation Demonstrate a Short Latency Hyperdirect Pathway in Humans. J Neurosci. 2018;38: 9129–9141.

27. Li Q, Ke Y, Chan DCW, Qian Z-M, Yung KKL, Ko H, et al. Therapeutic deep brain stimulation in Parkinsonian rats directly influences motor cortex. Neuron. 2012;76: 1030–1041.

28. Sermon JJ, Benjaber M, Duchet B, Anso J, Olaru M, Starr PA, et al. 1:2 entrainment is not a device-induced artefact, except when it is. Brain Stimul. 2024;17: 149–151.

29. Brown P, Oliviero A, Mazzone P, Insola A, Tonali P, Di Lazzaro V. Dopamine dependency of oscillations between subthalamic nucleus and pallidum in Parkinson's disease. J Neurosci. 2001;21: 1033–1038.

30. de Hemptinne C, Wang DD, Miocinovic S, Chen W, Ostrem JL, Starr PA. Pallidal thermolesion unleashes gamma oscillations in the motor cortex in Parkinson's disease. Mov Disord. 2019;34: 903–911.

31. Volkmann J, Allert N, Voges J, Sturm V, Schnitzler A, Freund H-J. Long-term results of bilateral pallidal stimulation in Parkinson's disease. Ann Neurol. 2004;55: 871–875.

32. Vitek JL, Bakay RAE, Freeman A, Evatt M, Green J, McDonald W, et al. Randomized trial of pallidotomy versus medical therapy for Parkinson's disease. Ann Neurol. 2003;53: 558–569.

33. Sandoval-Pistorius SS, Hacker ML, Waters AC, Wang J, Provenza NR, de Hemptinne C, et al. Advances in Deep Brain Stimulation: From Mechanisms to Applications. J Neurosci. 2023;43: 7575–7586.

Chapter 4:

Deep brain stimulation entrainment of gamma oscillations can be modelled by neuronal population models

INTRODUCTION

Deep Brain Stimulation (DBS) is a form of invasive neuromodulation, where electrical impulses are delivered to specific brain regions by implanted electrodes. In the context of Parkinson's disease (PD), high-frequency DBS (130-180 Hz) is primarily used to alleviate motor symptoms (bradykinesia, rigidity and tremor [1-2]) when medications provide inadequate benefit. While a diverse range of effects of DBS have been observed in both behavior and neuronal rhythms, the mechanisms underlying these responses are not fully understood.

Activity in the gamma band (approximately 30 to 100 Hz) has become a target for neuromodulation as it is associated with various cognitive performance features [3] as well as motor control [4]. However, it is necessary to distinguish between broadband gamma and finely-tuned gamma (FTG). While broadband gamma reflects neuronal spiking activity over a broad frequency range (which can be as wide as 30-200 Hz), FTG represents narrowband oscillatory activity with a peak frequency between 60-90 Hz [5, 6]. Here, we will be focusing on FTG oscillations, which were first revealed through invasive recordings of the basal ganglia in PD patients on antiparkinsonian medications [7, 8]. These have been thought to represent a “prokinetic” brain rhythm, in contrast to “antikinetic” beta rhythms (13-30 Hz). Recently, prominent FTG oscillations have been found during invasive recordings from motor cortical areas in PD [5, 9, 10], and may be associated with dyskinesias. Additionally, similar cortical oscillations have been observed in rat models of dyskinesia [11, 12].

Entraining FTG in patients with PD has potential to be beneficial (in the absence of dyskinesia). Transcranial alternating current stimulation (tACS) at gamma frequency was observed to increase motor velocity in PD, while tACS at beta frequency saw it decrease [13]. It was hypothesized that entrainment (specifically 1:1 entrainment at stimulation frequency) of both gamma and beta oscillations would explain this observation by enhancing “prokinetic” and “antikinetic” rhythms, respectively. Additionally, a shifted FTG peak frequency has been noted in the motor cortex in response to high-frequency DBS of the STN [5, 10, 14]. The gamma peak, off-stimulation between 65 and 80 Hz, locks to the half harmonic of stimulation, corresponding to 1:2 entrainment. Together, these studies suggest that the entrainment of FTG by DBS could play a role in ameliorating PD-associated motor symptoms. Moreover, the half-harmonic lock indicates that the response to stimulation is complex and goes beyond entraining rhythms solely at the frequency of stimulation or suppressing them. However, there is currently no theoretical understanding of 1:2 gamma entrainment in PD and generally no framework to predict the occurrence of specific entrainment regimes in response to brain stimulation.

In this study, we use a model-based approach that utilizes chronic invasive cortical recordings in PD patients to predict the properties of entrainment of cortical activity by basal ganglia DBS. We postulate that by constraining the parameters of a neuronal population model, it will be possible to predict stimulation parameters that lead to 1:2 gamma entrainment for patients with off-stimulation (medication induced) FTG. We provide a theoretical introduction to 1:2 gamma entrainment through the concepts of Arnold tongues (regions of entrainment in the stimulation frequency and amplitude space) and rotation number (the ratio of the average number of oscillation cycles to stimulation pulses). We proceed to develop a patient-specific approach by fitting a model representing interacting neural populations, the Wilson-Cowan model, to features of invasive chronic electrocorticography (ECoG) data recorded off stimulation from patients with PD. Using the fitted-models, we predict the regions of 1:2 entrainment in the stimulation parameter

(frequency and amplitude) space. We proceed to verify key features of the 1:2 entrainment regions with follow-up recordings from the same patients. Lastly, these results are discussed and the implications are highlighted for future stimulation therapies.

METHODS

Arnold tongues and rotation number

The frequency locking (entrainment) behavior of a neural rhythm to external stimulation across stimulation frequency and amplitude can be described by Arnold tongues [15]. Arnold tongues are the regions in the stimulation frequency and amplitude space where frequency-locking occurs. Frequency locking is observed when a rotation number of the form p:q, where p and q are coprime integers (i.e. no integer other than 1 divides both p and q), is maintained for several stimulation periods. In general, the rotation number may not be a ratio of integers (it is a ratio of integers only when there is frequency locking), and corresponds to the average number of oscillatory cycles achieved by the rhythm between two periodic pulses of the driving stimulation.

Previously, Arnold tongues have been used to describe 1:1 entrainment in response to noninvasive neuromodulation [16-19]. Depending on the system considered and the stimulation waveform, Arnold tongues can theoretically exist for various rotation numbers, including p:q with large p and/or q. However, in real systems, often only the tongues corresponding to the most stable rotation numbers, with low p and q values, will be observed. Arnold tongues often have different shapes for different dynamical systems. Generally, an Arnold tongue expands in width across larger frequency ranges as stimulation amplitude increases. This continues up until an amplitude where the tongue may border a region with another frequency-locking ratio or lose entrainment altogether.

Data collection

Human neural data were collected from three patients with Parkinson's disease (**Table 4.1**). Cortical data off-stimulation were collected to fit the Wilson-Cowan model. On-stimulation data (subcortical stimulation) at variable stimulation frequencies and amplitudes were then used to validate predictions from the fitted model. Patient clinical symptoms assessed 90 days pre-operation are summarized in **Table 4.2**. Patients were selected for participation in this study based on the presence of a peak in gamma band activity in the primary motor cortex off-stimulation (which is a necessary condition to fit a model to off-stimulation gamma activity). Patients were diagnosed with idiopathic Parkinson's disease by a movement disorders neurologist and underwent DBS surgery of either the subthalamic nucleus (STN) or globus pallidus (GP). Target choice was based on the patients' neuropsychological test results, which indicated pallidal implantation for patients with mild cognitive impairment or history of clinical depression [20, 21]. Patients were bilaterally implanted with the Medtronic Summit RC+S bidirectional neural interface (clinicaltrials.gov identifier NCT03582891, USA FDA investigational device exemption number 180097, IRB number 18-24454) quadripolar cylindrical leads into subcortical nuclei (Medtronic model 3389 or 3387 for STN and pallidum, respectively), and subdural paddle-type leads over the primary motor cortex in the subdural space (Medtronic model 0913025), see **Figure 4.1 A1-3** for RCS02, **Figure 4.1 B1-3** for RCS10 and **Figure 4.1C** 1-2 for RCS18. Implantations of subcortical leads were performed using frame-based stereotaxy, and confirmed by intraoperative cone beam CT and microelectrode recording (MER) in the awake state using standard methods in RCS02 and RCS10 [22], and by intraoperative cone-beam CT alone in RCS18 [23]. For RCS10, the active contact array was localized in the GP using MER mapping of single-unit cells to traverse the postero-lateral regions of the external globus pallidus (GPe) and globus pallidus internus (GPi), **Figure 4.1B1**. For RCS02, the motor territory of the STN was confirmed by eliciting movement-related single-cell discharge patterns during MER

when the DBS lead was placed with the middle two contacts in dorsal STN. Surgical placement of subdural cortical paddles has been previously described in detail [24]. Similar to subcortical contacts, localization of subdural paddles was confirmed by computationally fusing a postoperative CT scan to the preoperative planning MRI scan, see **Figure 4.1**.

Prior to the initiation of standard therapeutic DBS, we recorded four-channel LFPs of the cortical, and pallidal (n = 1) or subthalamic (n = 2) sites of each hemisphere between two and four weeks post implantation. The data were streamed from patients during normal activities of daily living and while on their schedule of antiparkinsonian medication. Only the cortical prestimulation data were used to fit the model. The recording methods and data processing were similar to those described by Gilron et al. [10]. Briefly, neural data were recorded from subcortical (STN or GP, as per patient's DBS target; Figure 4.1A1, B2, C1) and cortical (contact pairs 11-9 and 10-8 for RCS02, 11-10 and 9-8 for RCS10 and RCS18, Figure 4.1 B3, C2) sensing electrodes via a patient-facing graphical user interface application. Neural data were collected at 250 Hz. The Summit RC+S has two onboard filters applied after digitization that were set to a high pass of 0.85 Hz and a low pass of 450 Hz before amplification followed by 1700 Hz low pass filter after amplification.

After several months of continuous subthalamic (n = 2) or pallidal (n = 1) stimulation at clinically optimized parameters, we conducted a follow-up in-clinic recording session with each subject in their on-medication state to validate the initial model predictions. During recordings, we cycled through a range of stimulation frequencies and amplitudes to further explore the DBS parameter space (**Table 4.1**). In each participant, we delivered stimulation at their clinical contact in the STN or GP, while recording from cortical sensing contacts 11-10 and 9-8. In each trial, we tested a single frequency-amplitude combination for 30 seconds while the patient was at rest. Sessions lasted two to three hours, and the number of data points collected was different in each patient

due to patient fatigue. While it is not clear if fatigue plays into 1:2 entrainment, the testing order of stimulation parameters was not predetermined, making the point at which each tongue boundary was tested effectively random. In particular, the top tongue boundaries were not tested only later in the sessions when we would expect fatigue to be higher. It should also be acknowledged that non-stationary medication levels, associated with intermittent medication intake, could affect 1:2 entrainment at certain stimulation parameters. Filter settings for cortical contacts were the same as during off-stimulation recordings.

RESULTS

We fit the Wilson-Cowan model, a model of interacting neuronal populations, to prestimulation ECoG recordings in three patients with PD. Using the fitted models, we predicted for each patient the stimulation parameters leading to 1:2 entrainment of FTG. We then verified these predictions in follow-up on-stimulation recordings from the same patients.

Prediction of 1:2 entrainment of FTG using a fitted Wilson-Cowan model

For all patients, the Wilson-Cowan model fitted to the patient's prestimulation cortical FTG successfully reproduced all three FTG features. The top ranked model parameter sets had average $R2$ values (across 50 simulations) of 0.961, 0.944 and 0.868 for RCS02, RCS10 and RCS18 respectively, with good or satisfactory fits across all three The fitted models oscillate at the patient's FTG natural frequency (between 75-80 Hz in the absence of stimulation).

In the presence of low amplitude stimulation, all three models display a 1:2 Arnold tongue (i.e. entrainment region) around a stimulation frequency between 150-160 Hz (the 1:2 tongue stems from twice the natural frequency of the model). This is shown by the green 1:2 Arnold tongue in **Figure 4.2 A**, **D** and **G**, which correspond to a region of 1:2 entrainment (constant rotation number of 0.5). The 1:2 Arnold tongue is bordered by a larger zone of 1:1 entrainment, indicated by the

red regions. When stimulation is provided at 130 Hz (indicated by the black line), the excitatory population can be entrained at 65 Hz for a range of stimulation amplitudes. In all three fitted models, the 1:2 tongue is left leaning (more of the tongue is to the left of the frequency it stems from, see **Figure 4.2 A**, **D** and **G**), which suggests that stimulation frequencies lower than the stem of the tongue are more likely to lead to 1:2 entrainment. The range of stimulation frequencies that can give rise to 1:2 entrainment (given an appropriate stimulation amplitude) is the narrowest in RCS02 (110-160 Hz), and the broadest in RCS18 (60-160 Hz). In all cases, we note that increasing stimulation amplitude above a certain value will result in the loss of 1:2 entrainment. The left lean of the 1:2 Arnold tongues does not depend on whether stimulation is applied to the inhibitory population or the excitatory population. Additionally, the 1:2 entrainment region exhibits a left lean regardless of whether the stimulation being applied is in the form of a single time step pulse train, pulse trains with various recharge durations or more complicated waveforms. Additionally, the fitted Wilson-Cowan models predict that the highest spectral peaks will occur at the lowest frequencies for which 1:2 entrainment arises, as seen in **Figure 4.3 B**, **E** and **H**.

DISCUSSION

Here, we studied entrainment of cortical FTG by basal ganglia deep brain stimulation, using a computational model in conjunction with sensorimotor cortex ECoG sensed from chronically implanted bidirectional interfaces in three patients with PD. We show that through fitting a model of interacting neuronal populations to off-stimulation data, we can predict the region of stimulation parameters (frequency and amplitude) for which 1:2 entrainment is possible. Our model predicts that 1:2 entrainment is lost when stimulation amplitude is increased above a certain value. Furthermore, the 1:2 Arnold tongue is generally left leaning, implying that 1:2 entrainment can be achieved for stimulation frequencies markedly lower than twice the frequency of the natural gamma rhythm, but not for frequencies markedly higher. Lastly, the model further predicts that there would be a greater entrained gamma power at lower stimulation frequencies that result in

1:2 entrainment. Data recorded during therapeutic neurostimulation, after the modelling results were obtained, showed 1:2 Arnold tongues that generally validate these predictions. Hence, the model can capture a range of sub-harmonic entrainment features without being constrained by entrainment data. The work indicates that effects of DBS at clinically relevant stimulation parameters can be understood using the conceptual framework of a mathematical model representing interacting neural populations being externally perturbed by the periodic neurostimulation.

Entrainment and adaptive DBS

By solely analyzing the presence of 1:2 entrainment, we avoid the prominent artifact at stimulation frequency. Hence, this analysis of the data provides a valuable insight into the neuronal responses to stimulation. Bounding the 1:2 tongue from above, as we lose 1:2 entrainment at increased stimulation amplitudes (all three patients at 150 Hz), provides further evidence that the gamma peak at half stimulation frequency is unlikely to be artifactual. This is aligned with the model prediction that 1:2 entrainment will be lost when amplitude is increased beyond a certain point. Additionally, the model predicts that parameter changes that result in the loss of 1:2 entrainment would see a transition to 1:1 entrainment. However, the presence of 1:1 entrainment is difficult to assess as the resulting power spectral peak can be masked by the stimulation artifact.

1:2 entrainment presents opportunities for adaptive deep brain stimulation (aDBS). aDBS relies on a closed-loop control policy where a biomarker is used to adjust DBS parameters. Cortical gamma-band activity was shown to be a promising candidate biomarker for aDBS [5], [10], and stimulation-entrained gamma has been used to control clinically successful aDBS [26]. Additionally, entrainment in the gamma frequency band has been linked with dyskinesia [5]. Moreover, 1:2 entrainment has an entirely predictable frequency, which simplifies implementation,

particularly for chronic devices with limited spectral recording frequency bands (such as the Medtronic Percept).

Entrainment in the Wilson-Cowan model

1:2 entrainment is not an intrinsic property of the Wilson-Cowan model (large regions of parameter space do not lead to 1:2 entrainment). Additionally, if the parameters of the Wilson-Cowan model do produce 1:2 entrainment, the 1:2 tongue can also be right leaning or symmetrical about the central frequency. Hence, the parameters of the Wilson-Cowan model need to be tuned to reproduce the data. Among the top-ranked Wilson-Cowan fits, there is some variability between the parameter sets and the corresponding entrainment predictions. This demonstrates that the model parameters are non-identifiable. However, as the best fits converge on results that all include a left leaning 1:2 tongue and given the validation of some of the model predictions by follow-up recordings, we can conclude that the fitted model remains a good candidate to make predictions for future investigations. It would be possible to fit Wilson-Cowan model parameters to on-stimulation entrainment data, which may or may not reproduce off-stimulation data. This is not something we are investigating as more value is provided by predicting the response from off-stimulation fits.

While only 1:2 entrainment is investigated here, entrainment will occur at other sub-harmonics of stimulation if there is a neuronal rhythm present to entrain and the corresponding Arnold tongue is large enough to encompass the neuronal rhythm. Similarly to 1:2 entrainment, sub-harmonic entrainment at every harmonic of stimulation is not an intrinsic property of Wilson-Cowan models. However, other sub-harmonic entrainment ratios can be observed for certain model parameter sets. By increasing stimulation frequency, for example to around 225 Hz, it would be possible to investigate other sub-harmonic entrainment ratios such as 1:3 entrainment of the FTG rhythm.

The observation of the highest spectral peaks occurring at the lowest frequencies of stimulation in the model may be somewhat counter-intuitive, since one could expect more stimulation energy to provide more oscillatory power. However, due to the increased time between successive pulses of stimulation at lower frequencies, the trajectory of the population activity covers a larger distance in phase space. This means that the range of values that activity reaches for each population is greater, producing a higher power spectral peak for the given resultant frequency. Population activity having a larger range can also be interpreted as there being greater synchrony of neurons within the populations, as increased peak firing rates and decreased minima suggest more neurons are firing together.

Because the endogenous FTG is stronger for RCS02 and stimulation amplitude is lower, more variability in the on-stimulation entrained power is expected, which may explain the worse model performance for this patient (**Figure 4.2**). Specifically, the off-stimulation features of RCS02 show a higher gamma peak in the PSD, a larger peak amplitude of the envelope PDF, and a shallower slope at lower amplitudes of the envelope PDF than RCS10 and RCS18. Therefore, it is expected to be more difficult to perturb the underlying oscillators away from the natural gamma frequency of the network, which leads to a 1:2 tongue with a much smaller width over the stimulation frequency axis. Given that the stimulation amplitude used for RCS02 is also smaller than for the other patients (see **Figure 4.2**), the strength of the endogenous FTG relative to stimulation amplitude is significantly greater, and natural fluctuations in the endogenous FTG have a larger impact on the power measured. This leads to more variability in **Figure 4.2C** and a worse correspondence with the fitted model. However, the fitted model still manages to predict a 1:2 tongue with a smaller area and a significantly lower top boundary compared to the other models, as observed in the entrainment data. Hence, the model can predict features of the 1:2 tongue even with stronger endogenous rhythms.

Our modelling approach is based on ECoG recordings, but alternatives could be explored in future work. While non-invasive electroencephalography (EEG) has been used to study cortical gamma cross-frequency coupling with DBS [25], ECoG recordings have a markedly better signal-to-noise ratio. Thus, whether FTG features obtained from EEG are sufficiently accurate to enable reliable FTG entrainment predictions through model fitting requires further investigation.

Study limitations

As a pilot study, there was no systematic mapping of tongue boundaries, with large regions of untested parameters for some patients and a non-standardized approach to selecting stimulation parameters. Both shortcomings will be the focus of further investigations. However, extensive mapping of the 1:2 Arnold tongue boundary may be limited by patient fatigue and discomfort as some parameters tested are subtherapeutic and thus likely to lead to brief exacerbation of motor signs. In particular, there are relatively few data points to show the disappearance of 1:2 entrainment at high stimulation amplitudes (see **Figure 4.2C F**, and **I**). At these higher amplitudes, patients often experienced adverse effects which could be mildly unpleasant. Hence, following the documentation of loss or reduction of entrainment, higher amplitudes were not explored further. Provided these adverse effects can be better mitigated, the disappearance of 1:2 entrainment at high stimulation amplitudes will be confirmed in future studies.

Additionally, the absence of data on the clinical significance of gamma entrainment is a major limitation of this study and will be a focus for future work. However, Oehrn et al. recently reported that FTG power entrained at the half stimulation harmonic can predict hyperkinetic states in PD patients at home, and was identified as the optimal control signal for aDBS aimed at reducing residual motor fluctuations [40]. FTG-controlled aDBS resulted in improved motor symptoms and

quality of life during normal daily activities at home compared to standard-of-care continuous stimulation.

Given that ECoG data represents the activity of populations of neurons, the Wilson-Cowan model (a neural population model) is the appropriate level of description for this type of data. However, this doesn't allow us to observe or model the behaviour of individual neurons in response to stimulation and during 1:2 entrainment. Our approach is nonetheless adequate to predict stimulation parameters leading to 1:2 entrainment. Additionally, we have not included a population to represent the basal ganglia in our model. This was because there was no consistent subcortical off-stimulation gamma peak to fit a Wilson-Cowan network to for these patients. Subcortical narrowband oscillations in the basal ganglia have been recorded in long term recordings in other patients [10]. It may also be possible to observe 1:2 entrainment in the subcortex and while this study only considers cortical populations, the methodology presented here can be translated to any network of interacting excitatory and inhibitory populations of neurons. Furthermore, we did not consider plasticity in our model. While short-term response to stimulation (such as during the follow-up on-stimulation recordings reported here) can be described by models without plasticity, the several months of chronic stimulation between the prestimulation and follow-up recordings are likely to have led to plasticity, which we did not account for here.

The orthodromic projections from STN or pallidum to cortex are all polysynaptic, and whether the effect of basal ganglia DBS on cortex is excitatory or inhibitory is not well understood. There exist strong connections from STN to GPe [27], [28] and direct GABAergic projections from ChAT (choline acetyltransferase) and prototypic neurons from the GPe to the cortex [28]. Hence, stimulation from these two sites may act primarily on inhibitory populations of the cortex. However, there is not sufficient understanding of the effects of DBS on the basal ganglia as well as the exact nature of the projections from the basal ganglia to the cortex. It is also unclear how

antidromic activation of the stimulation targets would effect the motor cortex. To accommodate for this uncertainty, we consider DBS with both GABAergic and glutamergic tendencies. Stimulation to our fitted models consistently produces 1:2 entrainment with a left leaning tongue regardless of the population being stimulated. Hence, this choice is inconsequential and the presence of 1:2 entrainment is more specific to the dynamics of the cortical populations than the excitatory bias of the stimulating pulse.

Implications

This work demonstrates that brain rhythms can have nonlinear responses to stimulation, such as entrainment at harmonics of stimulation frequency, and non-monotonic rhythmic responses to stimulation amplitude. We argue against the simple view that only brain rhythms close to the stimulation frequency can be entrained (through 1:1 entrainment).

These findings might have implications across frequencies. 1:1 entrainment has been reported for example in the alpha band through single pulse transcranial magnetic stimulation when treating depression [16], with rhythmic visual stimulation [17], and with tACS [29]. If rhythms can lock to harmonics of stimulation frequency, as supported by this study, it is possible that current stimulation protocols targeting any frequency band could induce unexpected responses at sub- or supra-harmonics of the stimulation frequency. Thus, when designing stimulation protocols one should be aware of potential ramifications of stimulation on neuronal rhythms at multiple frequencies. For instance, stimulation targeting lower frequency oscillations, such as beta rhythms, may be able to entrain gamma at a 2:1 rotation number, or even alpha at a 1:2 rotation number. Similar considerations have been employed when designing stimulation protocols in a canine with epilepsy [30]. More recently, a principled approach to selectively promote rhythms close to the stimulation frequency while preventing entrainment at sub- and super-harmonics was put forward in [31].

FIGURES

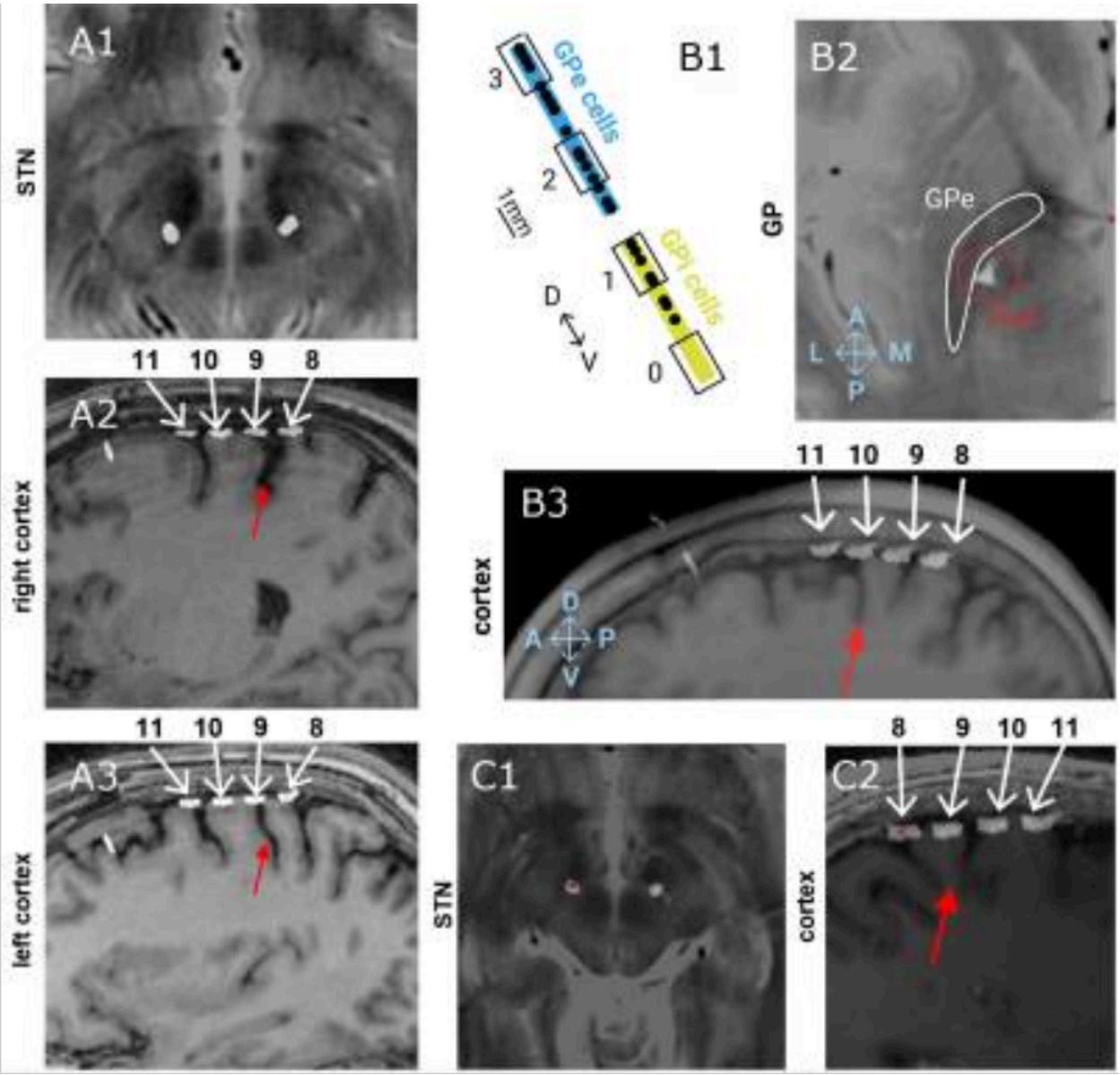

Fig. 4.1. Contact localization across three subjects.
The patients are presented as RCS02 (A1-3), RCS10 (B1-3) and RCS18 (C1 and 2). (A1-3, B2-3, C1-2) Localization of contacts with a postoperative CT scan that is computationally fused with the preoperative planning MRI scan. (A1 and C1) subthalamic nucleus (STN) lead on a T2-weighted MRI scan. In C1, the red dot indicates the left STN lead. (A2-3, B3, C2) Quadripolar subdural paddle lead on sagittal T1-weighted MRI shows the relationship between the central sulcus (red arrow) and contacts (white numbered arrows). For RCS10 (A2-3) and RCS18 (C2), contacts 11 and 10 were both over the pre-central gyrus whereas contact 9 was on the post-central gyrus. RCS02 (B3) was implanted slightly more anteriorly and contacts 9 and 10 were on the pre-central gyrus and 11 on the superior frontal gyrus. (Figure caption continued on next page)

(Figure caption continued from previous page) (B1) globus pallidus (GP) contact localization (black numbered rectangles) with respect to the boundaries of the internal globus pallidus (GPi) (yellow) and external globus pallidus (GPe) (blue) as defined by micro-electrode recording mapping of single-unit cells (black dots). (B2) GP lead on an axial T2-weighted MRI, which visualizes the GP as regions of T2 hypointensity (GPe highlighted by a white contour).

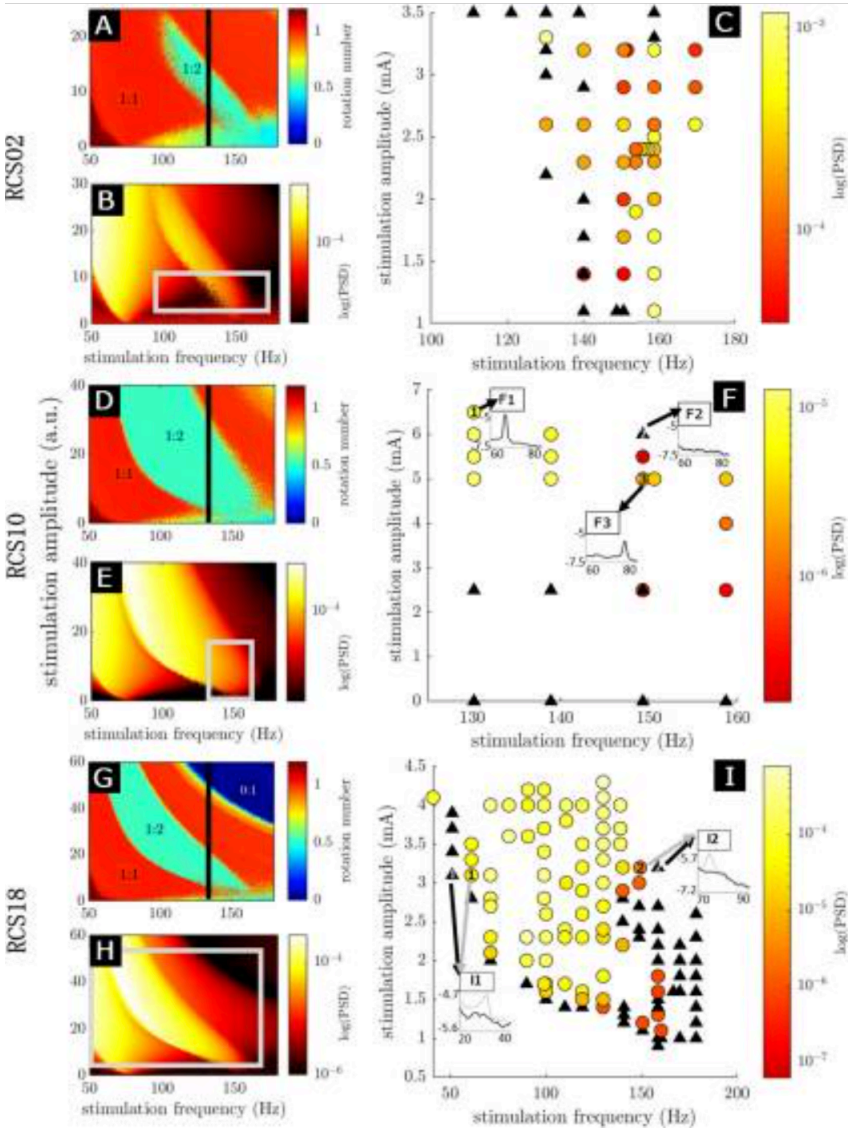

Figure 4.2: Testing model predictions of a cortical circuit's response to an external stimulus using human neural data during neurostimulation. Stimulation frequency is the horizontal axis for all panels, while stimulation amplitude is the vertical axis for all panels. Stimulation amplitude has arbitrary units (a.u.) for all model panels (A, B, D, E, G, and H) and is in mA for the data panels (C, F and I). Panels A-C are for RCS02, D-F for RCS10 and G-I for RCS18. Panels A, D and G have colour scales indicating the rotation number (as explained in the Arnold tongues and rotation number section) resulting from the stimulation parameters at that point, where 1:1 entrainment is in red and 1:2 entrainment is in green. For these panels, the black line indicates the 130 Hz stimulation condition used in [5], [14]. (A, D, G) The entrainment field of the Wilson-Cowan model with the top ranked parameters. The stimulation applied is a single time step pulse with no recharge. (B, E, H) The maximum height of the entrained peaks as predicted by the top-ranked Wilson-Cowan model fit, calculated as laid out in the Providing stimulation and entrainment analysis in the model section. (Figure caption continued on the next page)

(Figure caption continued from the previous page) The grey rectangles indicate comparable stimulation parameter ranges to those used in the variable stimulation response data, with stimulation amplitude scaling calculated as outlined in the Correspondence between stimulation amplitude in the model and in the data section. (C, F, I) The height of entrained peaks obtained from patient recordings for a series of different stimulation parameters. Circles display peak height (represented by the color scale) of parameters that displayed entrainment (as seen e.g. in insert F1), while black triangles are for parameters that did not display entrainment (as seen e.g. in insert F2). The occurrence of both a black triangle and a circle at the point (140 Hz, 1.4 mA) in panel C and point (150 Hz, 2.5 mA) in panel F indicate intermittent entrainment, hence, this will likely be on the boundary of the tongue. Inserts F1-3 and I1-2 show the logarithm of PSDs over frequencies around half the stimulation frequency. For inserts I1-2 the grey arrow and line indicate stimulation parameters where 1:2 entrainment was observed and black where it was not.

TABLES

Table 4.1. Patient information summary.

LEDD: levodopa equivalent daily dose, UPDRS: Movement Disorders Society Unified Parkinson's Disease Rating Scale, UPDRS (off-on): percent change off vs on medication, STN: subthalamic nucleus. “Time of charting” refers to on-stimulation data collection to test model predictions. *RCS18's right lead was deactivated during testing since it was recently reimplanted and undergoing clinical optimization.

Patient	RCS02	RCS10	RCS18
Age (years)	54	64	67
Disease Duration (years)	7	13	7
Gender	M	F	M
LEDD (mg/day)	1425	1083	2031
UPDRS-III off med	49	89	49
UPDRS (off-on)	90%	53%	76%
DBS Target	STN	Pallidum	STN
Duration of chronic DBS prior to collection of entrainment data (months)	30	10	7
Clinical Stimulation Settings	R: 1-C+, 2.6 mA, 60 µs, 130 Hz L: 2-C+, 2.4 mA, 60 µs, 130 Hz	R: 1-2-C+, 5.0 mA, 90 µs, 150 Hz L: 2-C+, 5.0 mA, 90 µs, 150 Hz	R: 2-C+, 2.3 mA, 60 µs, 130 Hz L: 2-C+, 2.4 mA, 60 µs, 130 Hz
Titration Ranges	R/L: Freq.: 110-170 Hz, Amp.: 0.7-3.1 mA	R/L: Freq.: 130-150 Hz, Amp.: 0-6.5 mA	R: OFF* L: Freq.: 40-180 Hz, Amp.: 0.9-4.3 mA

Table 4.2. Patient clinical symptom summary.
All assessments were done 90 days pre-operation. A few supplemental sub-scores are included (*MDS-UPDRS Part IV,** sum of all MDS-UPDRS-III tremor scores for each side, off medication).

Patient	UPDRS III OFF-med	UPDRS III ON-med	% change UPDRS when ON	time with dyskineasia*	Functional impact of dykinesia*	OFF-med tremor score**
RCS02	49	5	90%	4	0	L: 2; R: 0
RCS10	89	42	53%	0	0	L: 9; R: 11
RCS18	30	7	76%	2	1	L: 1; R: 1

REFERENCES

1. Koller William, Pahwa Rajesh, Busenbark Karen, Hubble Jean, Wilkinson Steve, Lang Anthony, et al. High-frequency unilateral thalamic stimulation in the treatment of essential and parkinsonian tremor. *Ann Neurol.* 1997;**42**
2. Thomas, Palleis Carla, Hell Franz, Mehrkens Jan H., Bötzel Kai. Deep brain stimulation programming for movement disorders: current concepts and evidence-based strategies. *Front Neurol.* 2019;**10**
3. Bosman Conrado A., Lansink Carien S., Pennartz Cyriel M.A. Functions of gamma-band synchronization in cognition: from single circuits to functional diversity across cortical and subcortical systems. *Eur J Neurosci.* Jun. 2014;**39**(11):1982–1999.
4. Nowak Magdalena, Zich Catharina, Stagg Charlotte J. Motor cortical gamma oscillations: what have we learnt and where are we headed? *Curr Behav Neurosci Rep.* Apr. 2018;**5**(2):136–142.
5. Swann Nicole C., De Hemptinne Coralie, Miocinovic Svjetlana, Qasim Salman, Wang Sarah S., Ziman Nathan, Ostrem Jill L., et al. Gamma oscillations in the hyperkinetic state detected with chronic human brain recordings in Parkinson's disease. *J Neurosci.* Jun. 2016;**36**(24):6445–6458.
6. Wiest C., Torrecillos F., Tinkhauser G., Pogosyan A., Morgante F., Pereira E.A., et al. Finely-tuned gamma oscillations: spectral characteristics and links to dyskinesia. *Exp Neurol.* 2022;**351** Elsevier Enhanced Reader.
7. Cassidy Michael, Mazzone Paolo, Oliviero Antonio, Insola Angelo, Tonali Pietro, Di Lazzaro Vincenzo, et al. Movement-related changes in synchronization in the human basal ganglia. *Brain.* Jun. 2002;**125**(6):1235–1246.

8. Williams David, Tijssen Marina, Van Bruggen Gerard, Bosch Andries, Insola Angelo, Di Lazzaro Vincenzo, Mazzone Paolo, et al. Dopamine-dependent changes in the functional connectivity between basal ganglia and cerebral cortex in humans. *Brain.* Jul. 2002;**125**(7):1558–1569.

9. de Hemptinne Coralie, Wang Doris D., Miocinovic Svjetlana, Chen Witney, Ostrem Jill L., Starr Philip A. Pallidal thermolesion unleashes gamma oscillations in the motor cortex in Parkinson's disease. *Mov Disord.* Jun. 2019;**34**(6):903–911.

10. Gilron Ro'ee, Little Simon, Perrone Randy, Wilt Robert, de Hemptinne Coralie, Yaroshinsky Maria S., et al. Long-term wireless streaming of neural recordings for circuit discovery and adaptive stimulation in individuals with Parkinson's disease. *Nat Biotechnol.* May 2021;**39**(9):1078–1085.

11. Halje Pär, Tamtè Martin, Richter Ulrike, Mohammed Mohsin, Angela Cenci M., Petersson Per. Levodopa-induced dyskinesia is strongly associated with resonant cortical oscillations. *J Neurosci.* Nov. 2012;**32**(47):16541–16551.

12. Güttler Christopher, Altschüler Jennifer, Tanev Kaloyan, Böckmann Saskia, Kersten Haumesser Jens, Nikulin Vadim V., et al. Levodopa-induced dyskinesia are mediated by cortical gamma oscillations in experimental parkinsonism. *Mov Disord.* Apr. 2021;**36**(4):927–937.

13. Guerra Andrea, Colella Donato, Giangrosso Margherita, Cannavacciuolo Antonio, Paparella Giulia, Fabbrini Giovanni, et al. Driving motor cortex oscillations modulates bradykinesia in Parkinson's disease. *Brain.* Jul. 2021

14. Swann Nicole C., De Hemptinne Coralie, Thompson Margaret C., Miocinovic Svjetlana, Miller Andrew M., Gilron Ro'Ee, et al. Adaptive deep brain stimulation for Parkinson's disease using motor cortex sensing. *J Neural Eng.* May 2018;**15**(4)

15. Arnol'd V.I. Remarks on the perturbation theory for problems of Mathieu type. *Russ Math Surv.* Aug. 1983;**38**(4):215–233.

16. Fröhlich Flavio. Tuning out the blues – Thalamo-cortical rhythms as a successful target for treating depression. *Brain Stimul: Basic, Transl, Clin Res Neuromodulation.* nov 2015;**8**(6):1007–1009.

17. Notbohm Annika, Kurths Jürgen, Herrmann Christoph S. Modification of brain oscillations via rhythmic light stimulation provides evidence for entrainment but not for superposition of event-related responses. *Front Human Neurosci.* Feb. 2016;**10**(FEB2016

18. Ali Mohsin M., Sellers Kristin K., Fröhlich Flavio. Transcranial alternating current stimulation modulates large-scale cortical network activity by network resonance. *J Neurosci.* Jul. 2013;**33**(27):11262–11275.

19. Hanslmayr Simon, Axmacher Nikolai, Inman Cory S. Modulating human memory via entrainment of brain oscillations. *Trends Neurosci.* 2019;**42**(7):485–499. doi: 10.1016/j.tins.2019.04.004.

20. Okun Michael S., Fernandez Hubert H., Wu Samuel S., Kirsch-Darrow Lindsey, Bowers Dawn, Bova Frank, et al. Cognition and mood in Parkinson's disease in subthalamic nucleus versus globus pallidus interna deep brain stimulation: the compare trial. *Ann Neurol.* 2009;**65**

21. Follett Kenneth A., Weaver Frances M., Stern Matthew, Hur Kwan, Harris Crystal L., Luo Ping, et al. Pallidal versus subthalamic deep-brain stimulation for Parkinson's disease. *N Engl J Med.* 2010;**362**

22. Starr Philip A. Placement of deep brain stimulators into the subthalamic nucleus or globus pallidus internus: technical approach. *Stereotact Funct Neurosurg.* 2002;**79**

23. Shahlaie Kiarash, Larson Paul S., Starr Philip A. Intraoperative computed tomography for deep brain stimulation surgery: technique and accuracy assessment. *Neurosurgery.* 2011;**68**

24. Swann Nicole C., De Hemptinne Coralie, Miocinovic Svjetlana, Qasim Salman, Ostrem Jill L., Galifianakis Nicholas B., et al. Chronic multisite brain recordings from a totally

implantable bidirectional neural interface: experience in 5 patients with Parkinson's disease. *J Neurosurg.* 2018;**128**

25. Muthuraman Muthuraman, Bange Manuel, Koirala Nabin, Ciolac Dumitru, Pintea Bogdan, Glaser Martin, et al. Cross-frequency coupling between gamma oscillations and deep brain stimulation frequency in Parkinson's disease. *Brain.* Dec. 2020;**143**(11):3393–3407.
26. Oehrn Carina R, Cernera Stephanie, Hammer Lauren H, Shcherbakova Maria, Yao Jiaang, et al. Personalized chronic adaptive deep brain stimulation outperforms conventional stimulation in Parkinson's disease. 2023. MedRxiv.
27. Calabresi P., Picconi B., Tozzi A., Ghiglieri V., Di Filippo M. Direct and indirect pathways of basal ganglia: a critical reappraisal. *Nat Neurosci.* 2014;**17**(8):1022–1030. doi: 10.1038/nn.3743.
28. Dong Jie, Hawes Sarah, Wu Junbing, Le Weidong, Cai Huaibin. Connectivity and functionality of the globus pallidus externa under normal conditions and Parkinson's disease. *Front Neural Circuits.* 2021;**15**(8):3.
29. Huang Wei A., Stitt Iain M., Negahbani Ehsan, Passey D.J., Ahn Sangtae, et al. Transcranial alternating current stimulation entrains alpha oscillations by preferential phase synchronization of fast-spiking cortical neurons to stimulation waveform. *Nat Commun.* May 2021;**12**(1):1–20.
30. Zamora Mayela, Meller Sebastian, Kajin Filip, Sermon James J., Toth Robert, Benjaber Moaad, et al. Report: embedding “digital chronotherapy” into medical devices—a canine validation for controlling status epilepticus through multi-scale rhythmic brain stimulation. *Front Neurosci.* Sep. 2021;**15**:1196.
31. Duchet Benoit, Sermon James J., Weerasinghe Gihan, Denison Timothy, Bogacz Rafal. How to entrain a selected neuronal rhythm but not others: open-loop dithered brain stimulation for selective entrainment. *J Neural Eng.* Apr. 2023;**20**(2)

Publishing Agreement

It is the policy of the University to encourage open access and broad distribution of all theses, dissertations, and manuscripts. The Graduate Division will facilitate the distribution of UCSF theses, dissertations, and manuscripts to the UCSF Library for open access and distribution. UCSF will make such theses, dissertations, and manuscripts accessible to the public and will take reasonable steps to preserve these works in perpetuity.

I hereby grant the non-exclusive, perpetual right to The Regents of the University of California to reproduce, publicly display, distribute, preserve, and publish copies of my thesis, dissertation, or manuscript in any form or media, now existing or later derived, including access online for teaching, research, and public service purposes.

DocuSigned by:
Maria Olaru
AE7288762F1A497...
Author Signature

7/2/2024
Date